JETSET NOTE 91-21
14 November 1991

ORGANISATION EUROPÉENNE POUR LA RECHERCHE NUCLÉAIRE
CERN EUROPEAN ORGANISATION FOR NUCLEAR RESEARCH

CERN JETSET GROUP

FORWARD CHERENKOV COUNTERS AND SILICON DETECTOR PERFORMANCE DURING THE APRIL-JULY 1991 RUNS

D. Drijard, M. Ferro-Luzzi, N. Hamann, R. Jones, B. Mouëllic, J-M. Perreau, S. Ohlsson

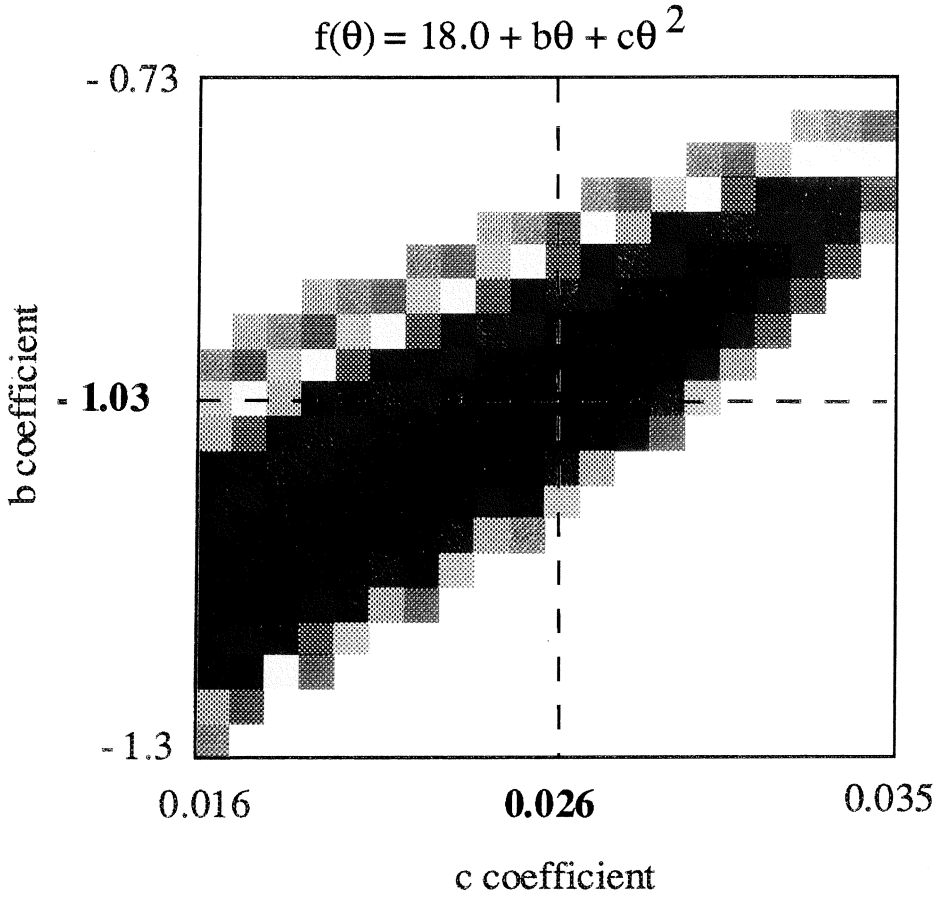

1. INTRODUCTION

The data acquired during the first two periods of JETSET running in 1991 have been examined in an effort to assess the performance of two detector systems on which our experiment is crucially dependent: the "*Forward Cherenkovs*" and the "*Silicon*".

In this note we describe a study of the events recorded under the label of "*elastic triggers*". Among these we have selected those which can be most safely assigned to the $\bar{p}p$ elastic scattering reaction. We use these events and exploit their convenient kinematical features to assess the response of our detectors under controlled conditions. We find that both systems have performed according to specifications, albeit with minor and partly unexplained faults.

One conclusion is that the *Cherenkovs* not only provide the expected threshold response (which is all they were supposed to do in the first place) but are also capable of providing an approximate measurement of the particle's β good enough to play a role in the event-identification procedure. On the negative side we confirm[1] that a few of them appear to have suffered from structural stresses resulting in some of the liquid-radiator having leaked out from cracks. This has reduced and in some cases nullified their operational capability. The reason for this occurrence is still under investigation but seems to be due to a mechanical deformation of the plexiglas containers under differential expansion (the cause of which has not yet been established) between radiator and wall materials. Mechanical tests are currently under way to understand this behaviour; in any case repairs and reconstructions where necessary are being done at the moment. A refurbished system will be put back in operation for next year's runs.

In the case of the *Silicons* we find a satisfactory and consistently reliable response from the elements along the tracks trajectories with respect to alignement and response. On the negative side we are somewhat puzzled by the large amount of apparently uncorrelated silicon hits. Also, we have not yet succeeded in explaining the low-β response of the data from the single (and unfortunately very short) run taken at the lowest energy. The detector response at 600 MeV/c appears to be far higher than expected on the basis of the higher energy calibrations. We suspect this to be due to factors other than the detector response. At the forward momenta available in $\bar{p}p$ elastic scattering at 600 MeV/c (which can be as low as a few hundred MeV/c) it is quite possible that the track-reconstruction procedure has been seriously affected by large multiple scattering effects and other vagaries such as antiproton annihilation, secondary decays, etc. This work is still going on, in particular trying to understand why our results are at variance with those obtained in an earlier preliminary study[2].

---

[1] See "Change of radiator from freon to water", (M.F.-L.) unnumbered note 26 September 1991.
[2] See "Silicon dE/dx for elastics at 600 MeV/c" (B.Stugu) unnumbered note 23 August 1991.

In all cases it should be stressed that this is not meant to be the last word on these detectors. These results are presented in the usual spirit of (a) informing the Collaboration on our progress and (b) soliciting useful remarks on possible misinterpretations and mistakes.

The presentation of the study follows a momentum-by-momentum approach of various subjects. You will find long and repetitive series of similar plots covering the full momentum region of the experiment preceded by a common explanation and commentary. We find it useful to present all results at various energies rather than only samples because they serve to show possible trends and anomalies easily unnoticed otherwise.

2. ELASTIC EVENTS

The manner by which we gathered our sample of *bona fide* elastic scattering events has been to proceed through the following steps. First, all the "*elastic triggers*" were analysed on the IBM with an *ad hoc* procedure based on a "reduction program" filtering out the most unlikely elastic events by applying a "coplanarity" requirement as described in previous notes[3] plus a number of checks on the track ingredients such as a minimum and maximum number of hits in the barrel and forward tracker. The results of this first selection ($\approx$ 25 % of the total) were converted into 8-mm cassettes and analysed on the Macintosh computers (which some of us are very happy to rely upon in place of using more ponderous and not easily accessible alternatives). The second selection applied to these events imposed more drastic requirements. The most important of them were:

(a) an ADC cut at 200 channels for the **straight-scintillator** and **gamma-veto** barrel elements for any additional hit beyond one (to reject possible neutrals and inelastic events);

(b) a strict **forward-pixel** association with the forward track (to make sure that the track had gone through the detectors under study);

(c) a correct forward and barrel track **reconstruction** (using a chi-square criterion based on the goodness of the track fit);

(d) agreement within $\pm$ 15^{o} between expected (via kinematics) and measured barrel-track **polar** directions and between the forward and barrel **azimuths**;

(e) existence of one and only one fitted forward track while allowing up to two fitted tracks in the barrel.

In the vast majority of the events thus selected the proton is observed in the straw-barrel in association with a barrel-pipe-scintillator and the antiproton in the forward-straws associated to a forward-pipe-scintillator. In the course of this study we will refer to these two tracks as barrel- and forward-track respectively. The portions of the forward-track

---

[3] See JETSET notes 90-12 (D. Drijard et al.) 22 July 1990 , 90-23 (M.F.-L.) 13 November 1990 and "Elastics" by S.Ohlsson undated, un-numbered note on the subject.

occasionally seen by the barrel straws is usually too short to allow an independent reliable reconstruction; here we have consistently ignored this information. Notice that also deliberatly missing in this study are those events where both proton and antiproton went through the forward tracker.

The result of the second "reduction" was to retain an average of $\approx 20\%$ of the events from the first selection (see Table 1). The notable exception is at 600 MeV/c where the number retained is very small indeed. Notice that requiring tracks to reach pixels compels these already low-energy particles the additional effort to go through a Cherenkov counter with its attendant slowing-down and annihilation hazards.

Table 1

Fraction of elastic triggers retained after each selection.

P (GeV/c)	1st selection	2nd selection	Total selection
0.6		0.006	
1.2		0.195	
1.3		0.143	
1.4		0.277	
1.5		0.214	
1.6		-	
1.7		0.225	
1.8		-	
1.9		0.212	
2.0		0.240	

The plots that follow illustrate the main geometrical and kinematical features of the final sample. Figs 2.1 to 2.10 show the azimuth and polar angle differences between the forward- and the barrel-track. These quantities are expected to be equal in the ideal case of zero measurement error and no material effects. The spread observed is quite consistent with the conditions of the experiment. Results of Gaussian fits of these quantities are shown by curves and tables on the figures themselves.

Notice that the acceptance criteria applied to these events are well beyond the limits of the observed distributions for the azimuth distribution. The polar-angle distributions instead are generally wider than those referring to the azimuth and furthermore appear somewhat cut, reflecting as they do the present charge-division uncertainties on the barrel-track angle.

It should also be mentioned that the current barrel-track polar angles turned out to be on the average 2.8^{o} larger than expected by the elastic kinematics; this correction has been applied throughout the analysis and we advise to apply it on the rest of the analysis[4].

Differently from the other figures the data in fig. 2.1 have been represented by lines rather than points because of the need to guide the eye in the midst of a widely fluctuating set of points.

[4] The lack of this correction may well be partly responsible for the anomalous behaviour of our 1B3F events in the 4K anlysis of JETSET note 91-11 (D.Drijard et al.) 27 September 1991.

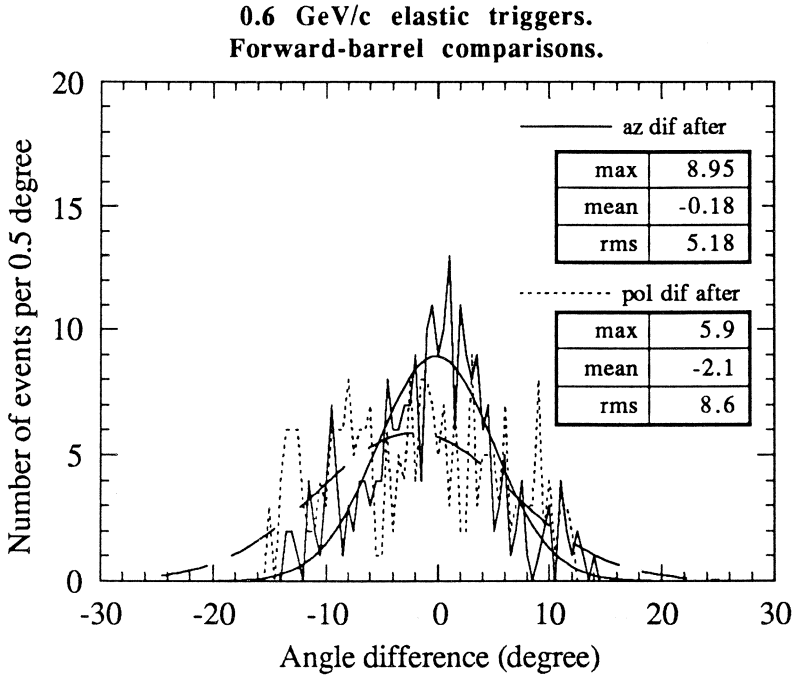

Fig. 2.1 Incident momentum 0.6 GeV/c.

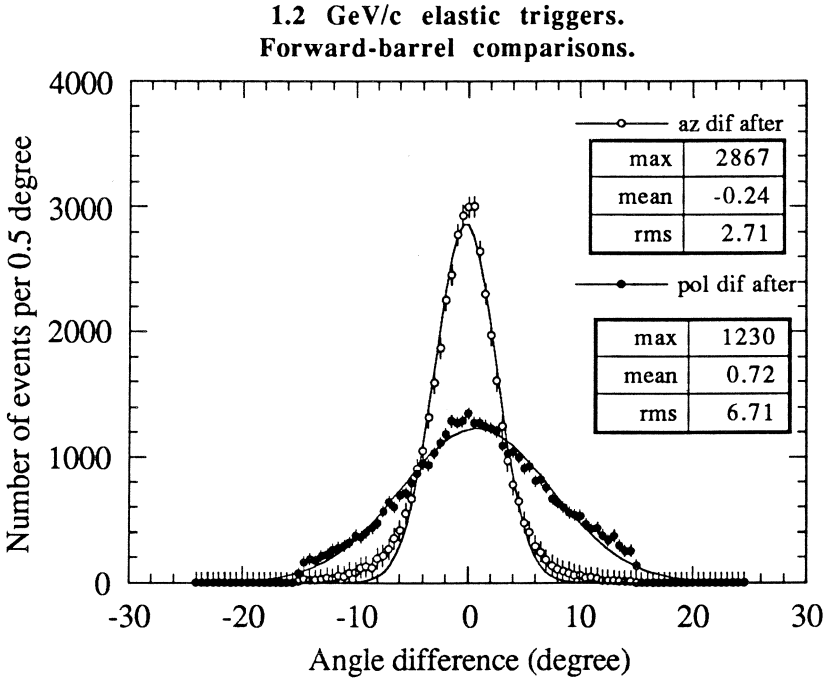

Fig. 2.2 Incident momentum 1.2 GeV/c.

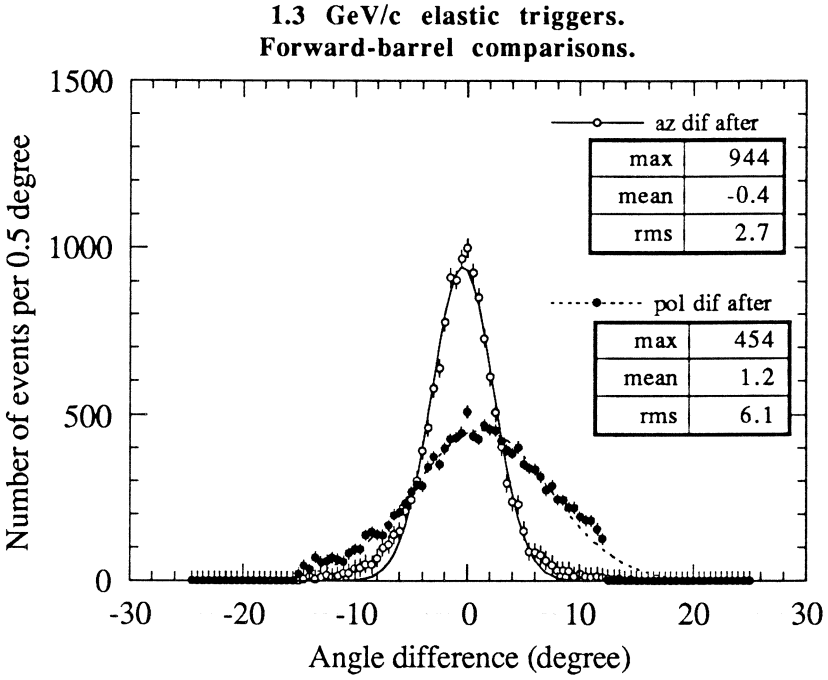

Fig. 2.3 Incident momentum 1.3 GeV/c.

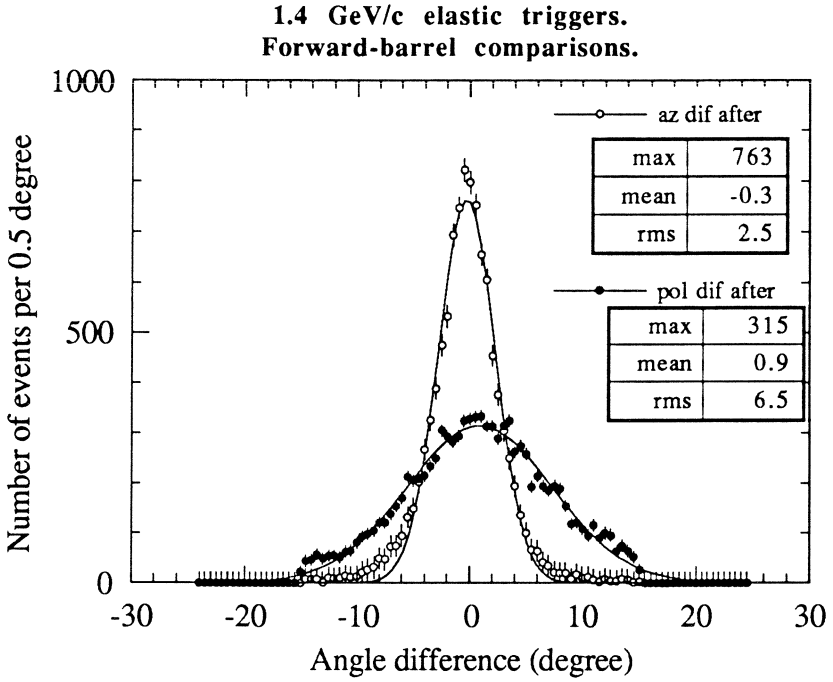

Fig. 2.4 Incident momentum 1.4 GeV/c.

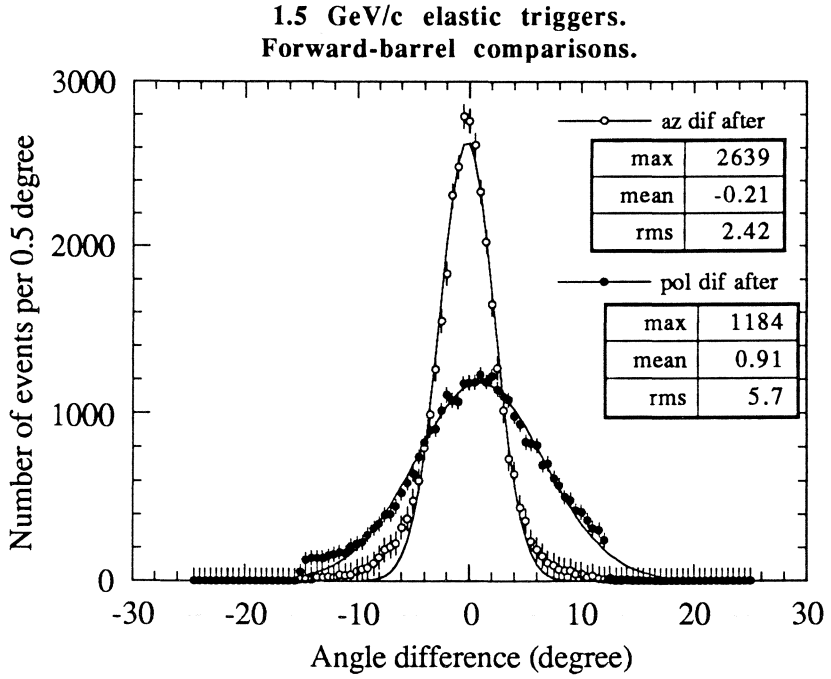

Fig. 2.5 Incident momentum 1.5 GeV/c.

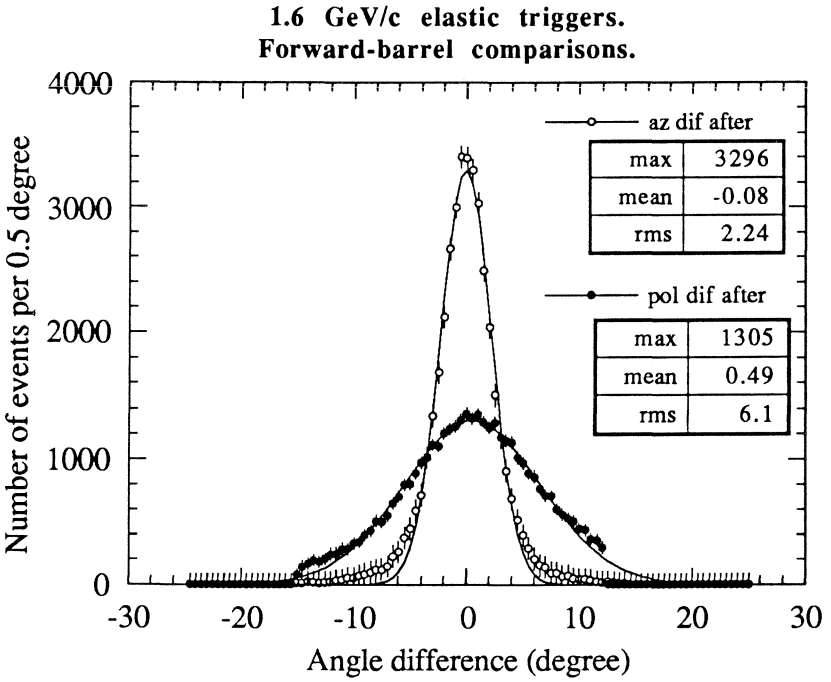

Fig. 2.6 Incident momentum 1.6 GeV/c.

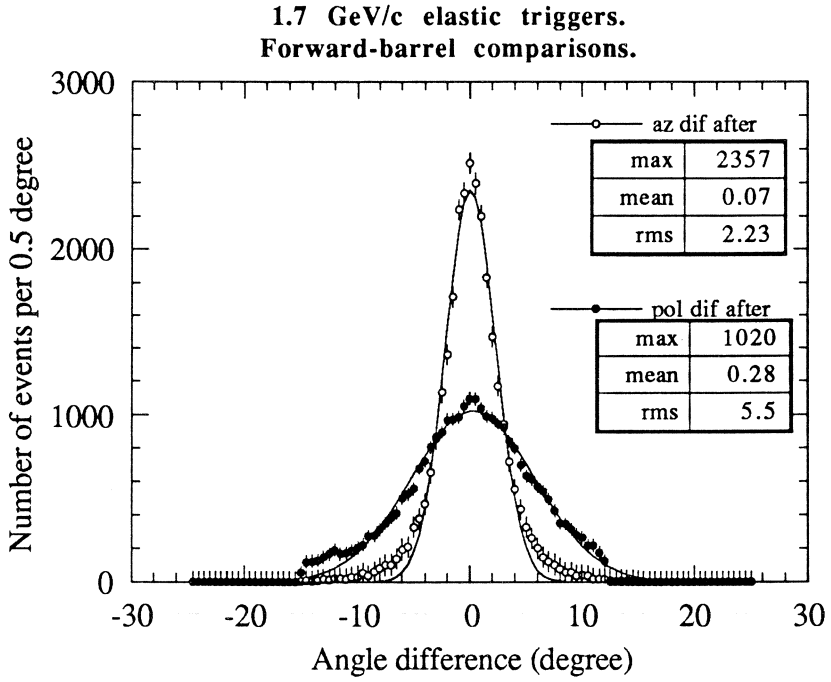

Fig. 2.7 Incident momentum 1.7 GeV/c.

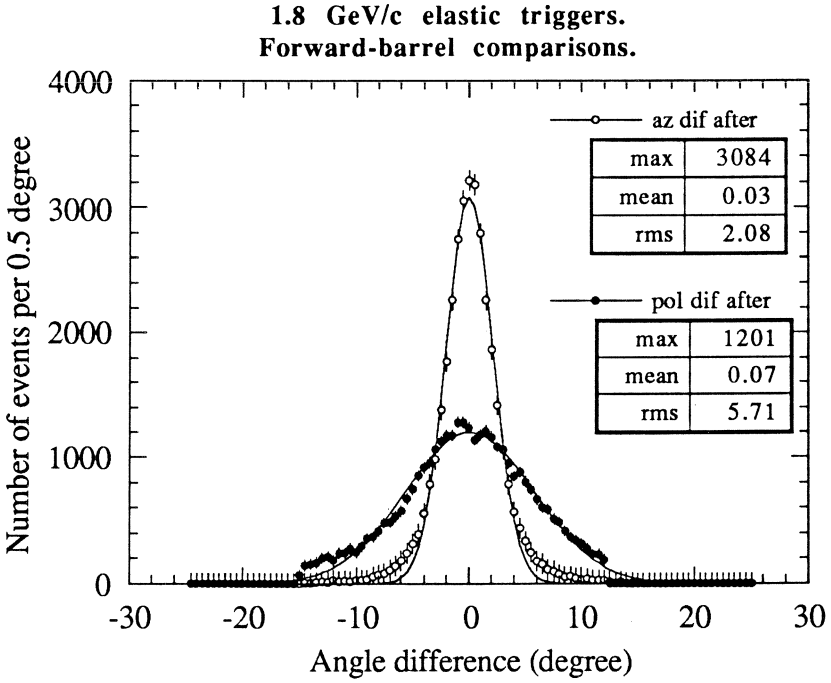

Fig. 2.8 Incident momentum 1.8 GeV/c.

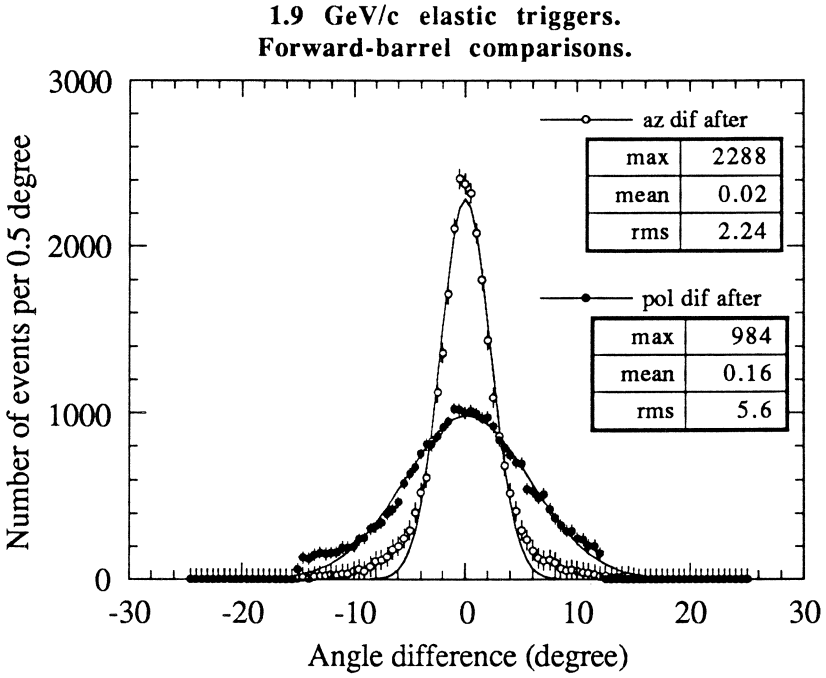

Fig. 2.9 Incident momentum 1.9 GeV/c.

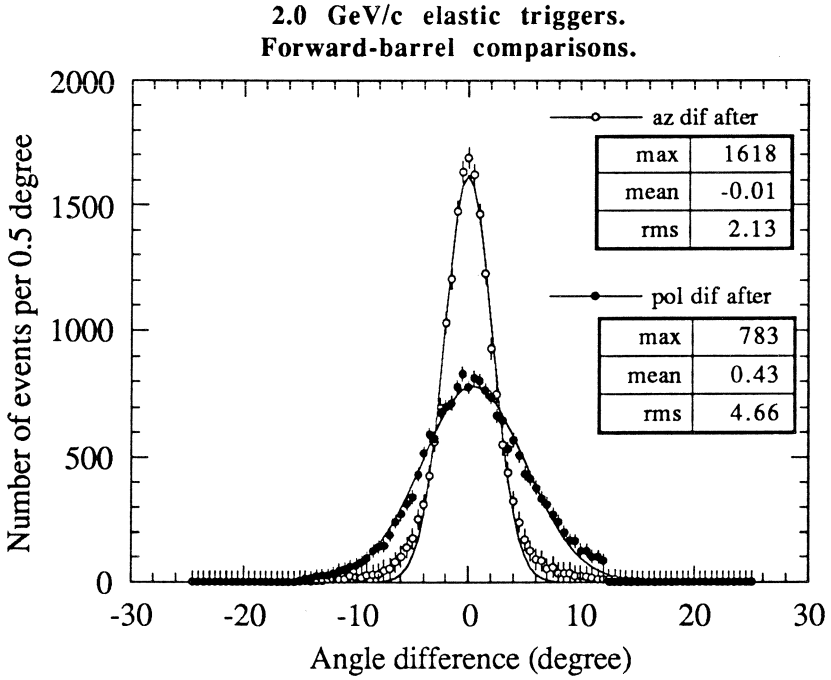

Fig. 2.10 Incident momentum 2.0 GeV/c.

In figures 2.11 to 2.20 we show — more for reassurance of our selection capabilities than other purposes — the angular distributions of the selected elastic events. The angles are in the laboratory system and refer to the assumed (fixed) incident antiproton direction along the vacuum pipe axis. Do not forget that the incident beam has an intrinsic spread and so has the target region; we have not taken into account either of them. The limits of the individual distributions (15° to 45° and 45° to 65°) are those imposed by the trigger acceptance criterion: one hit in the forward- and one in the barrel-pipes.

We have reassured ourselves that the dips noticeable here and there in these plots are **not** the effect of faulty detector acceptance or inefficiency (as we feared when first noticing them) but are simply the reflection of the diffraction minima present in the original differential cross sections.

The corresponding momenta calculated via the elastic kinematics are shown in figs 2.21 to 2.30; the same features are observable here as in the previous angular plots.

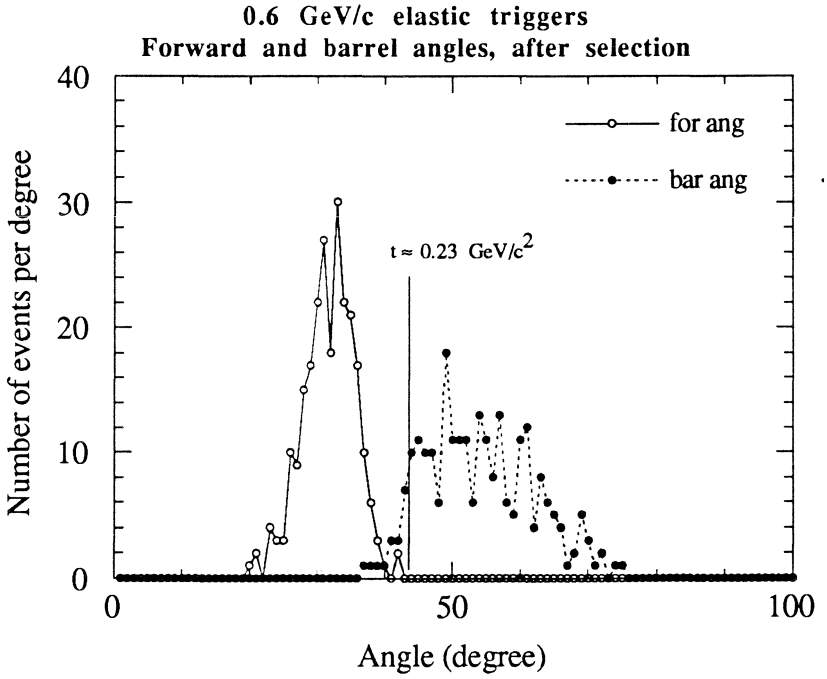

Fig. 2.11 Incident momentum 0.6 GeV/c.

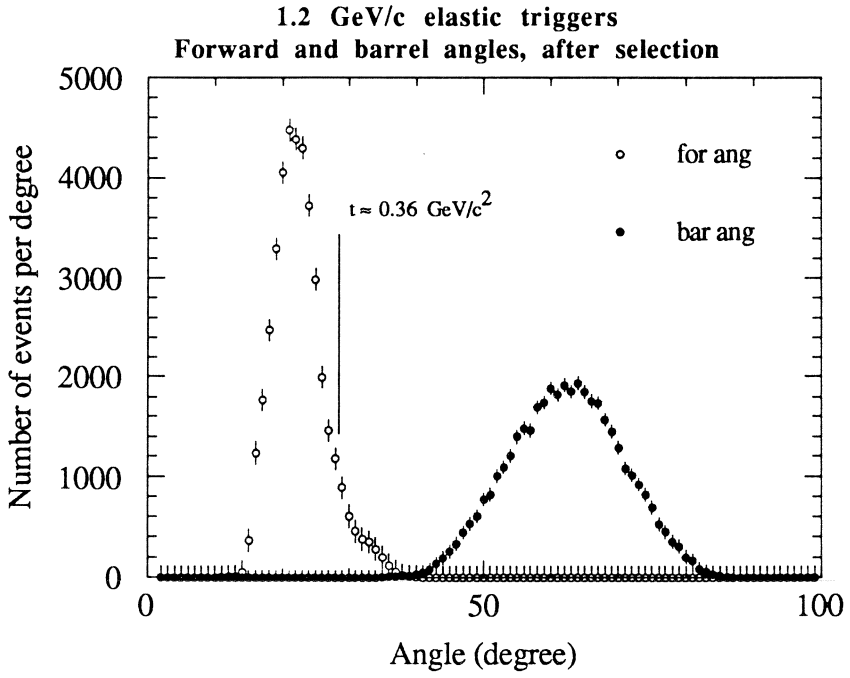

Fig. 2.12 Incident momentum 1.2 GeV/c.

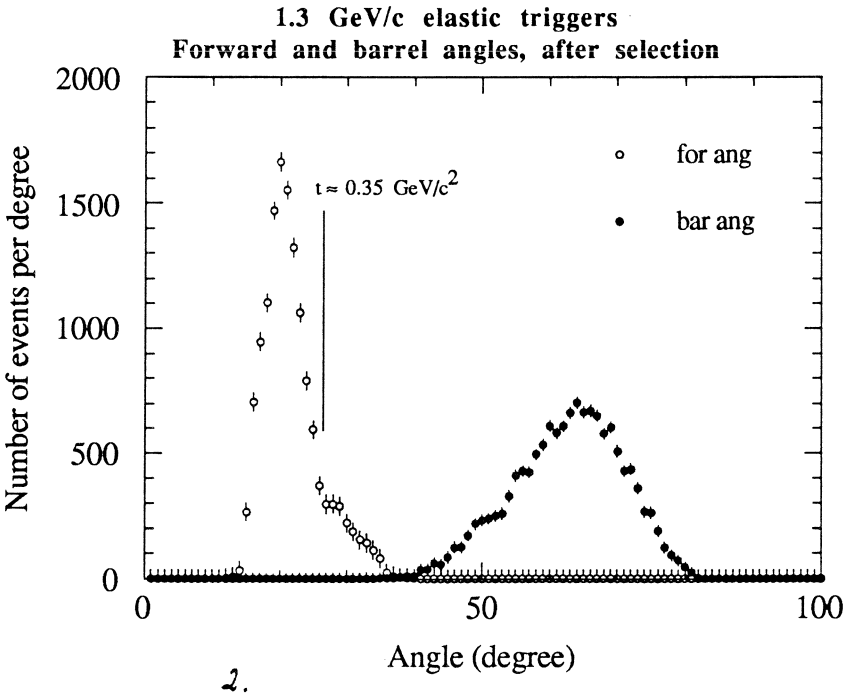

Fig. 2.13 Incident momentum 1.3 GeV/c.

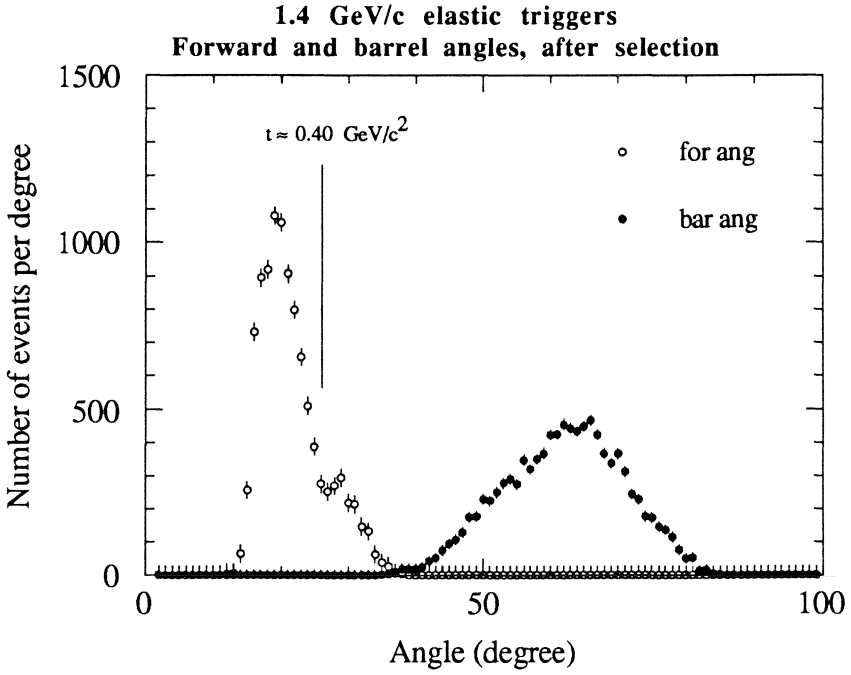

Fig. 2.14 Incident momentum 1.4 GeV/c.

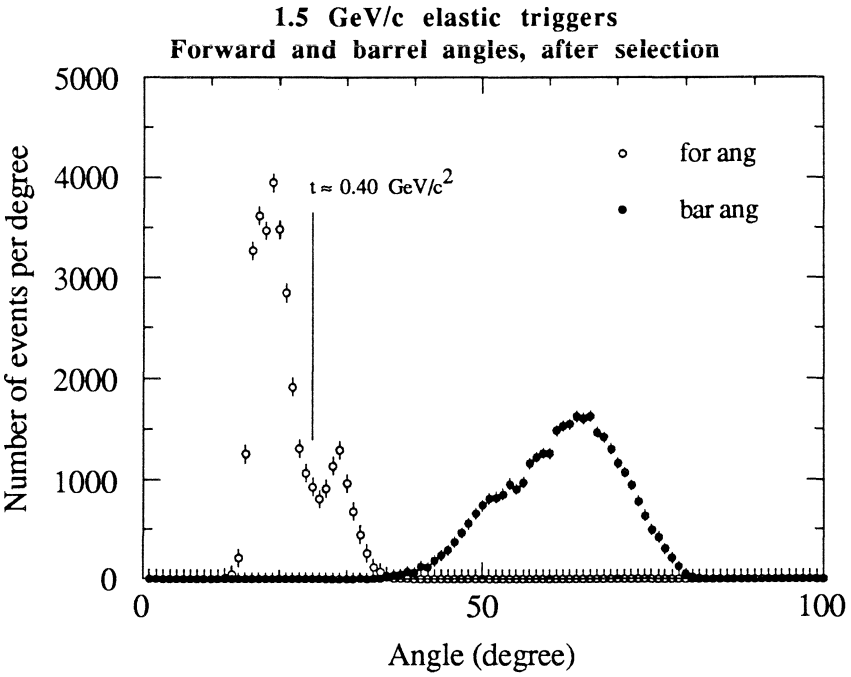

Fig. 2.15 Incident momentum 1.5 GeV/c.

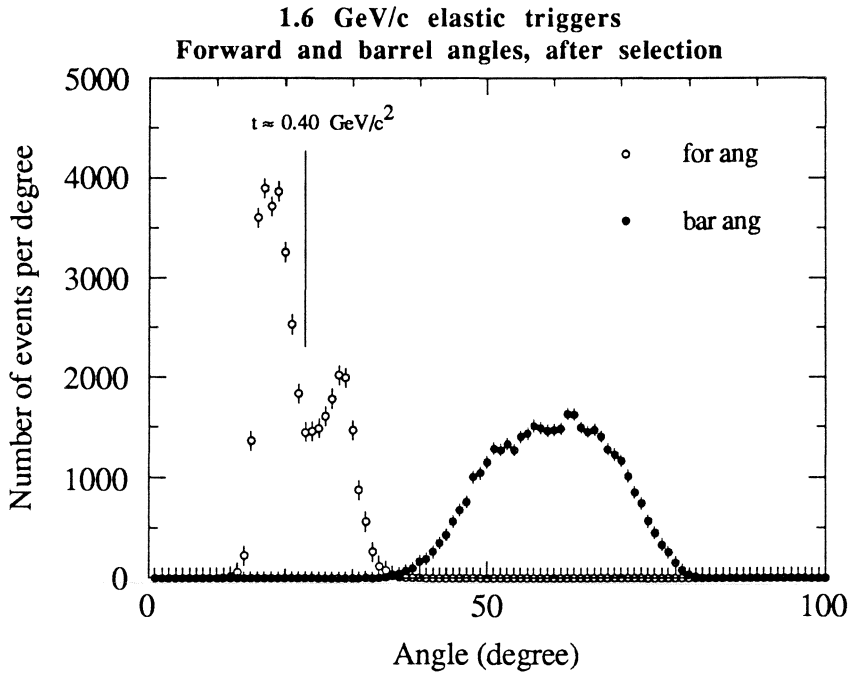

Fig. 2.16 Incident momentum 1.6 GeV/c.

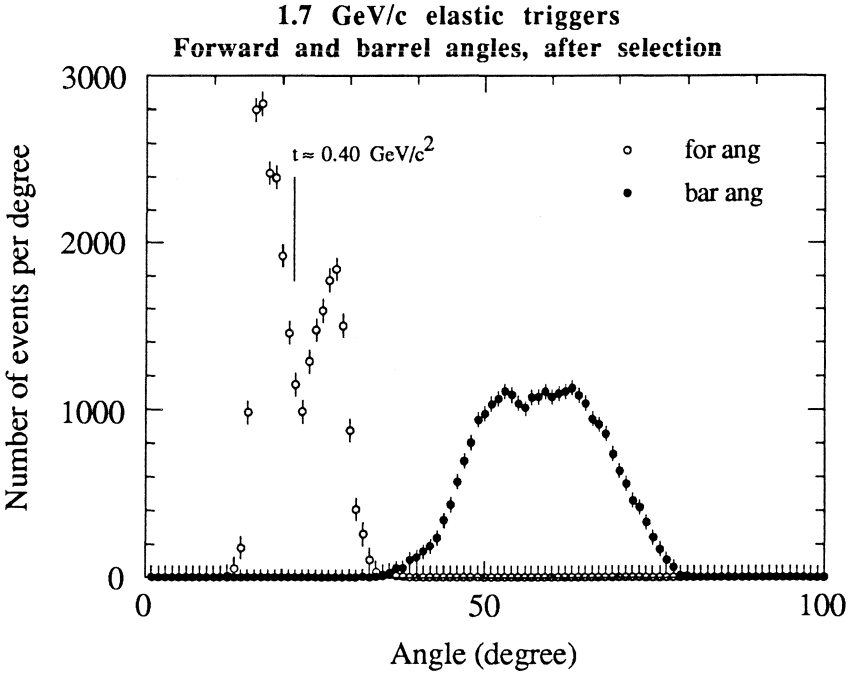

Fig. 2.17 Incident momentum 1.7 GeV/c.

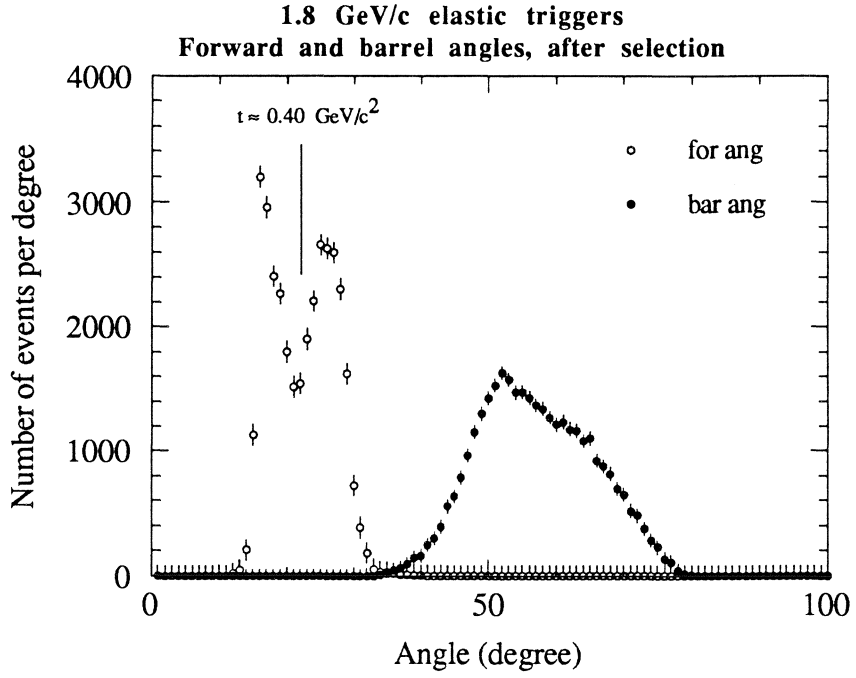

Fig. 2.18 Incident momentum 1.8 GeV/c.

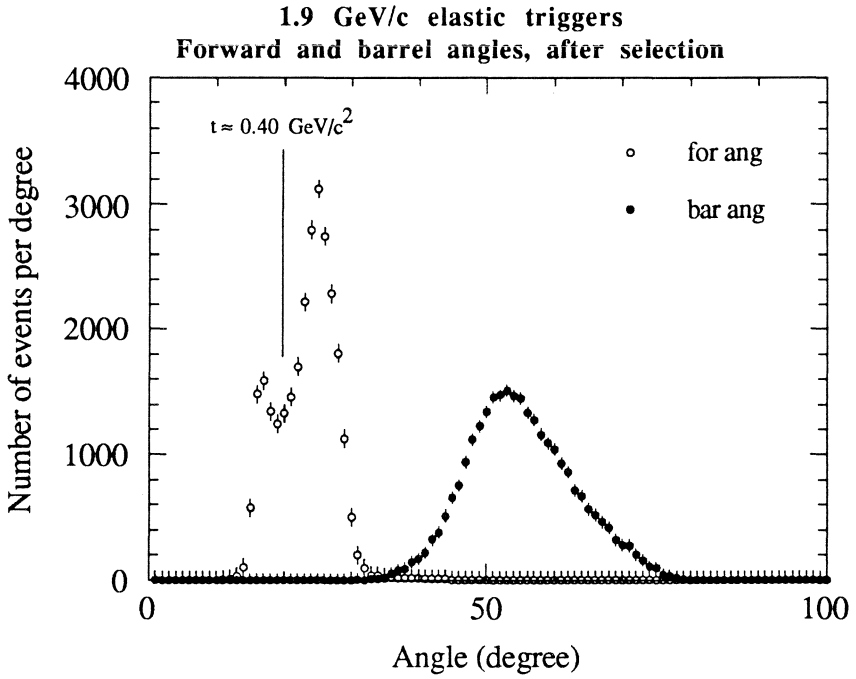

Fig. 2.19 Incident momentum 1.9 GeV/c.

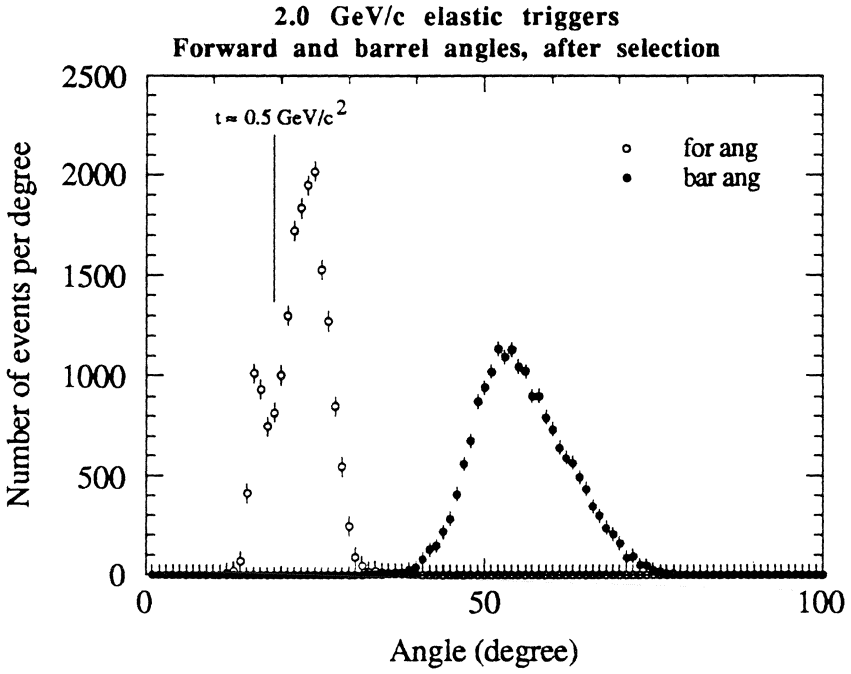

Fig. 2.20 Incident momentum 2.0 GeV/c.

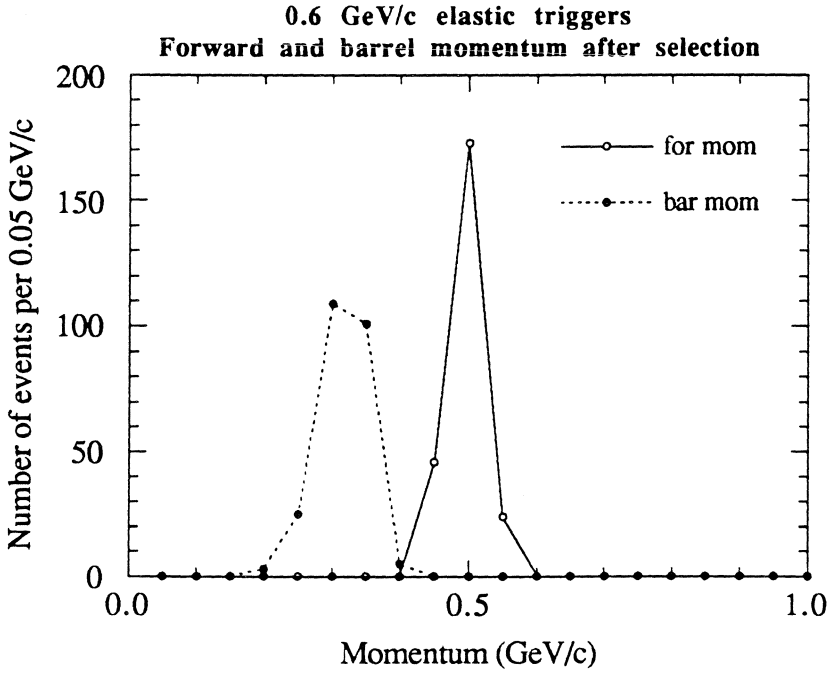

Fig. 2.21 Incident momentum 0.6 GeV/c.

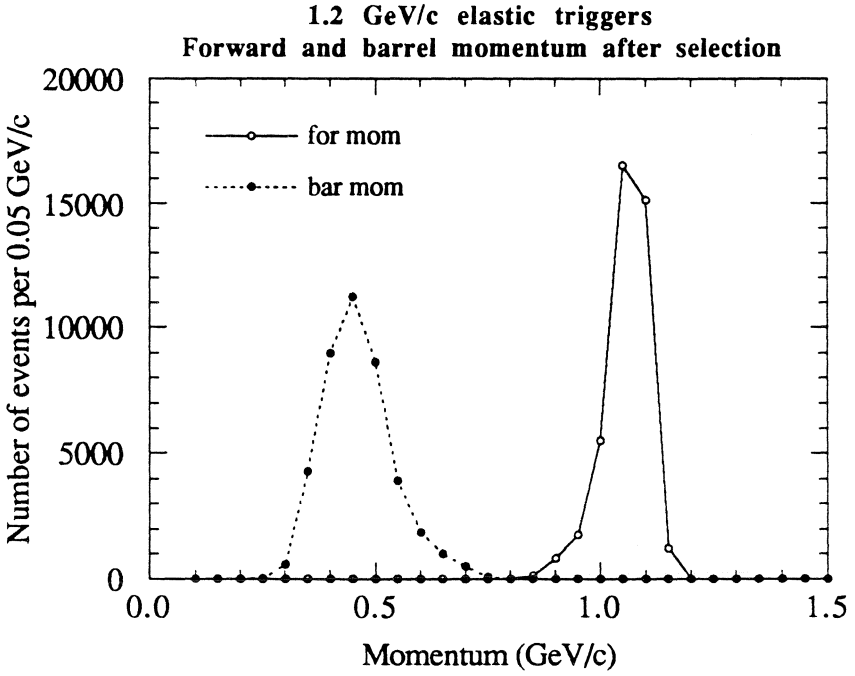

Fig. 2.22 Incident momentum 1.2 GeV/c.

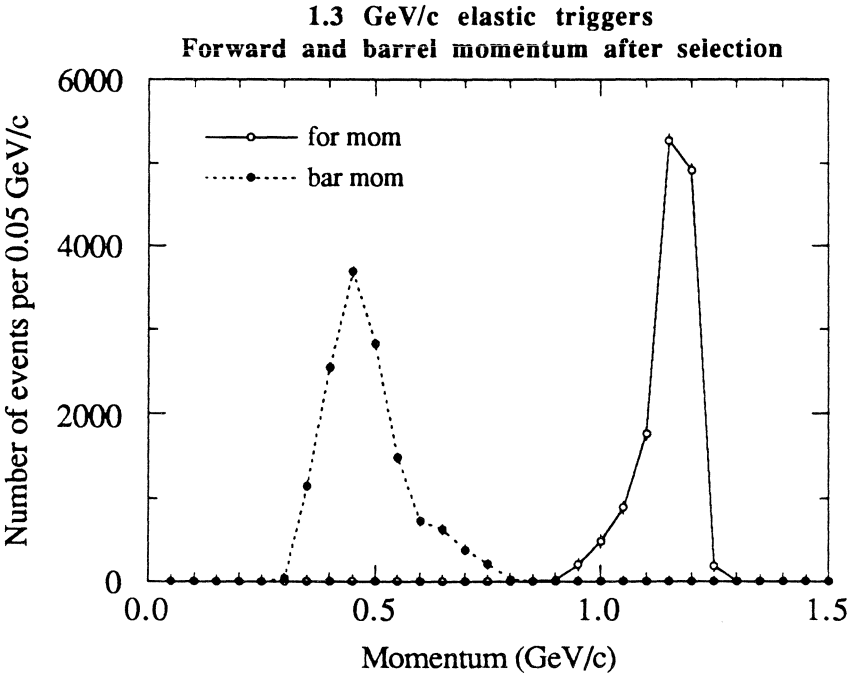

Fig. 2.23 Incident momentum 1.3 GeV/c.

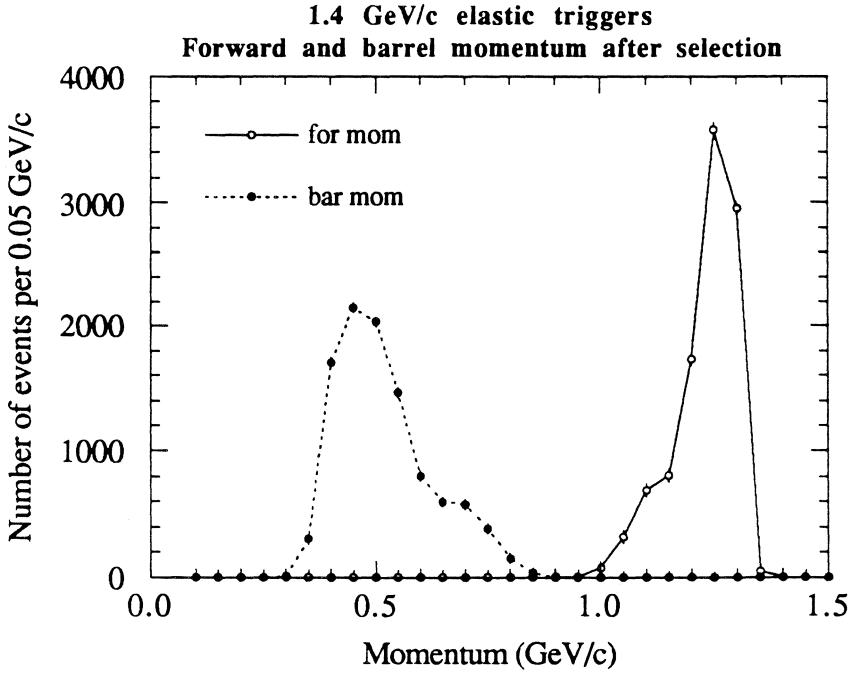

Fig. 2.24 Incident momentum 1.4 GeV/c.

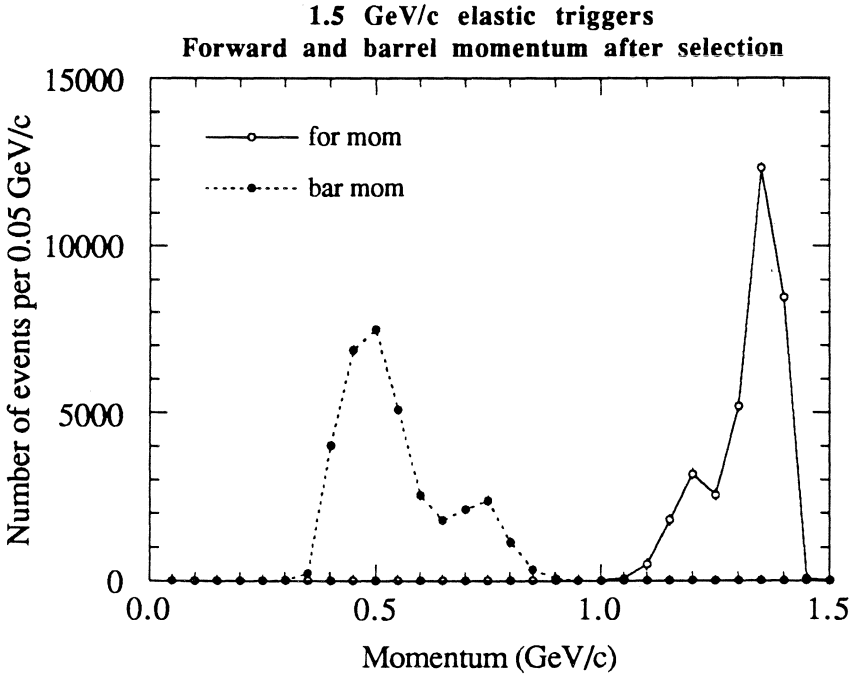

Fig. 2.25 Incident momentum 1.5 GeV/c.

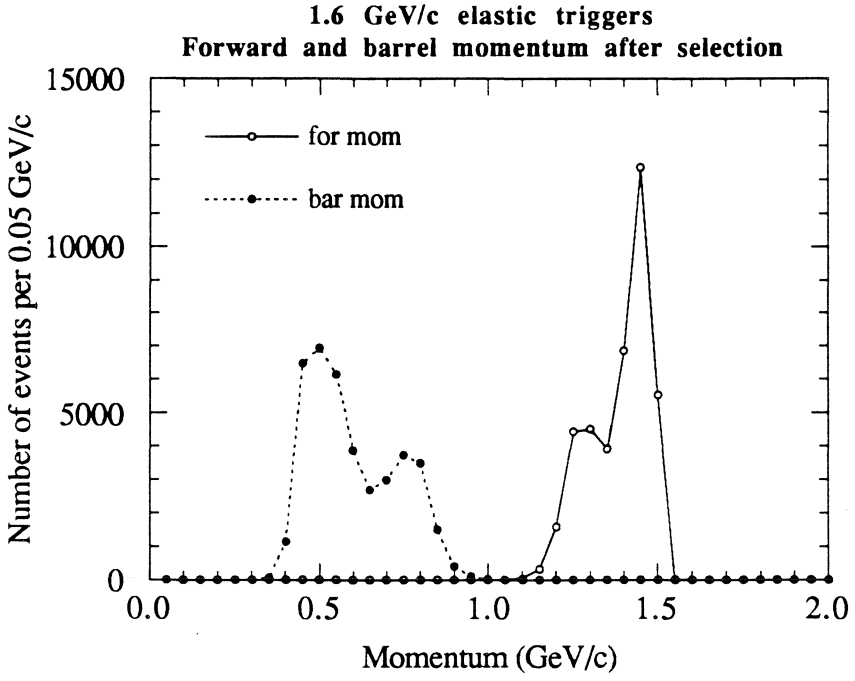

Fig. 2.26 Incident momentum 1.6 GeV/c.

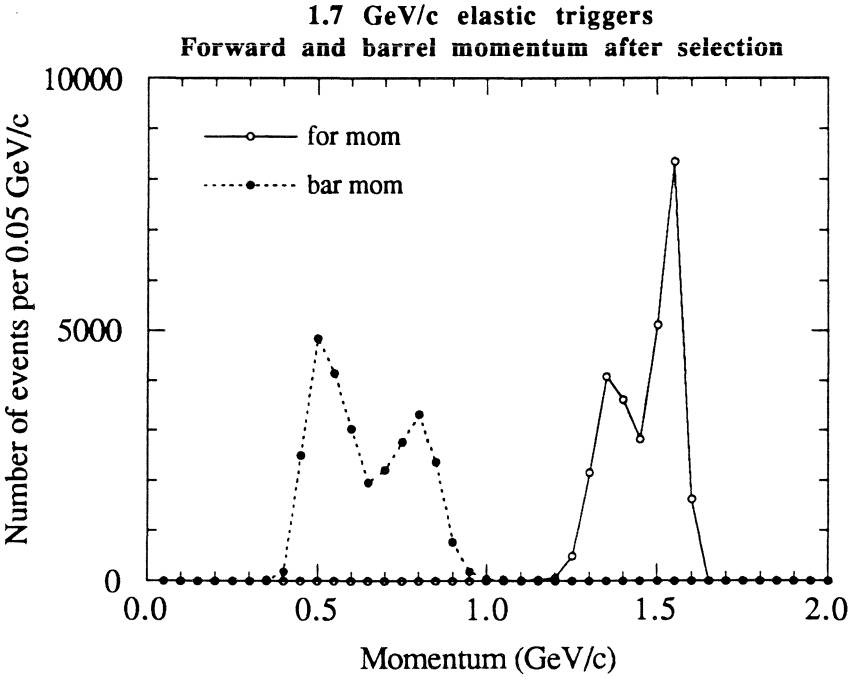

Fig. 2.27 Incident momentum 1.7 GeV/c.

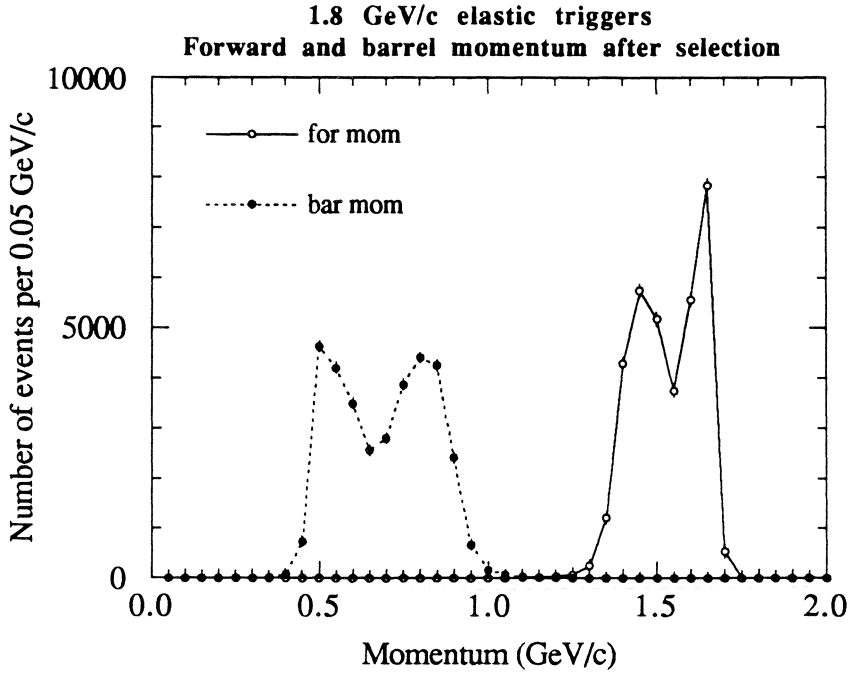

Fig. 2.28 Incident momentum 1.8 GeV/c.

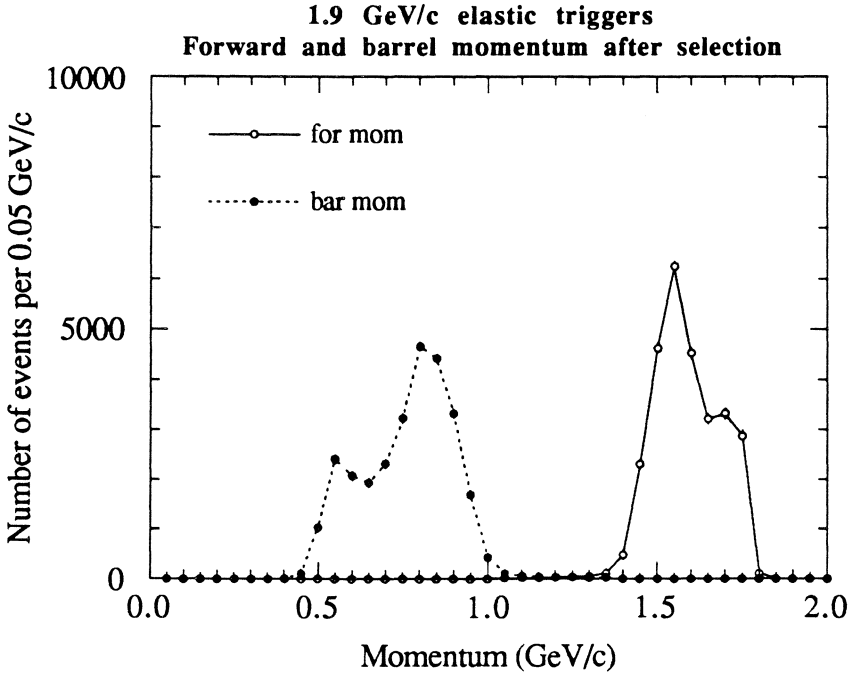

Fig. 2.29 Incident momentum 1.9 GeV/c.

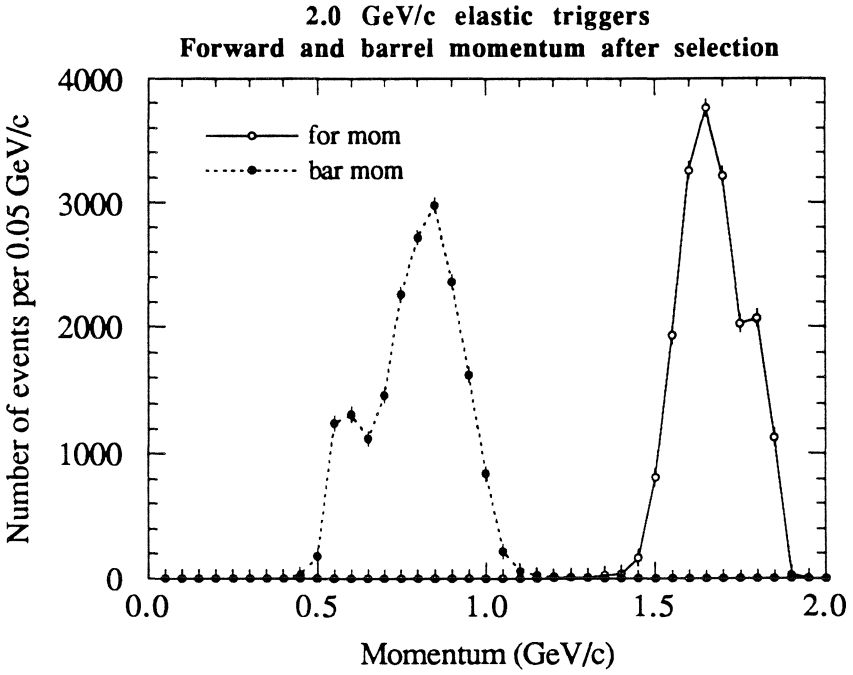

Fig. 2.30 Incident momentum 2.0 GeV/c.

3. CHERENKOV RESPONSE

Having convinced ourselves that we are dealing with a good sample of elastic events we have then used it to test the Cherenkov response when the counters are traversed by known particles of known β at known angles[5].

Measurements performed earlier on a Cherenkov prototype module in the T_{11} beam[6] had already provided us with a detailed knowledge of the amount of photo-electrons expected to be produced on the photo-cathode by light emitted from incident particles at different angles. The measurements were done under geometrical conditions illustrated in fig. 3.1. and the main results are shown in fig. 3.2.

---

[5] The radiator used was the one currently referred to as "liquid freon" (not a freon at all, by the way), also called "FC-72" and produced under this trade name by the 3M company. Its proper chemical name is hexane-perfluoro and its composition C_6F_{14}. Its refraction index is given as n=1.276 at 6eV and n=1.2515 in the visible. It has density ρ=1.6995, radiation length X_o=31.59 g/cm^2 and coefficient of expansion = 0.0016 cm^3/ (cm^3 °C). We list these boring details because each time we need them we have to make extensive searches ....

[6] See JETSET notes 88-21, 89-03, 89-15, 89-20 and logbook Vol III pages 32 and ff.

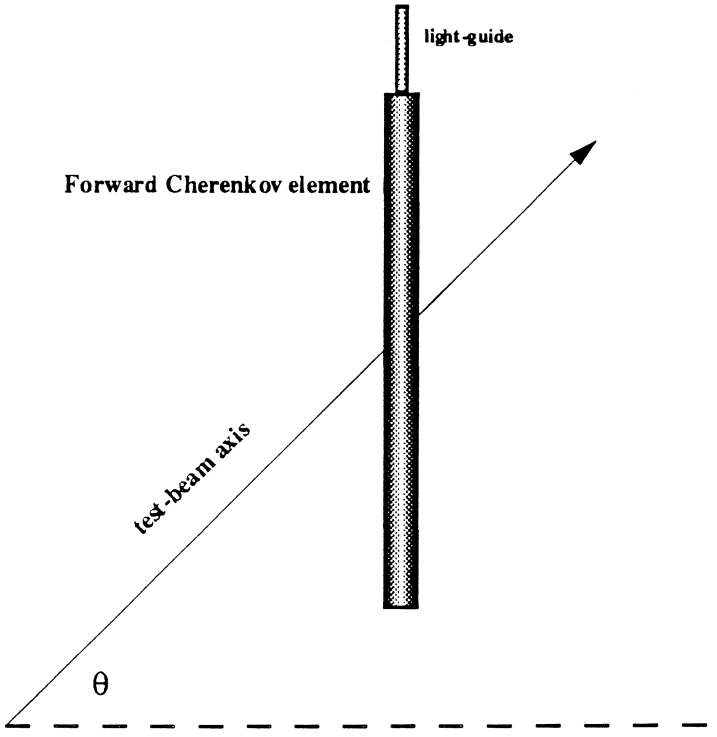

Fig. 3.1 Detector set-up for the measurement of the Cherenkov counter response at various incident angles (θ).

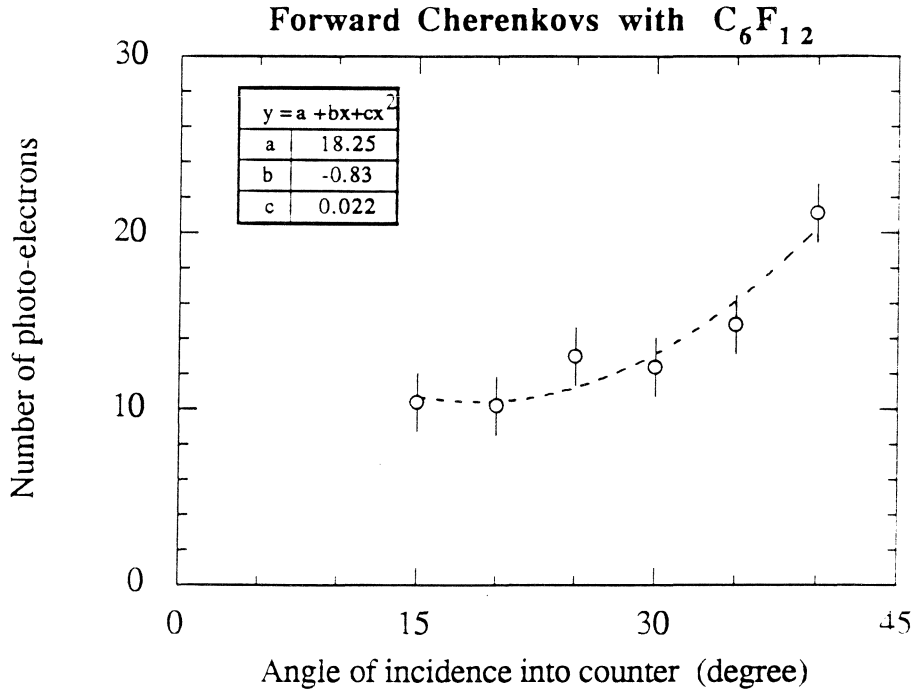

Fig. 3.2 Cherenkov counter response as a function of the incident angle. The dotted curve represents a second-order fit to the data. The variable x in the inset stands for the angle of incidence.

These calibration measurements indicated that in our detectors (in the same condition as in the experiment) the light-output resulting from the collection of Cherenkov radiation due to radiator and walls shape has the following empirical angular dependence:

$$f(\theta) = 18.25 - 0.83\,\theta + 0.022\,\theta^2.$$

The above should not be misunderstood for the behaviour of the Cherenkov-radiation emission which depends on the usual Cherenkov opening angle and which can be represented as a function of β by:

$$f(\beta) = \frac{1 - (\frac{\beta_x}{\beta})^2}{1 - \beta_x^2}$$

where $\beta_x = 1/n$ is the threshold-β (n is the index of refraction).

The light output and consequently the Cherenkov signal are proportional to the product of the above two functions.

The final expression must then be multiplied by a suitable normalisation factor to give the **expected** Cherenkov signal for a given track. In order to determine if the above functional dependence is correct and to determine the value of the normalisation factor we have dealt with each counter individually (there exist large variations between different elements because of variability of phototubes and reflectivities). For each counter we have divided the measured signal amplitude by the unnormalised expected amplitude and obtained individual normalisation factors.

In figs. 3.3 and 3.4 we show these results for two incident momenta: 2.0 and 1.9 GeV/c respectively. The blank spaces indicate that the data from the counter which should have appeared in that position were not available.

Notice that there had been a deliberate re-adjustment of the HV settings of all the photomultipliers between the April and July runs. Purpose of the operation was to reduce the photomultipliers gains by a factor of ≈ 2 to improve their resolution. The effect of this HV difference is clearly visible in the spectra, showing larger and wider normalisation values for the former setting.

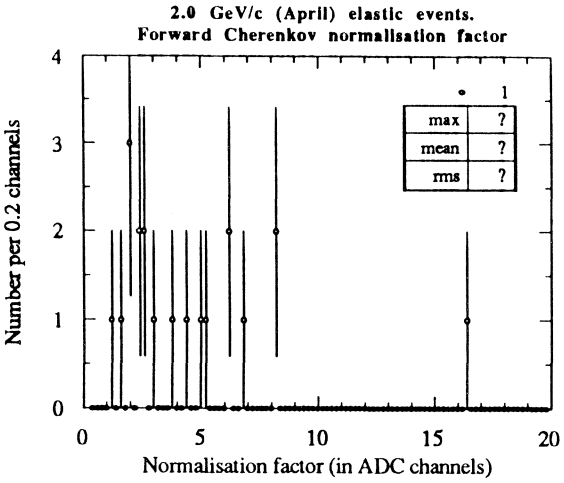

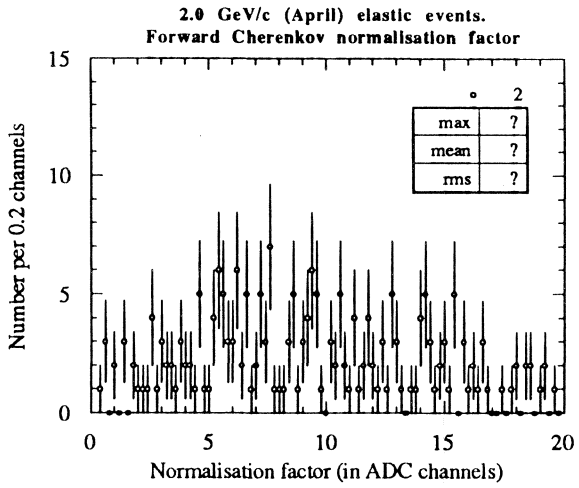

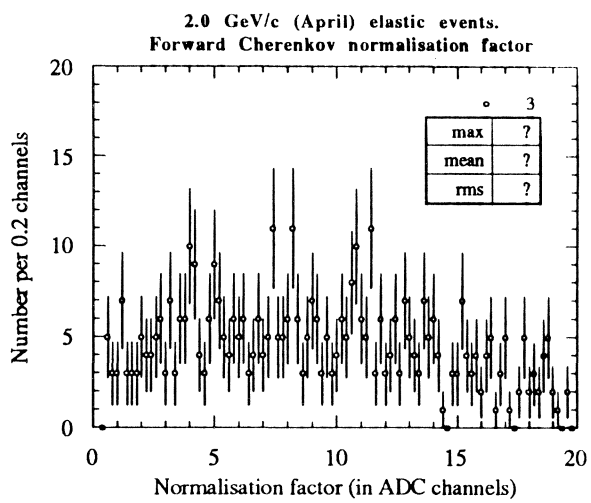

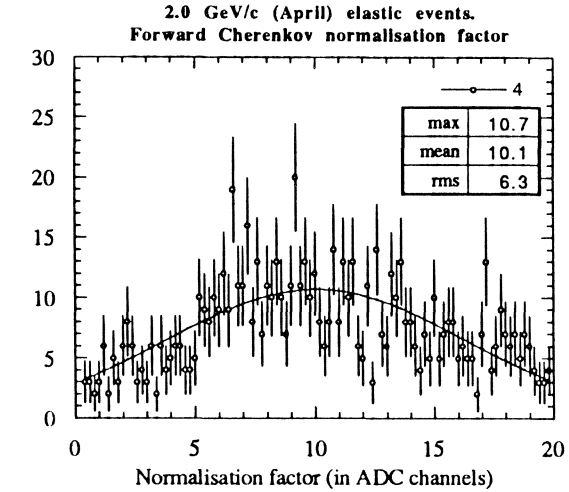

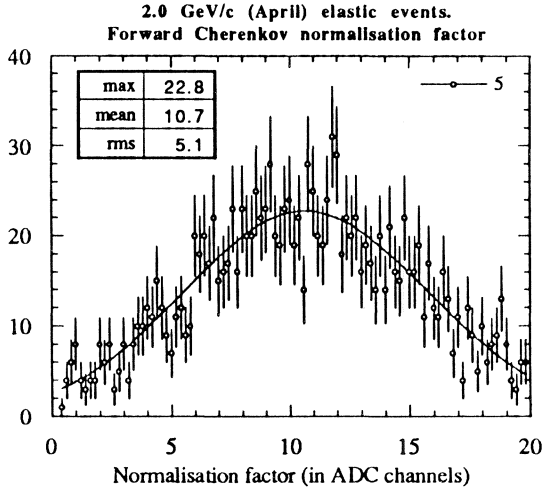

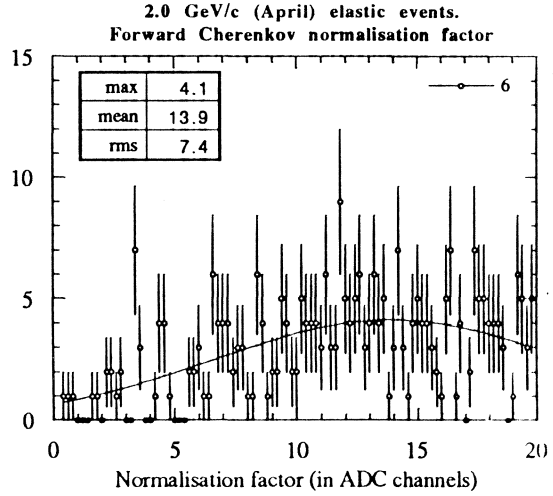

Fig. 3.3 a Incident momentum 2.0 GeV/c. Counters 1 - 6.

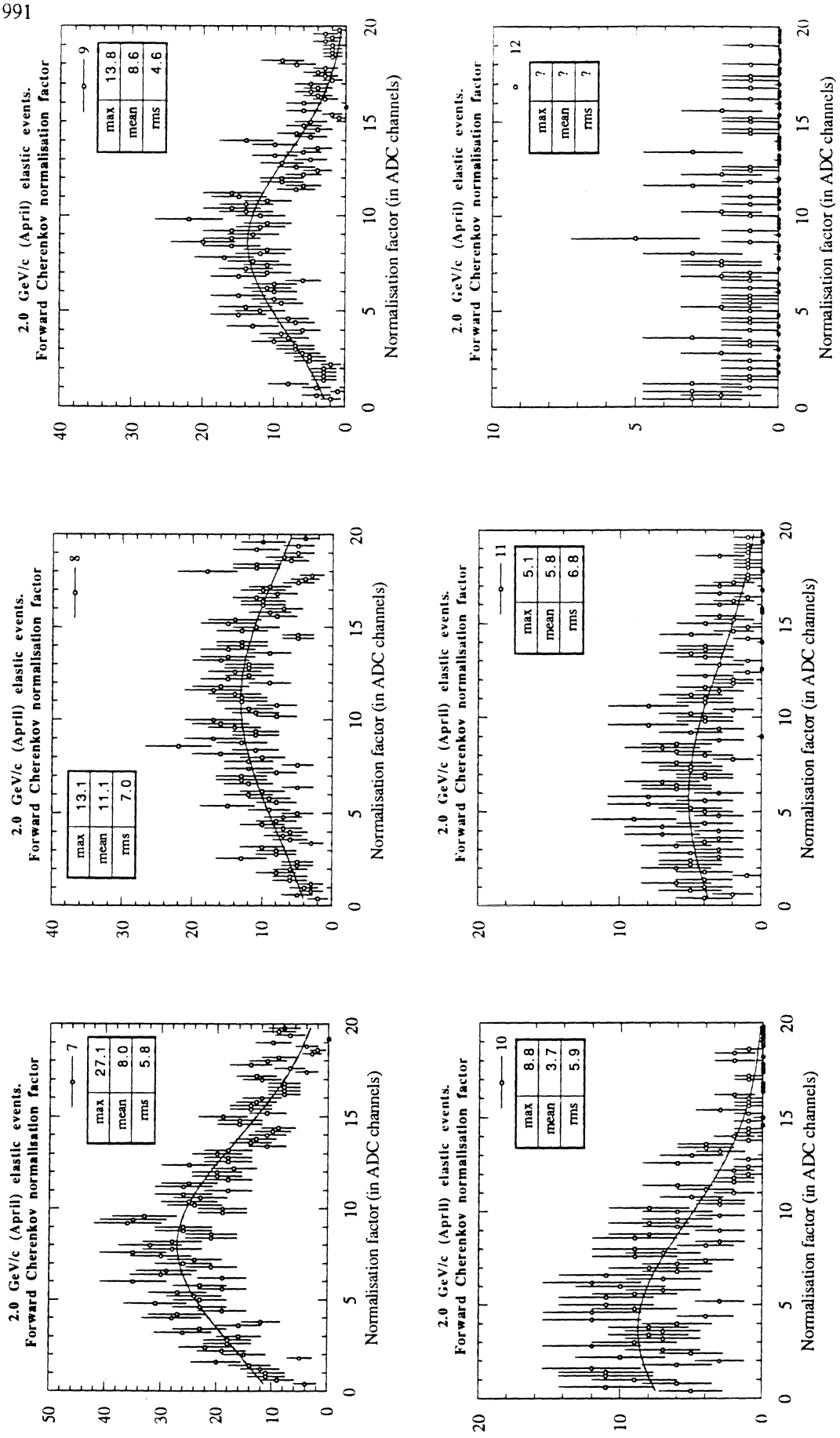

Fig. 3.3 b Incident momentum 2.0 GeV/c. Counters 7 - 12.

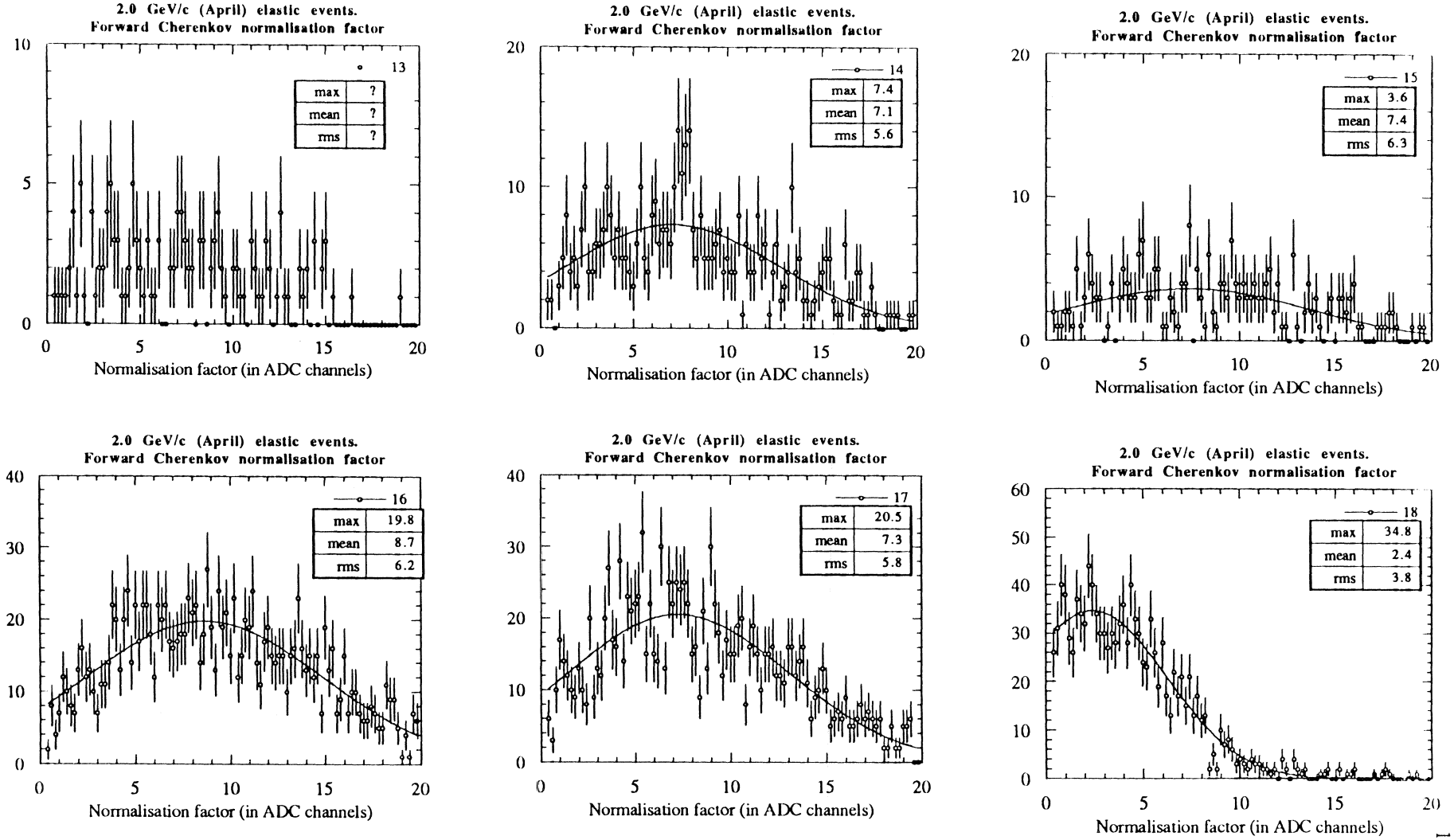

Fig. 3.3 c Incident momentum 2.0 GeV/c. Counters 13 - 18.

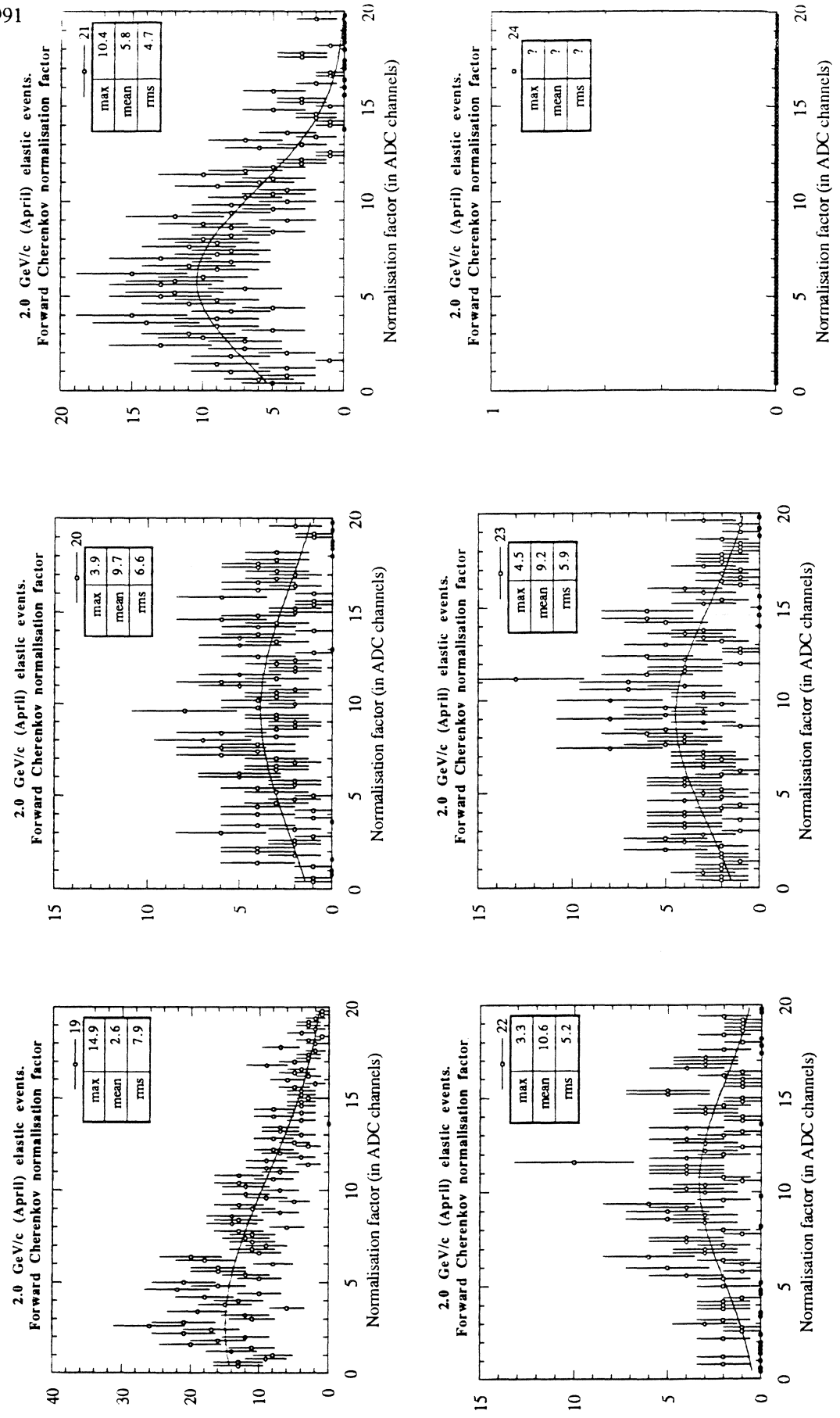

Fig. 3.3 d Incident momentum 2.0 GeV/c. Counters 19 - 24.

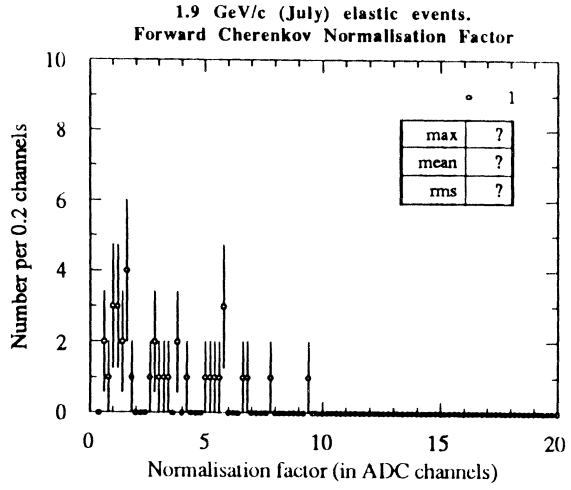

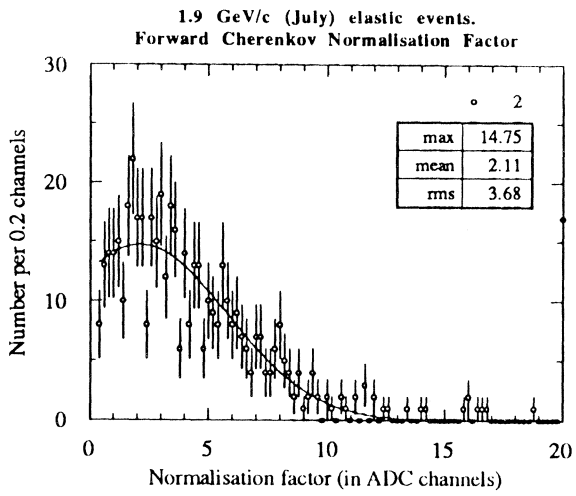

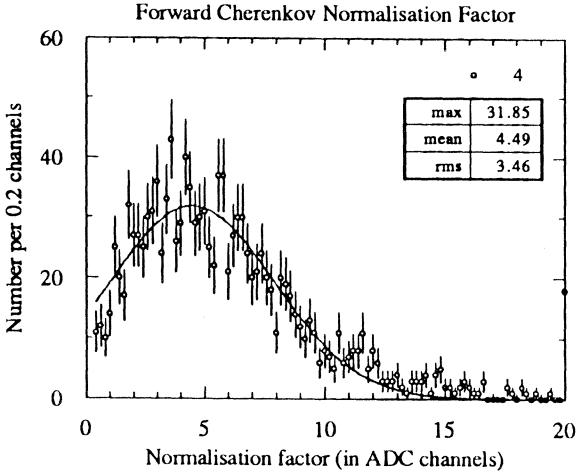

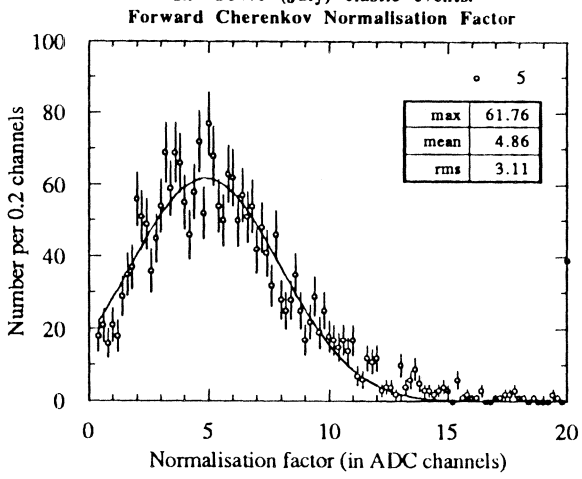

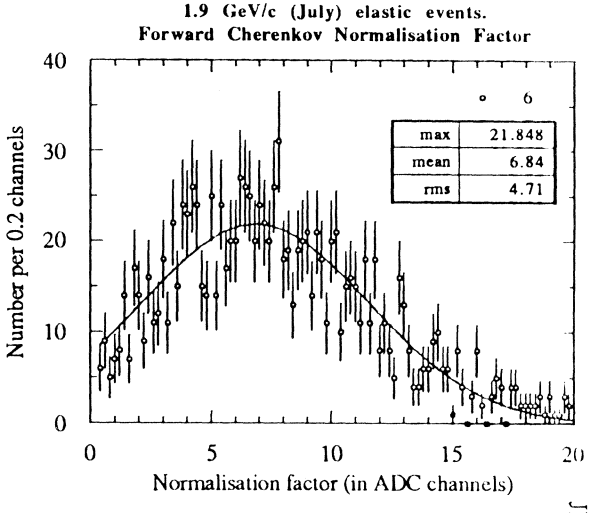

Fig. 3.4 a Incident momentum 1.9 GeV/c. Counters 1 - 6.

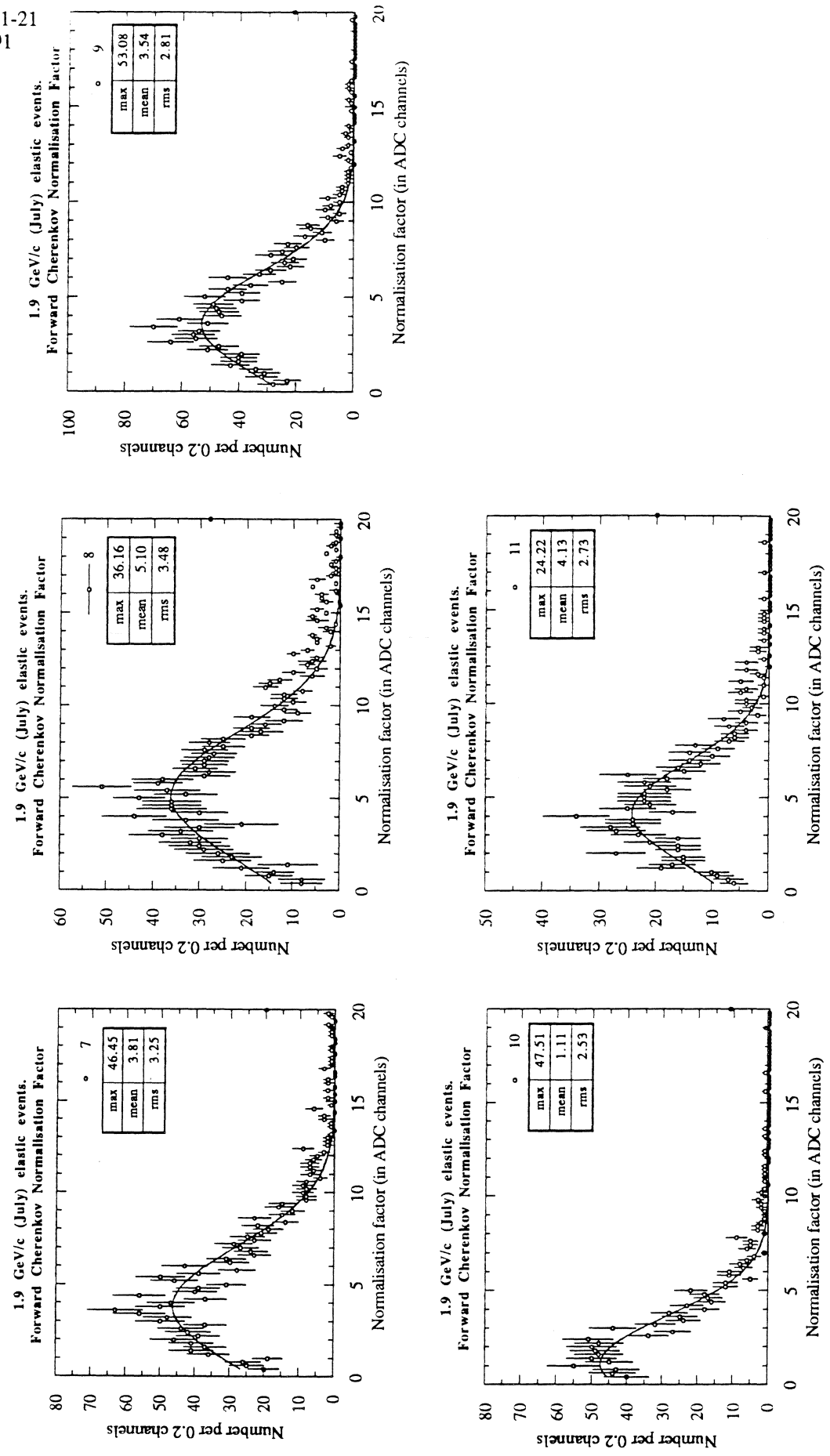

Fig. 3.4 b Incident momentum 1.9 GeV/c. Counters 7 - 12.

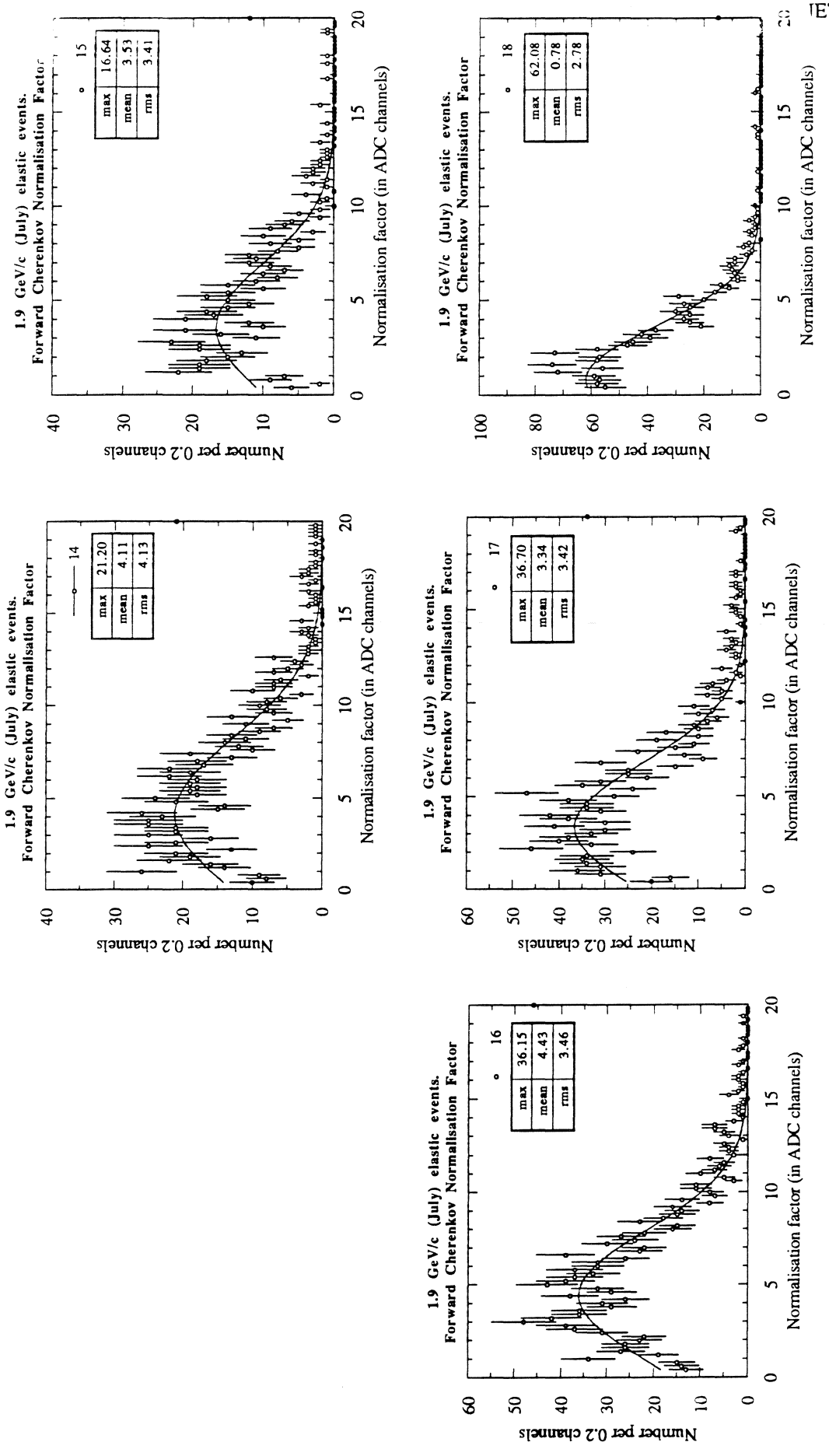

Fig. 3.4 c Incident momentum 1.9 GeV/c. Counters 13 - 18.

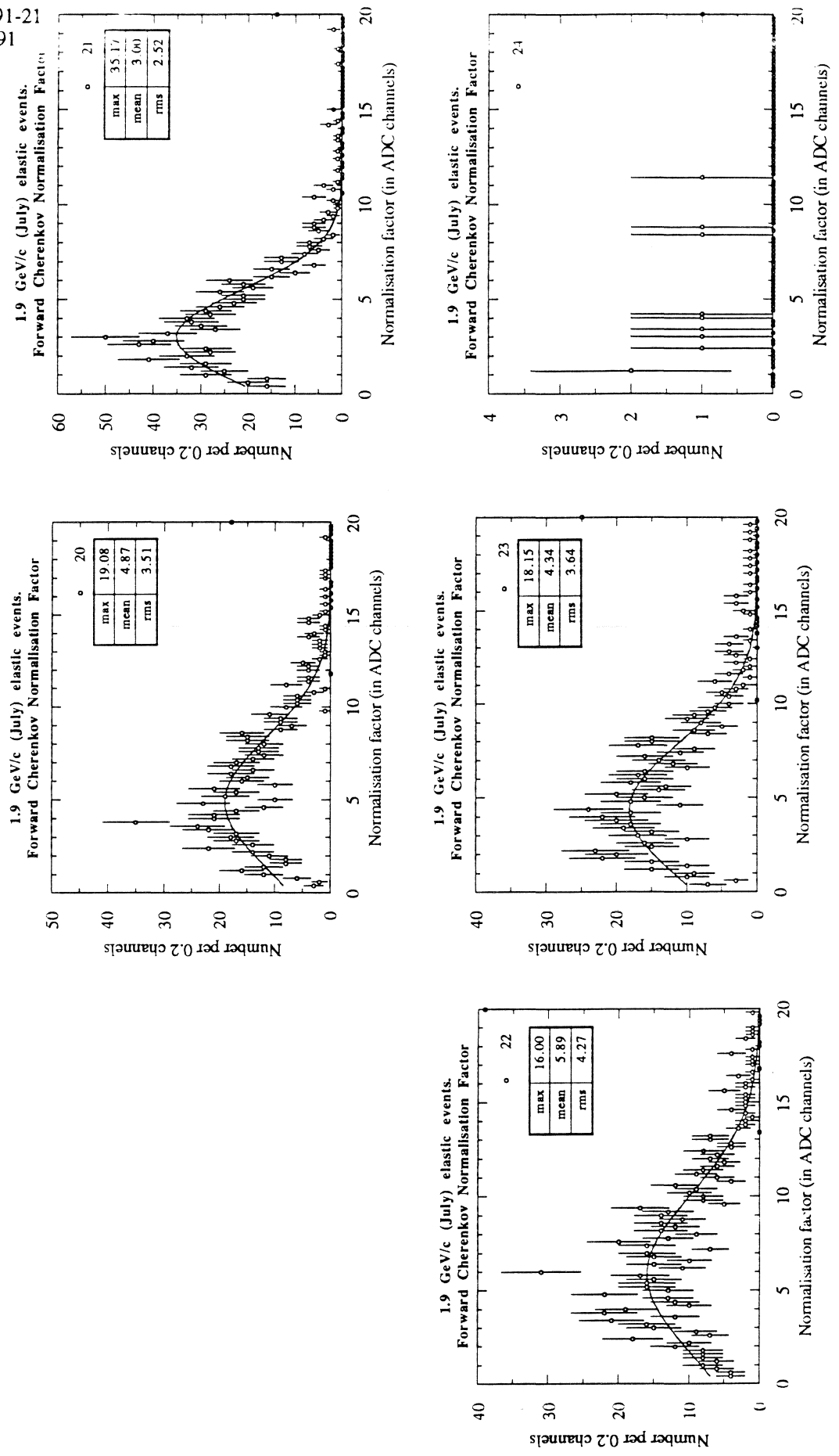

Fig. 3.4 d Incident momentum 1.9 GeV/c. Counters 19 - 24.

From the above individual spectra we have derived the shapes of the normalisation factors via simple Gaussian fits represented on these plots. The mean values and the corresponding rms have then been introduced in the expected-signal evaluation and an overall comparison has been made between measurements and expectations.

The differences between these quantities are shown in the plots of figs. 3.5 to 3.11. Notice that the entries refer to events where the scattered particles had values of β above threshold (obviously no results can be shown for those incident momenta where all the forward scattered particles were below threshold).

The first plots (figs. 3.5-3.7) are distinctly skewed and in very poor agreement with the Gaussian fit. The others look better but still show marked irregulartities here and there. These are due to differences between the spectra of the individual counters (some being much wider than others). We have checked that a **weighted** superposition (where each contribution is divided by the corresponding rms) gives rise to a much more regular distribution of this quantity. This has not been done systematically and we are able to present only the case at 1.9 GeV/c in fig. 3.12.

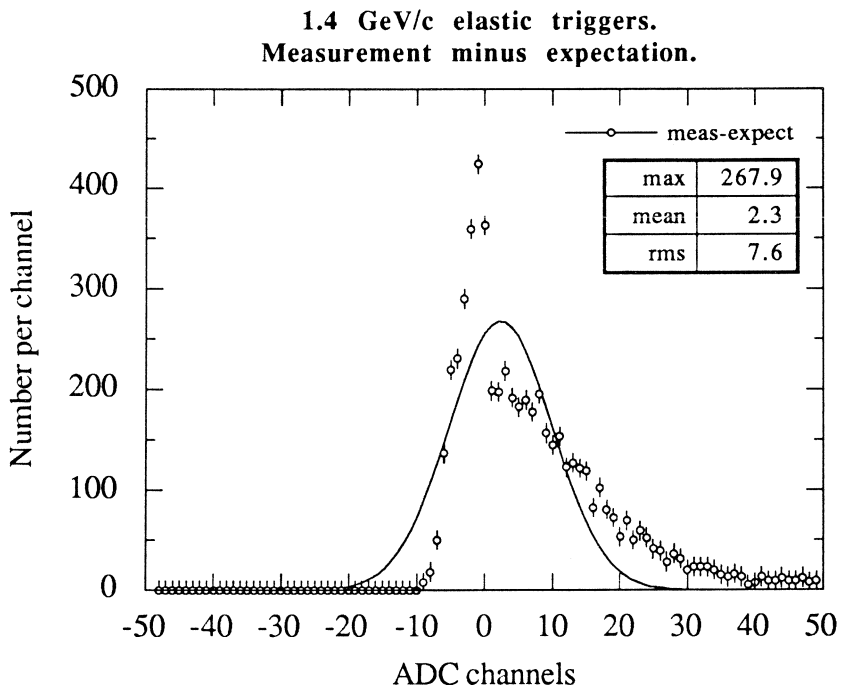

Fig. 3.5 Incident momentum 1.4 GeV/c.

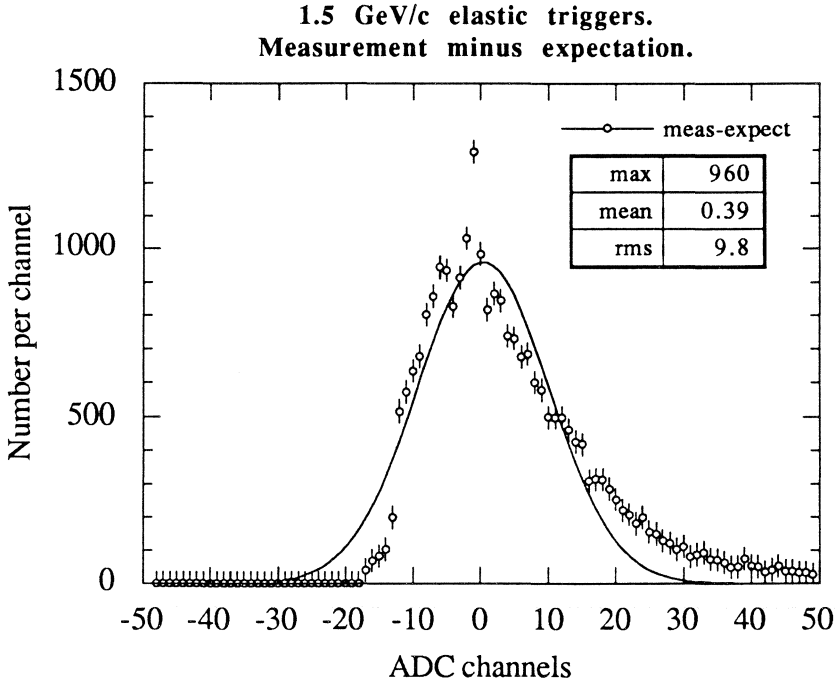

Fig. 3.6 Incident momentum 1.5 GeV/c.

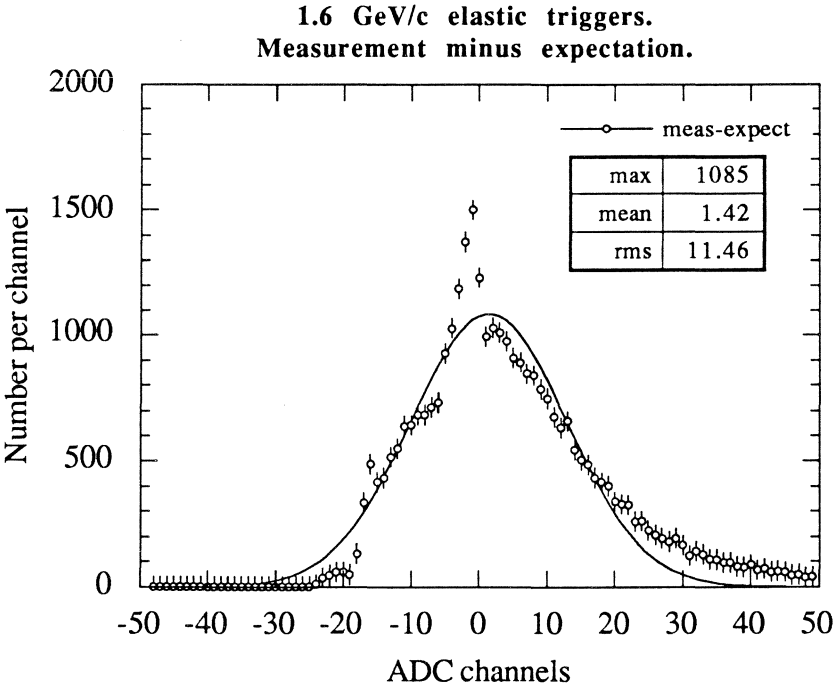

Fig. 3.7 Incident momentum 1.6 GeV/c.

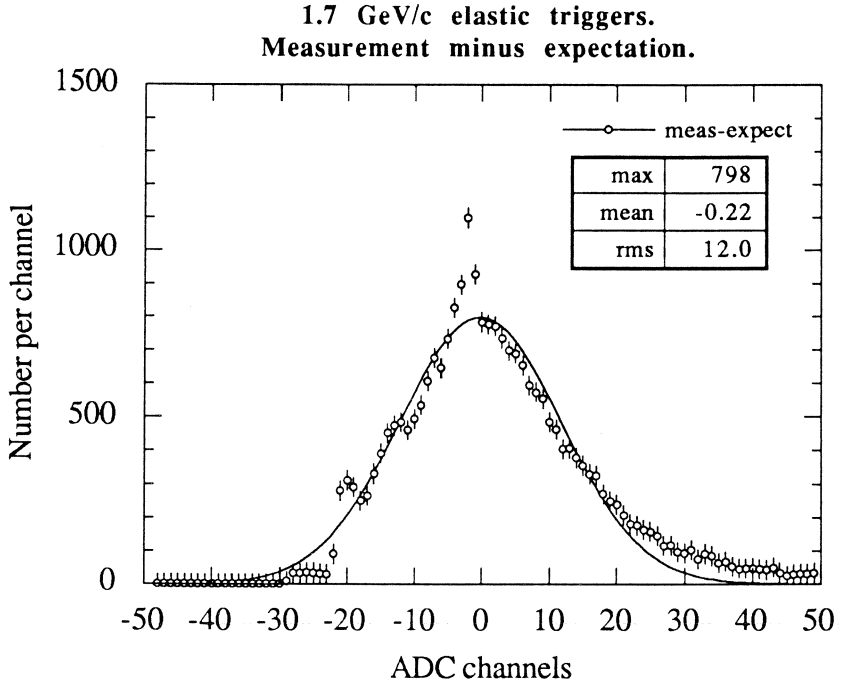

Fig. 3.8 Incident momentum 1.7 GeV/c.

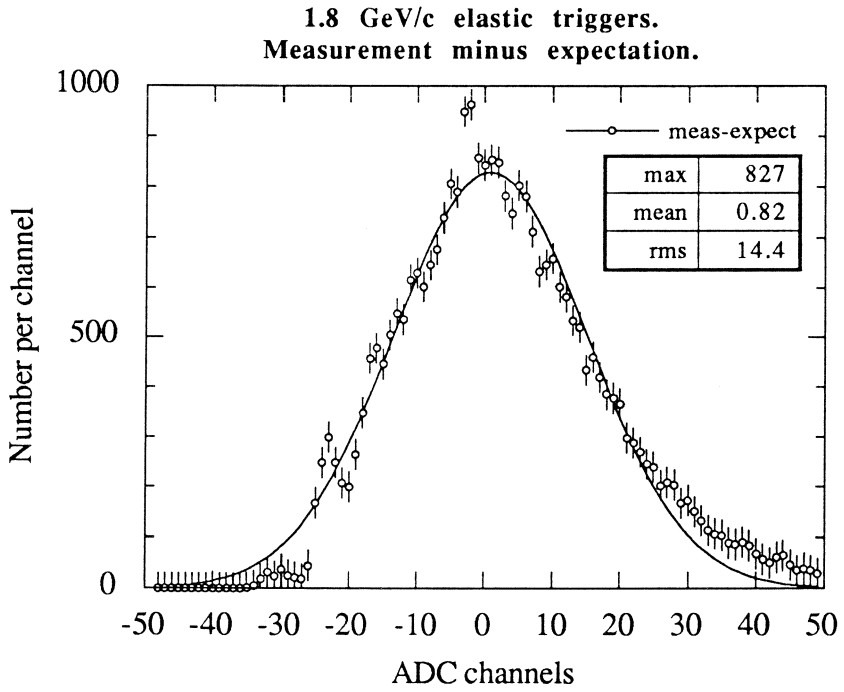

Fig. 3.9 Incident momentum 1.8 GeV/c.

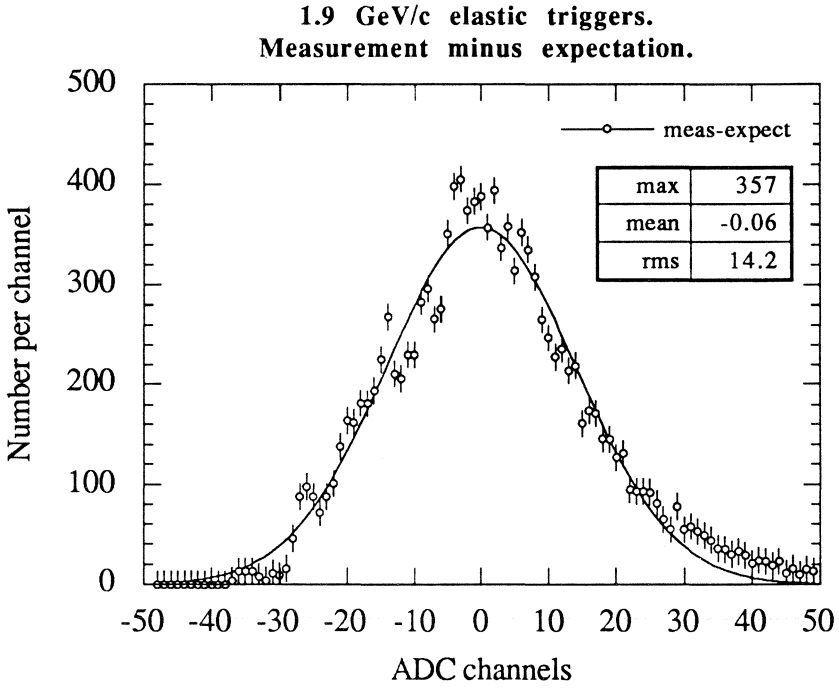

Fig. 3.10 Incident momentum 1.9 GeV/c.

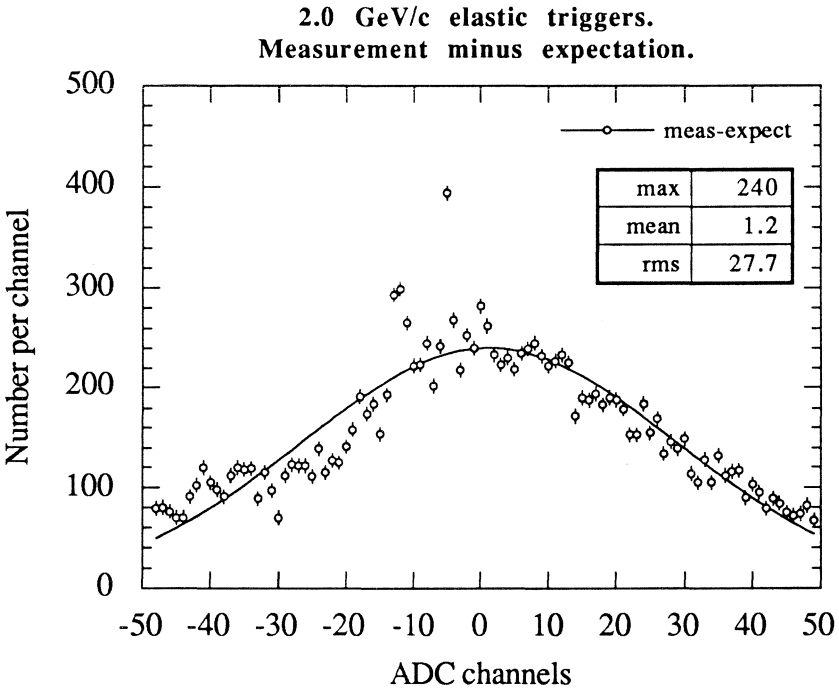

Fig. 3.11 Incident momentum 2.0 GeV/c.

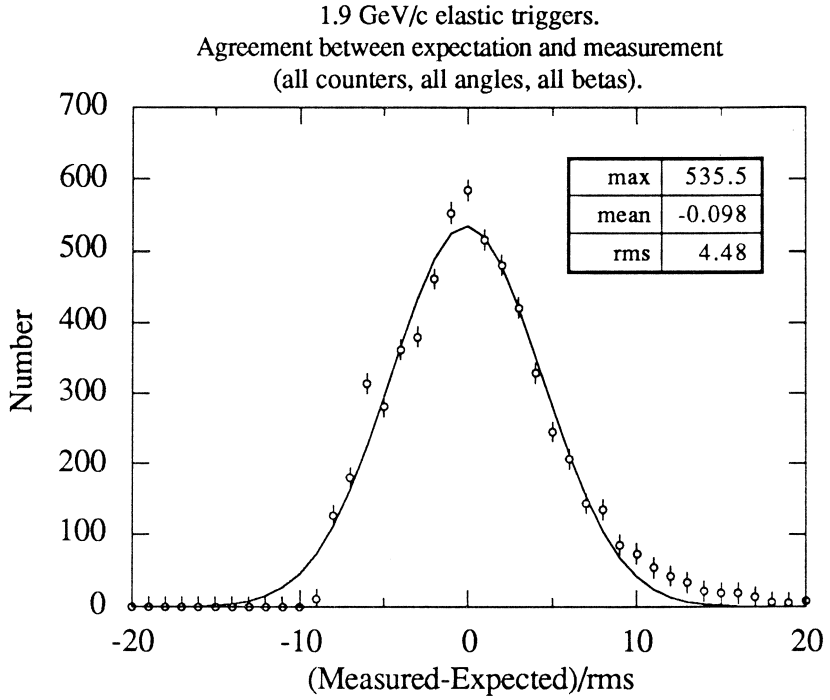

Fig. 3.12 Distribution at 1.9 GeV/c of the measured-minus-expected signal divided by the rms of the individual counters.

One more control over the correct handling of the data comes from what we have labelled as "probability distributions" in figs. 3.13 to 3.19. For each event we have calculated the chi-square of the forward track using the *Cherenkov* "measurement" and the expectation (i.e. the value of β determined via kinematics). From these we have calculated and plotted the **confidence level** of the events.

Please ignore the dotted curves on all these graphs (they were meant to show a combined *Cherenkov&Silicon* probability but unfortunately something went wrong and it is too late now to recalculate the quantity correctly).

One expects a uniform distribution of the data in these plots. What we see is something reasonably uniform apart from the peak at 0 which is probably due to wrong events or wrong detector response. From the width of this peak we guess that the measurement errors used in this calculation are somewhat underestimated.

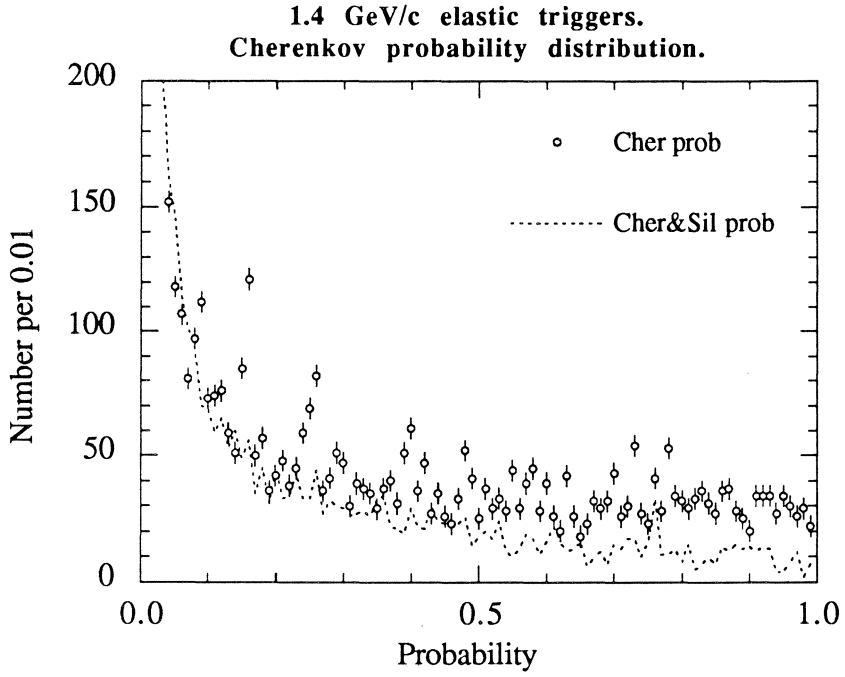

Fig. 3.13 Incident momentum 1.4 GeV/c.

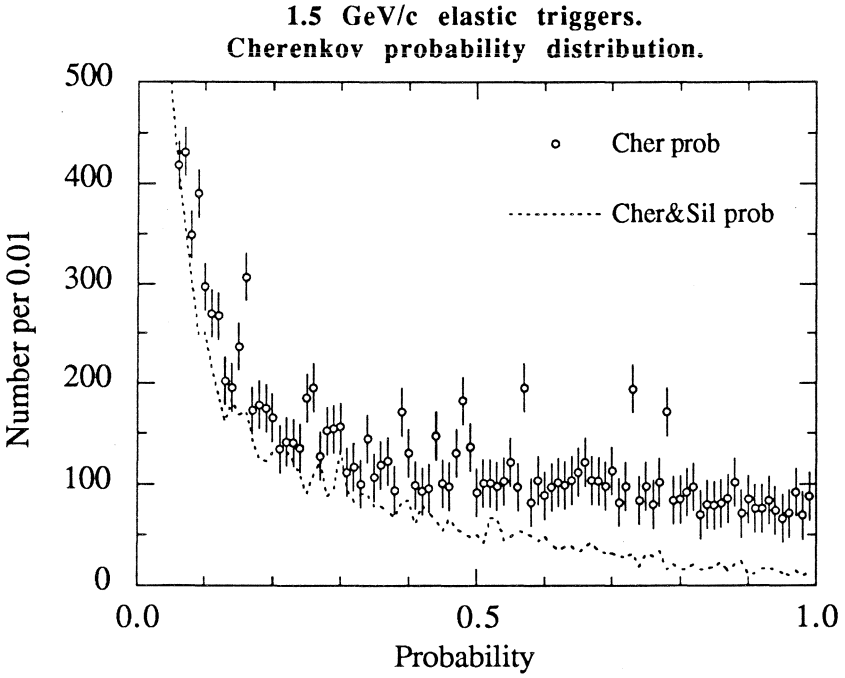

Fig. 3.14 Incident momentum 1.5 GeV/c.

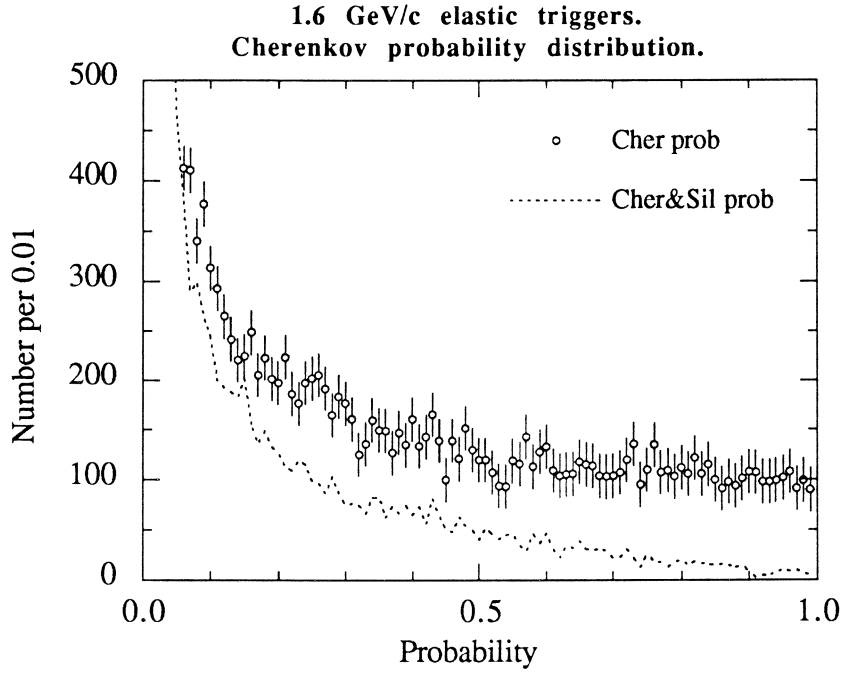

Fig. 3.15 Incident momentum 1.6 GeV/c.

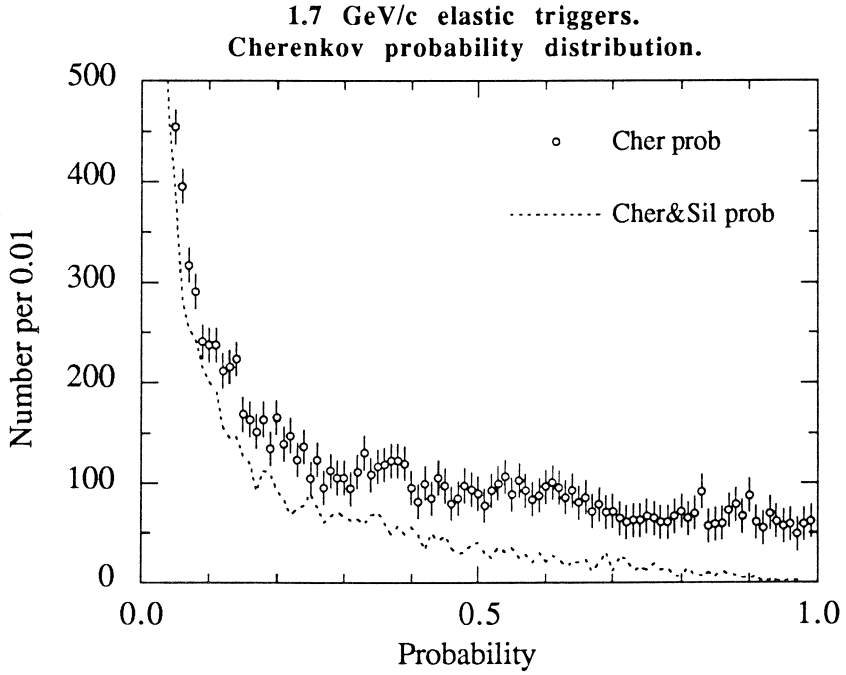

Fig. 3.16 Incident momentum 1.7 GeV/c.

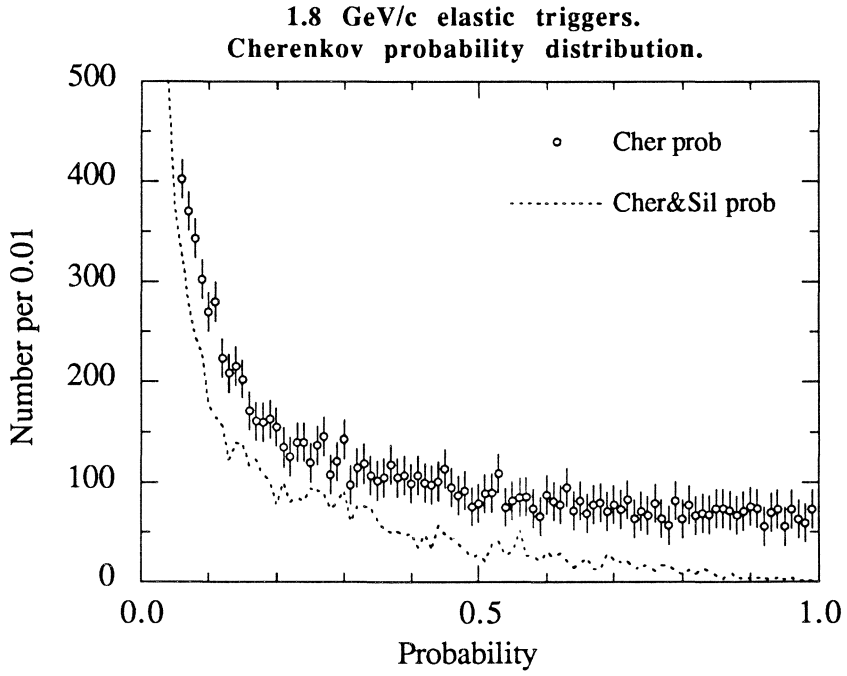

Fig. 3.17 Incident momentum 1.8 GeV/c.

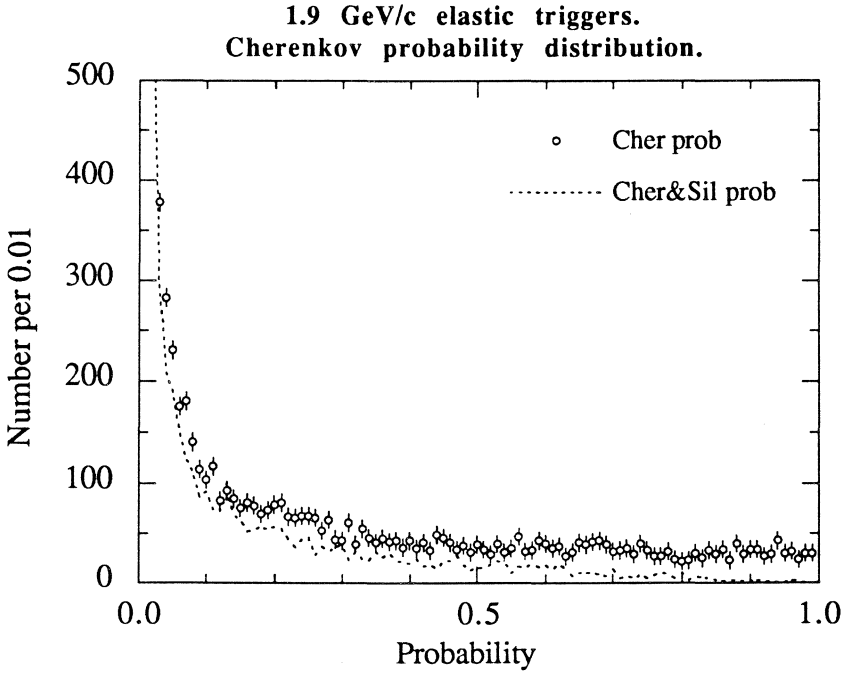

Fig. 3.18 Incident momentum 1.9 GeV/c.

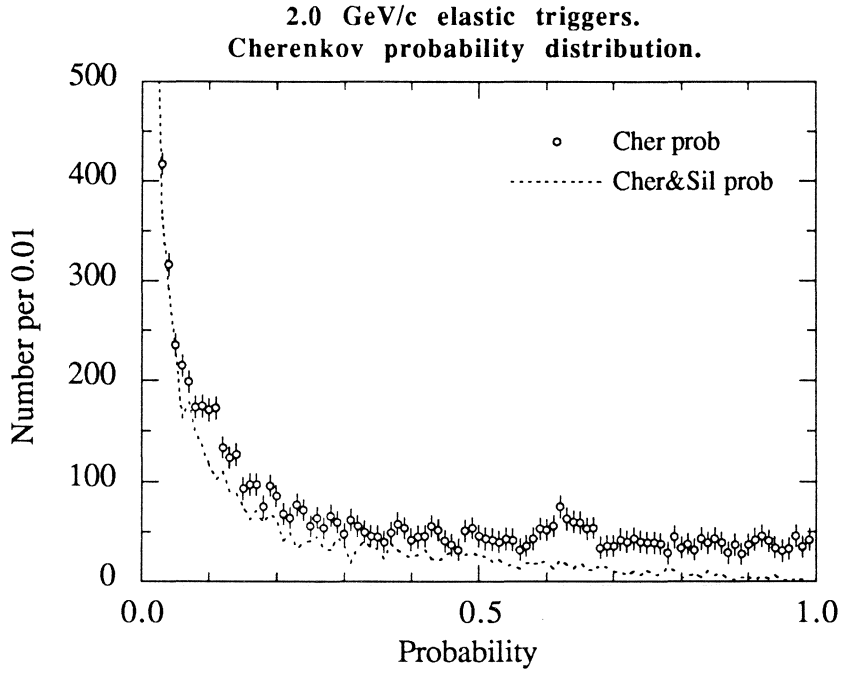

Fig. 3.19 Incident momentum 2.0 GeV/c.

A further check on the correctness of the above results was obtained by performing (only at one momentum: 1.9 GeV/c) an elaborate "maximum likelihood" type of analysis over the individual events. In this procedure we have allowed the coefficients in the $f(\theta)$ expression given above to describe the detector response as a function of the particle angle to vary so as to agree as well as possible with the data. The normalisation factor of each counter was left free to adjust itself as well as it could. Three different estimates of the normalisation factors were obtained. The essential result of the fit is contained in the figure appearing on the frontispiece where we have represented with a graded colour-scale a "chi-square"[7] level as a function of the b- and c-coefficients in $f(\theta)$. The point of maximum probability corresponds to the position of the darkest patch; the "chi-square" decrease over the surrounding blank level is of 41.3.

The coefficients thus found are almost indistinguishable from those obtained from the data of fig. 3.2. This can also be seen in fig. 3.20 which shows very little difference between the calculated and fitted curves giving the number of photoelectrons calculated with the two procedures.

[7] We have not introduced a variance in the calculation, so the "chisquare" mentioned above is simply a quantity proportional to the latter.

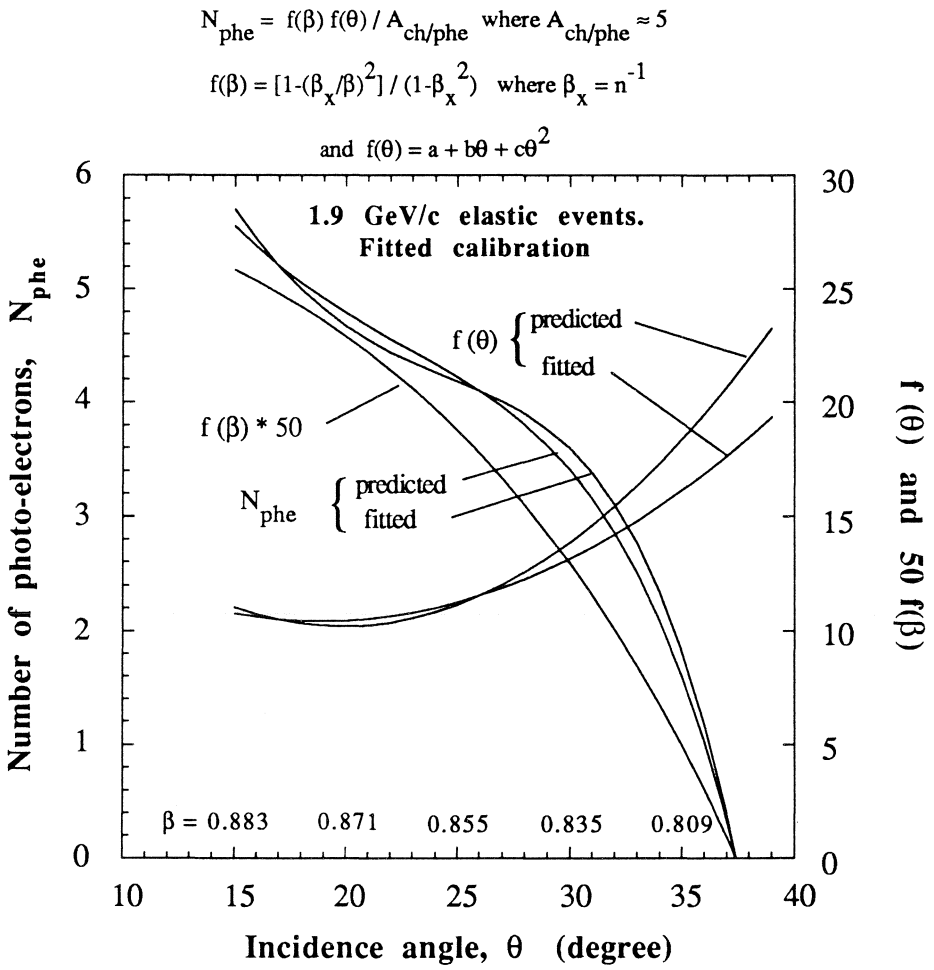

Fig. 3.20 Comparison between fitted and measured expectations at 1.9 GeV/c.

The final expression adopted for the expected Cherenkov signal is the formula given on page 21 multiplied by the normalisation factors listed below in Table 2. Here we also give the values of the pedestals and the rms of the distributions. Notice that this recipe is meant to supersede the earlier formulation given in the note describing the 4K analysis[8].

Table 2

Pedestals of the Forward Cherenkovs (1 to 24) :
21, 2,27,29,22,30,23,27,23,35,28,29,20,17,20,16,18, 8,16,21,22,21,19,19
Add 3 channels to these pedestals to make sure you are above pedestal.

Normalisation factors:

first set = April 1991 data
1.00,1.00,1.00,10.1,10.7,13.9,8.0,11.1,8.6,3.7,5.8,1.00
1.00,7.1,7.4,8.7,7.3,2.4,2.6,9.7,5.8,10.6,9.2,1.00
second set = July 1991 data
1.00,2.11,1.00,4.49,4.86,6.84,3.81,5.10,3.54,1.11,4.13,1.00
1.00,4.11,3.53,4.43,3.34,0.78,1.00,4.87,3.00,5.89,4.34,1.00

---

rms values of the normalisation factors :
first set = April 1991 data
10.00,10.00,10.00,6.3,5.1,7.4,5.8,7.0,4.6,5.9,6.8,10.00
10.00,5.6,6.3,6.2,5.8,3.8,7.9,6.6,4.7,5.2,5.9,10.00,
second set = July 1991 data
10.00,3.68,10.00,3.46,3.11,4.71,3.25,3.48,2.81,2.53,2.73,10.00
10.00,4.13,3.41,3.46,3.42,2.78,10.00,3.51,2.52,4.27,3.64,10.00

Other results which are also worth presenting are those concerning the Cherenkov **inefficiency**, summarised in fig. 3.21. This figure shows, as a function of the track's angle of incidence, the measured inefficiencies (i.e. the fraction of zero-signal events over the total when the particle's β was above threshold). We observe a 10 to 20% inefficiency level at low angles increasing to $\approx$30% at the largest angles. On the same figure we show an estimate of the *geometrical inefficiency* expected from the separation between counters (i.e. dead space). In view of the pie-shaped configuration of the elements the amount of dead space relative to sensitive space decreases when the angle increases. An evaluation of the various pieces of material between elements suggests that there are at least 3 mm separating the sensitive regions of two adjacent elements. This value gives the curve labelled "*geom.ineff.*" on the plot.

On the other hand, because we are dealing with elastic scatterings, there is a well defined β-dependence of the scattering angle; along the abscissa we have indicated values of β corresponding to certain angles. Now, for a given value of β we expect a Poisson distribution

[8] Jetset note 91-11

in the number of photo-electrons; from this we can estimate the zero-photoelectron fraction, viz. the inefficiency. This is the curve labelled "*Poisson ineff.*" on the plot. The right-hand scale shows the number of photo-electrons expected at each angle. The combined inefficiency of the losses due to geometrical and photo-electron-statistics is shown by the solid curve. Clearly the inefficiency should become 100% below threshold (vertical line). The fact that this is not the case is simply a reflection of the existence of background noise in the counters due to many sources such as scintillation effects, light emission in the plexiglass walls, secondary interactions, δ-rays, etc. The fact that this background is more noticeable at these angles than elsewhere is probably related to the larger area of counter exposed at large angles (don't forget the pie-shape of the elements !). Notice that the inefficiency measurements which refer to β above threshold agree surprisingly well with the predictions of the naive model described above.

In conclusion, we feel reasonably satisfied with the performance of these counters. They certainly perform as desired from the "threshold-counter" point of view. From what we have seen above it seems that we can also use them as rough estimators of β, not a mean feat for a cheap set of unsophisticated counters.

Of course, if they hadn't leaked we would have been even more happy.....

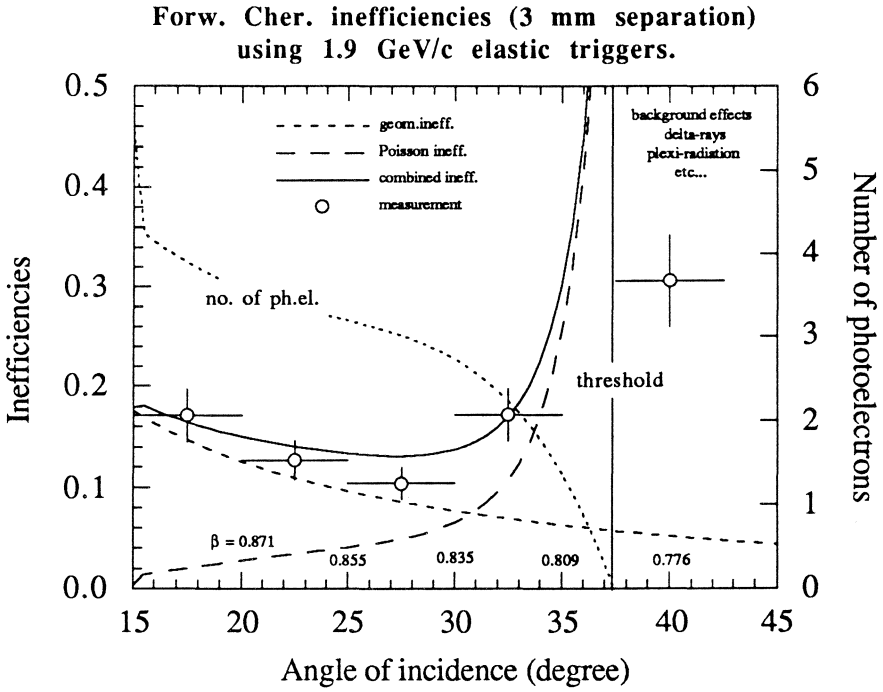

Fig. 3.21 Cherenkov inefficiency at 1.9 GeV/c.

4. SILICON RESPONSE

While analysing the detector for which we feel more directly responsible we have also been able with little extra effort to inspect the behaviour of the *Silicon* counters. In fact, for each track examined in the course of the Cherenkov study we also automatically read out the *Silicon* measurement and can compare it with the expectation value based on the energy loss in the 300 μm of the silicon thickness.

The analysis has followed the same lines as for the *Cherenkovs*. We have used the same events and selected among them the tracks associated to one or two Silicon hits. The background of wrong-hits has been rejected following the recipe provided by Maurizio a few months ago.

In fig. 4.1 we show, as a typical example, the **multiplicity** distribution at 1.8 GeV/c. The number of hits per event appears to be more or less uniformly distributed between 0 and 40 (the latter being the maximum number of hits considered in our analysis). This distribution is somewhat disconcerting in view of what is expected from a single track in the forward direction. Why does it look like this and what should be done to avoid this behaviour is a series of questions which we gladly leave to others for an answer.

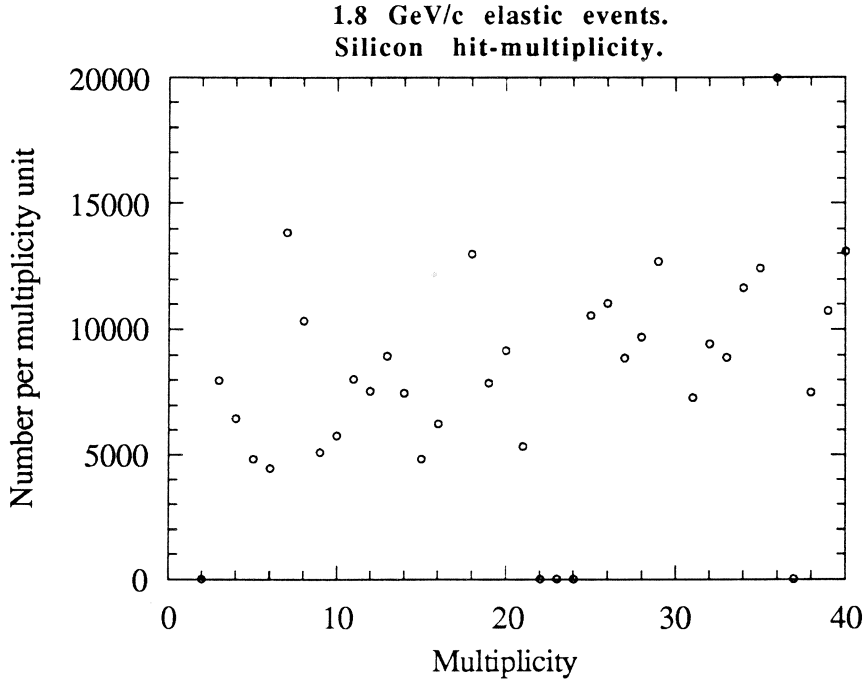

Fig. 4.1 Silicon multiplicity distribution at an incident momentum of 1.8 GeV/c.

The **correlation** between silicon-pads and tracks appears on figs. 4.2 to 4.11. Here we see the azimuth and polar angle differences between track and closest silicon element. The general agreement looks quite good.

The apparent larger width of the azimuthal as compared to the polar distributions is due to the difference between solid angle acceptance of the Silicon pads in the vertical and horizontal planes; we have not studied this effect in more detail. Notice a common feature of the polar distributions: there is a slight skewness for large angle-differences. Here again we have no ready explanation for the phenomenon.

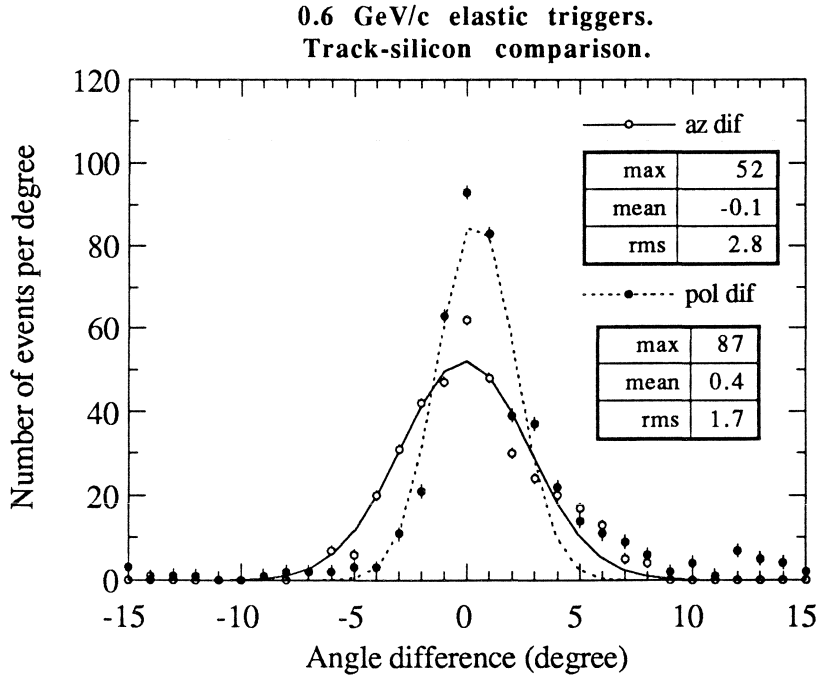

Fig. 4.2 Incident momentum 0.6 GeV/c.

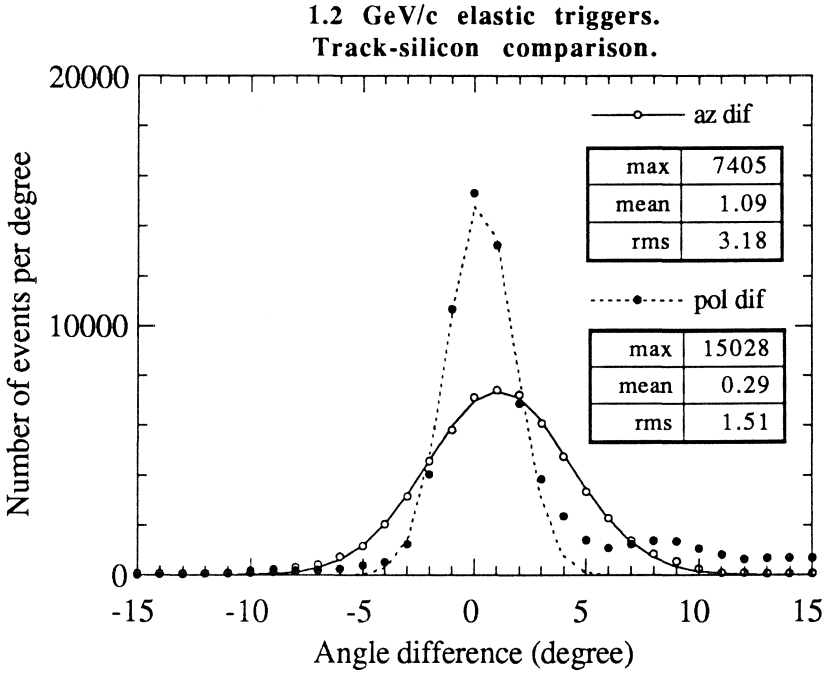

Fig. 4.3 Incident momentum 1.2 GeV/c.

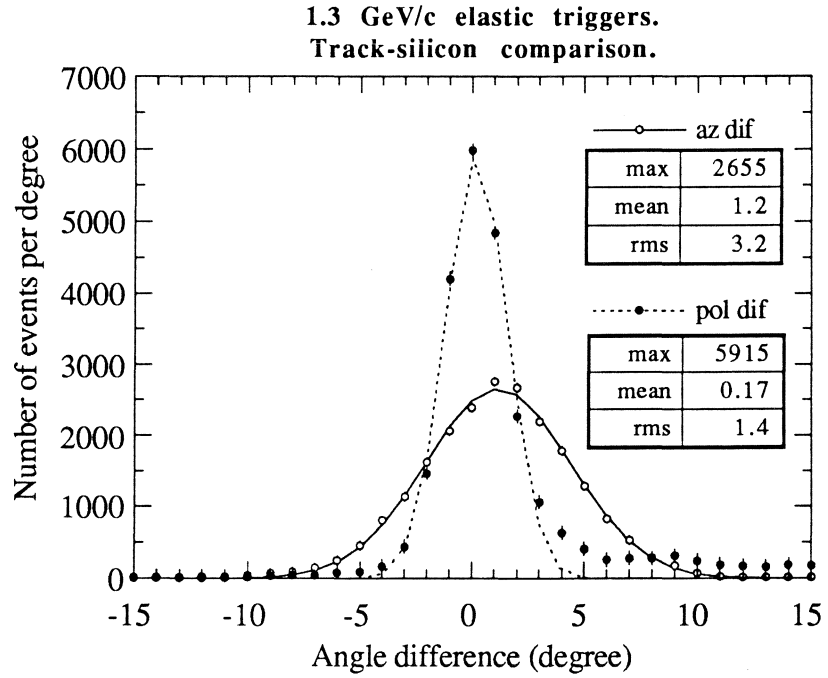

Fig. 4. 4 Incident momentum 1.3 GeV/c.

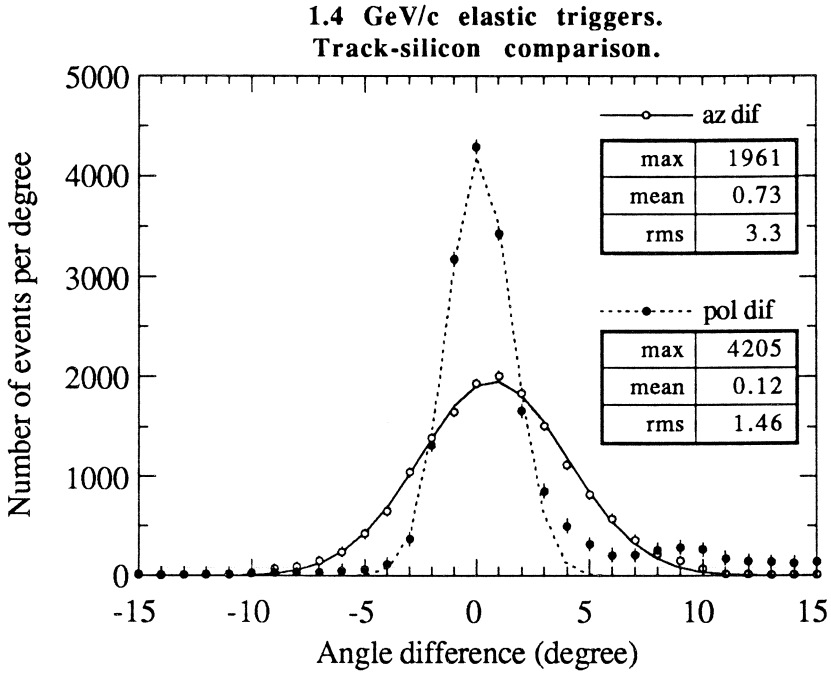

Fig. 4.5 Incident momentum 1.4 GeV/c.
Azimuth and polar angle differences between track and closest silicon element.

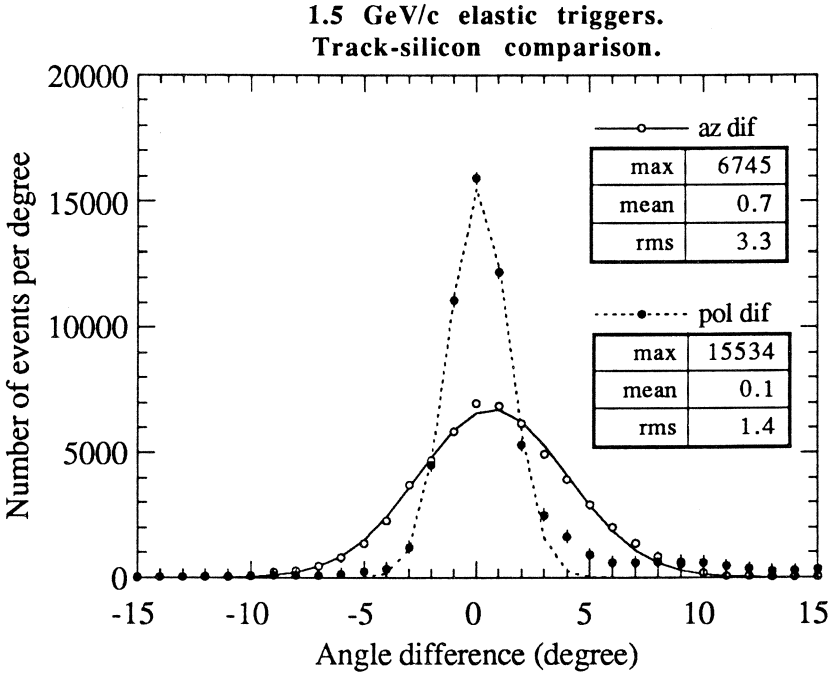

Fig. 4.6 Incident momentum 1.5 GeV/c.

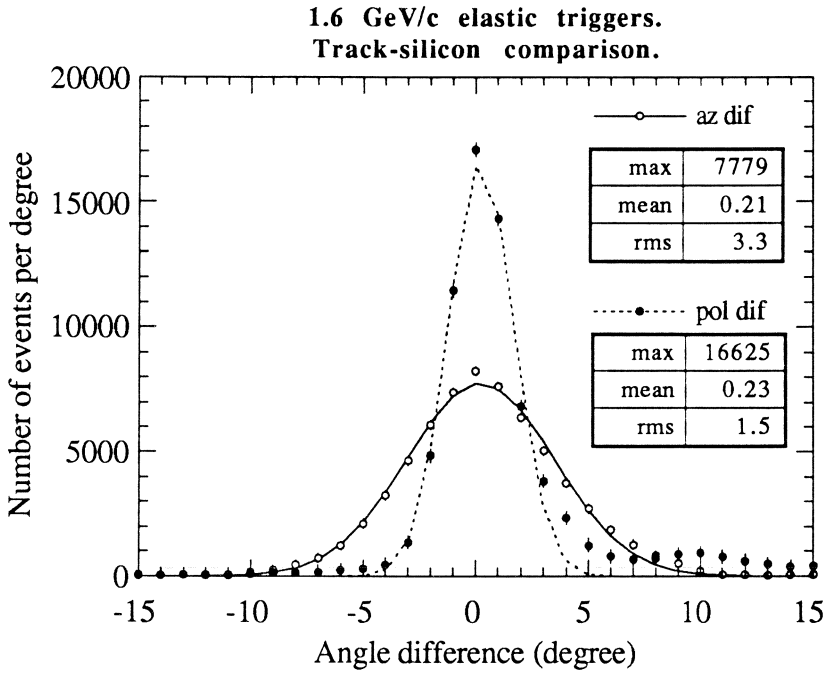

Fig. 4.7 Incident momentum 1.6 GeV/c.

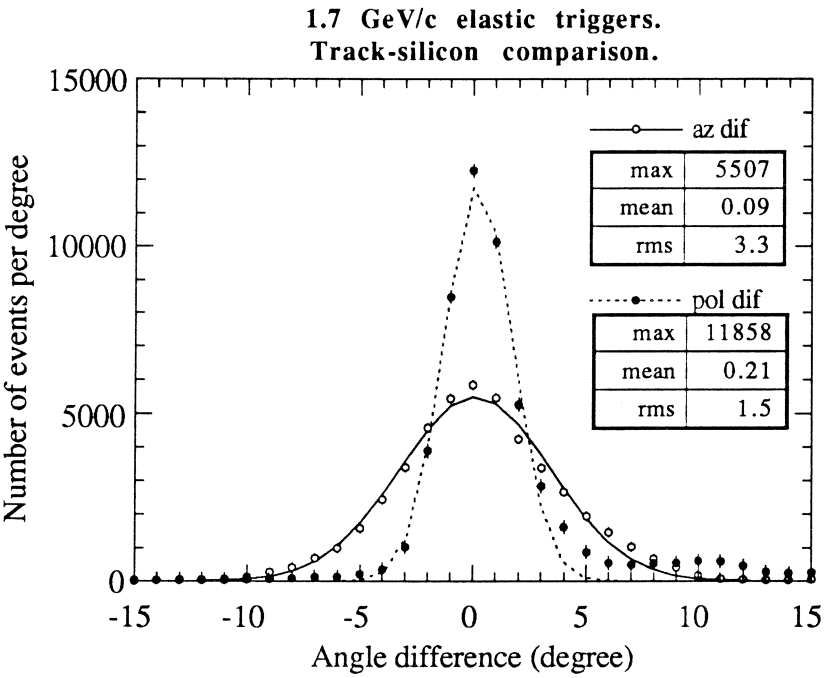

Fig. 4.8 Incident momentum 1.7 GeV/c.

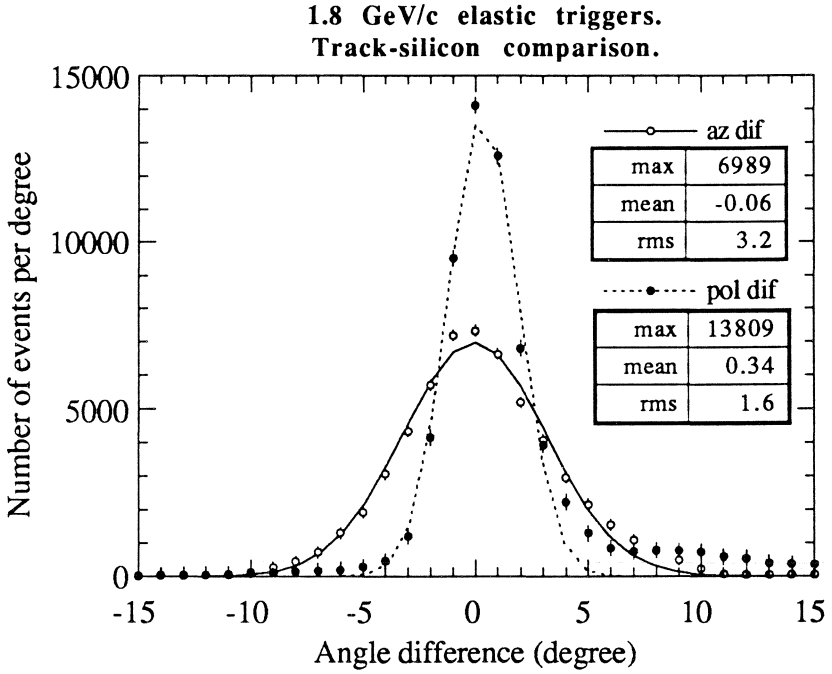

Fig. 4.9 Incident momentum 1.8 GeV/c.

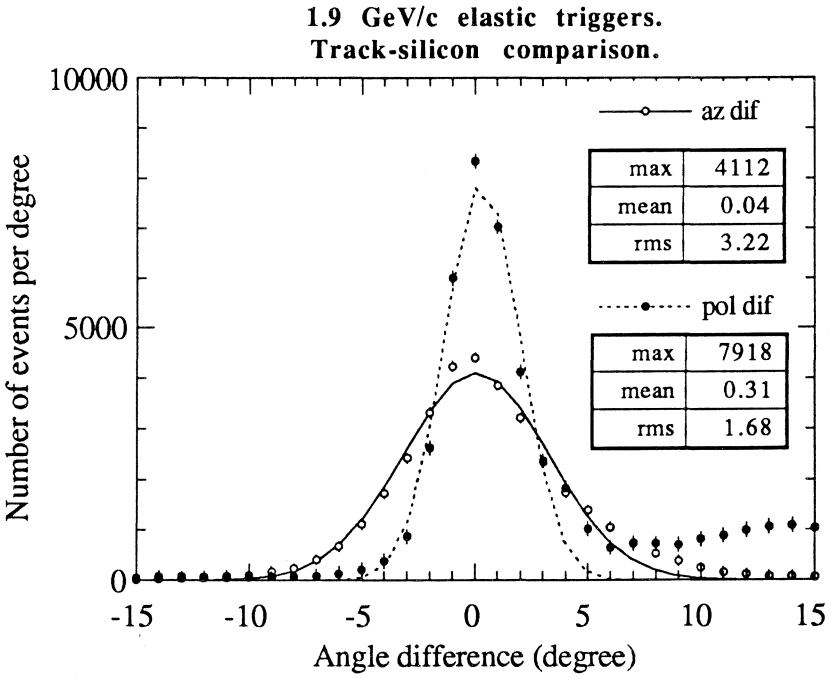

Fig. 4.10 Incident momentum 1.9 GeV/c.

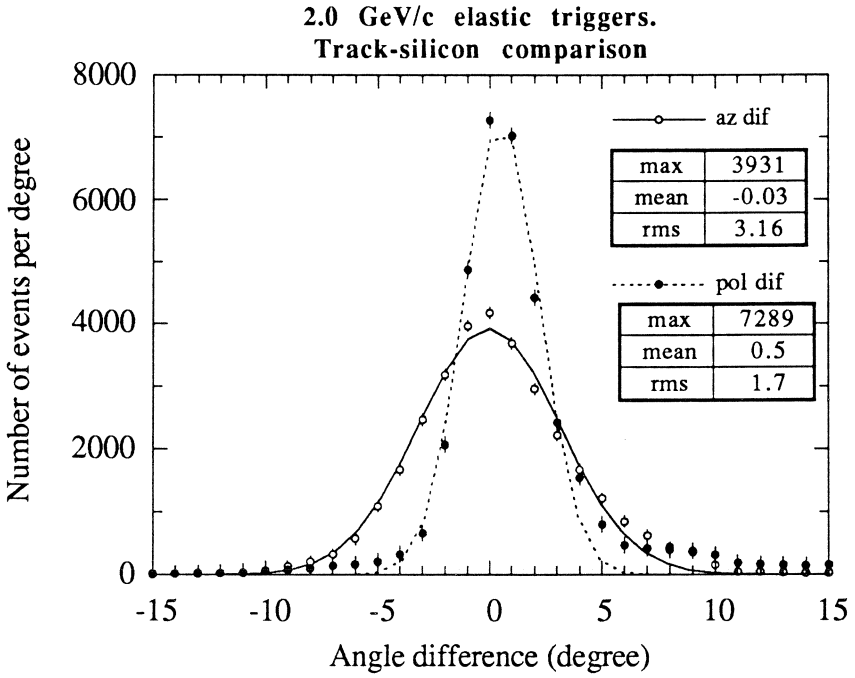

Fig. 4.11 Incident momentum 2.0 GeV/c.

The β distributions of the particles traversing the silicon are shown in figs. 4.12 to 4.21. These are the same which allow our Cherenkov study. It so happens that over most of the momentum region explored the values of β are very close to those giving the *minimum ionising* response. This is good for the Cherenkov but not so good for the Silicon.

It goes without saying that out of these data we cannot hope to learn much about the behaviour of the detector in the sensitive low-energy region where it really matters. This region is unfortunately reacheable only by the data at 0.6 GeV/c where we have already mentioned (and shown on Table 1) that track reconstruction — or else — reduces the statistics of useful events to an insignificant level.

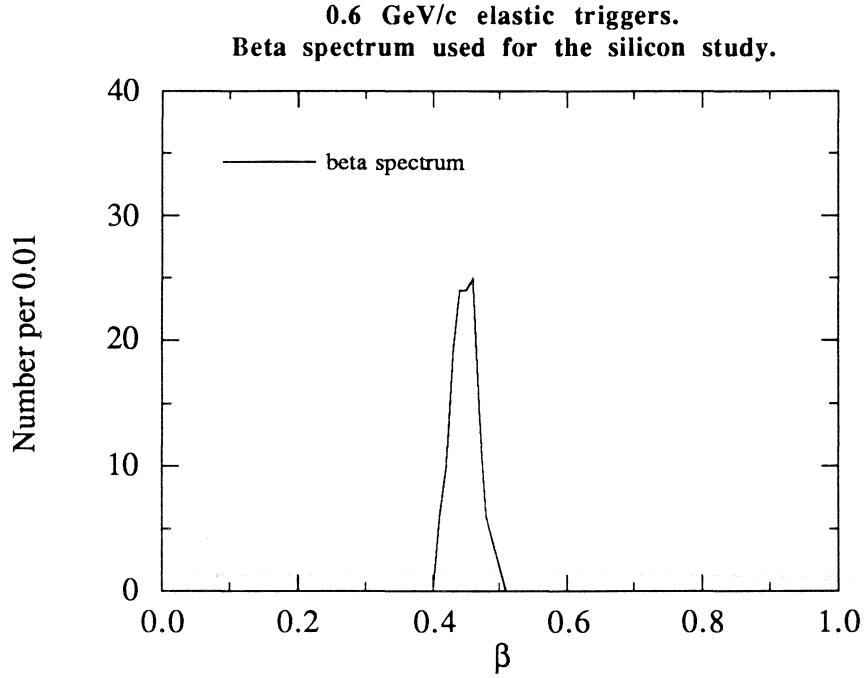

Fig. 4.12 Incident momentum 0.6 GeV/c.

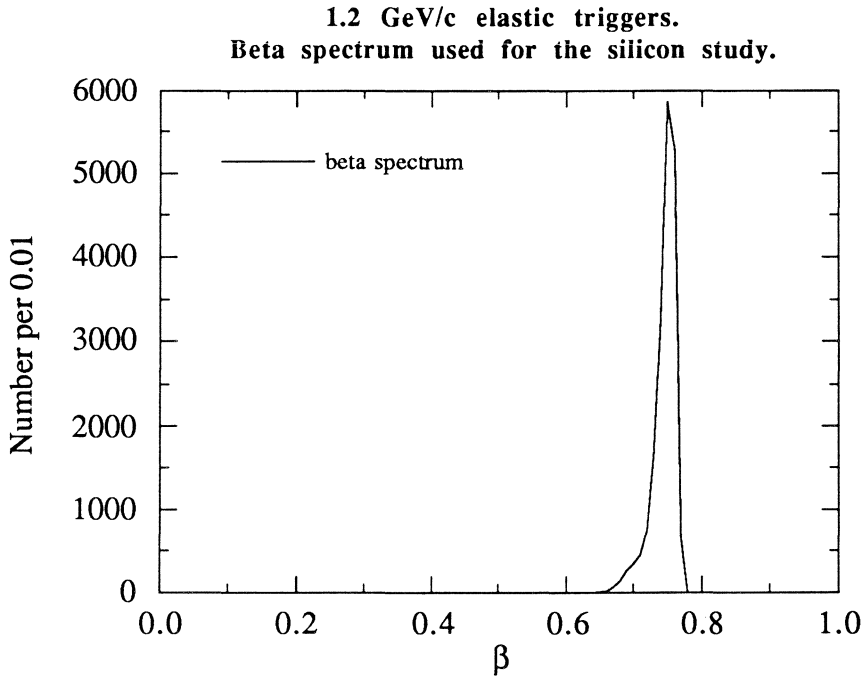

Fig. 4.13 Incident momentum 1.2 GeV/c.

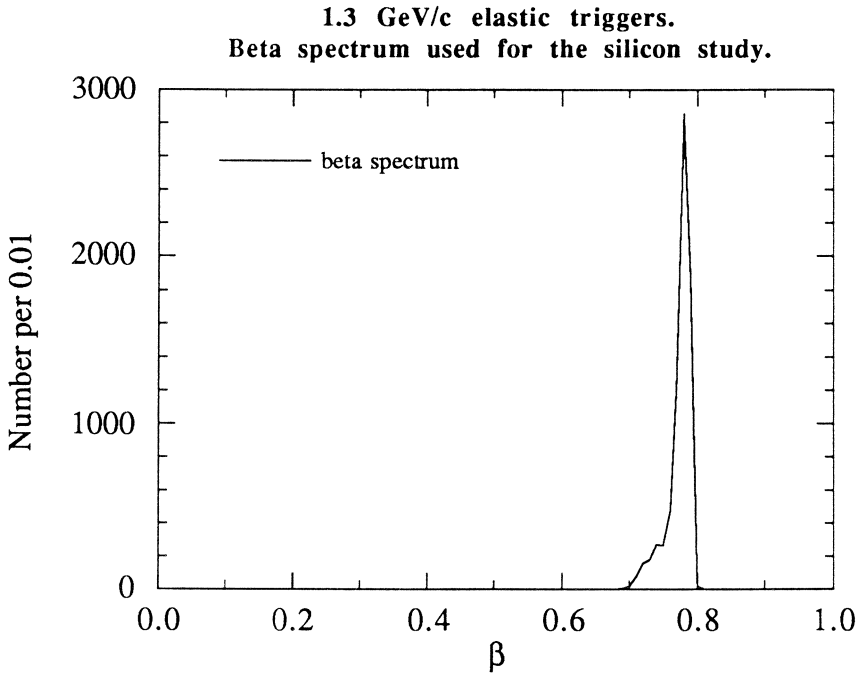

Fig. 4.14 Incident momentum 1.3 GeV/c.

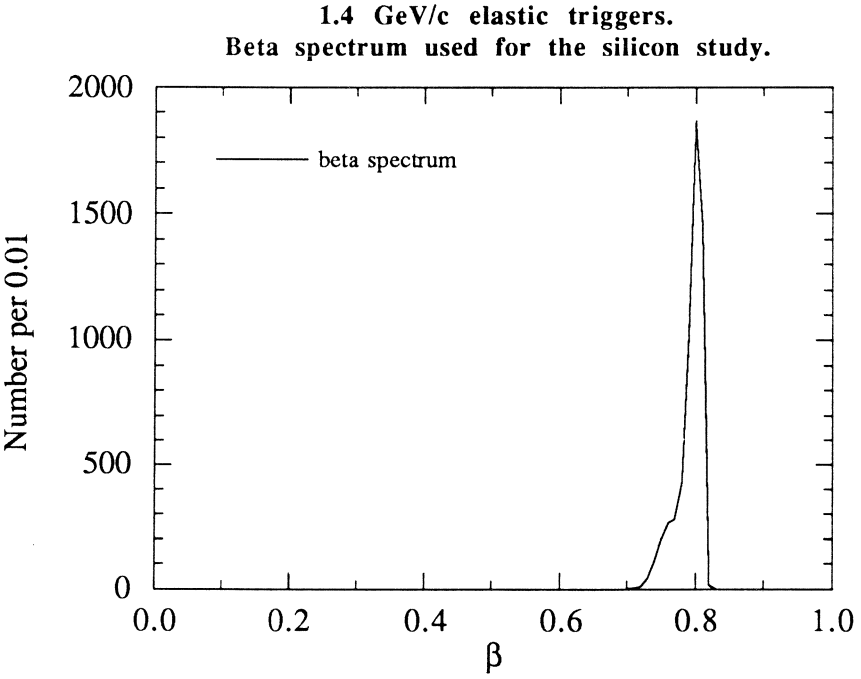

Fig. 4.15 Incident momentum 1.4 GeV/c.

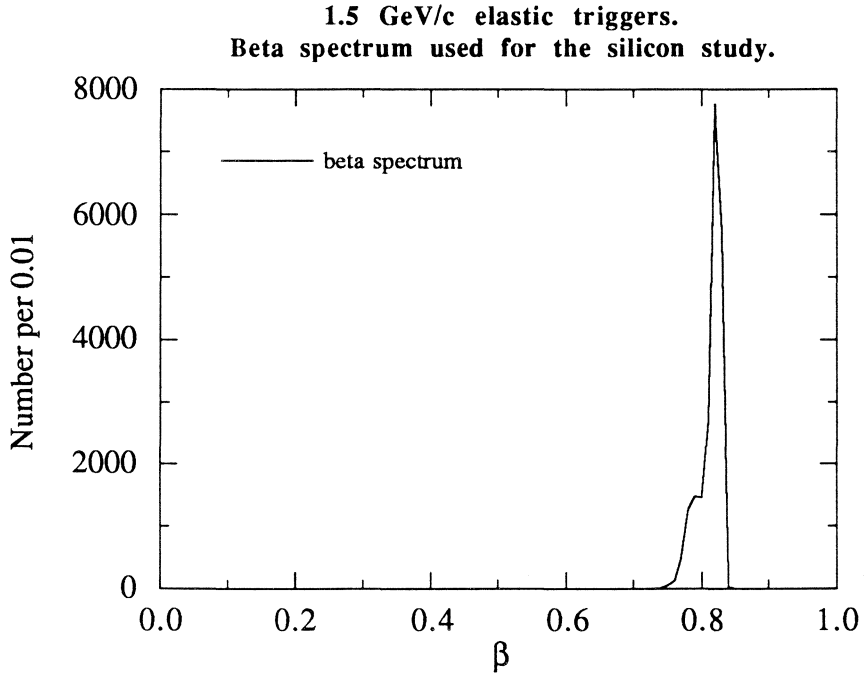

Fig. 4.16 Incident momentum 1.5 GeV/c.

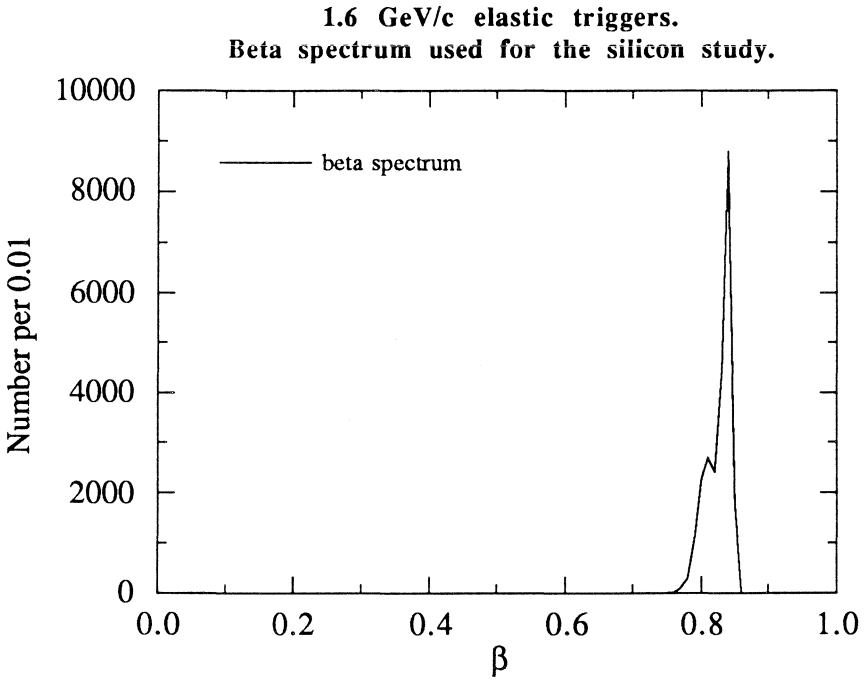

Fig. 4.17 Incident momentum 1.6 GeV/c.

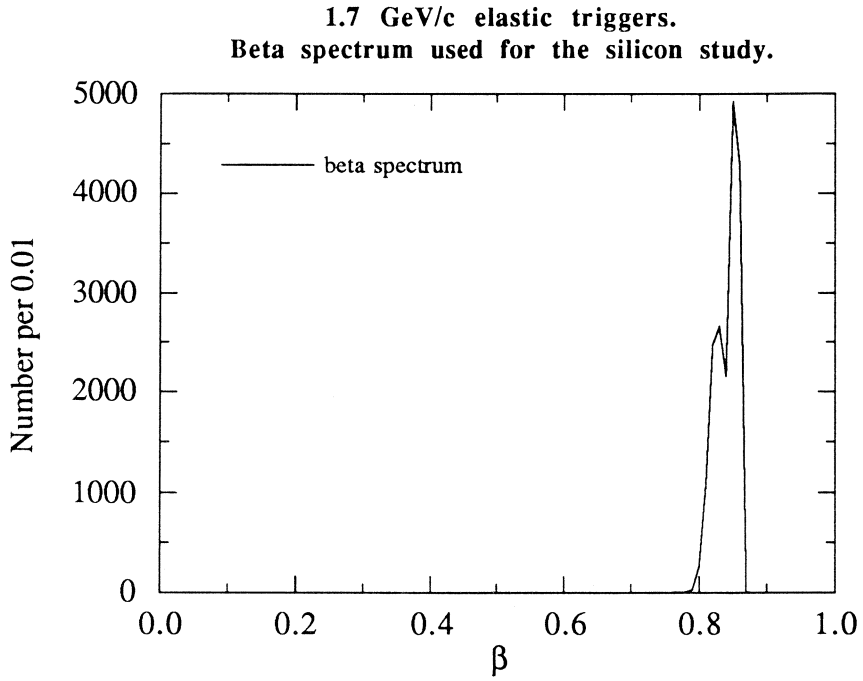

Fig. 4.18 Incident momentum 1.7 GeV/c.

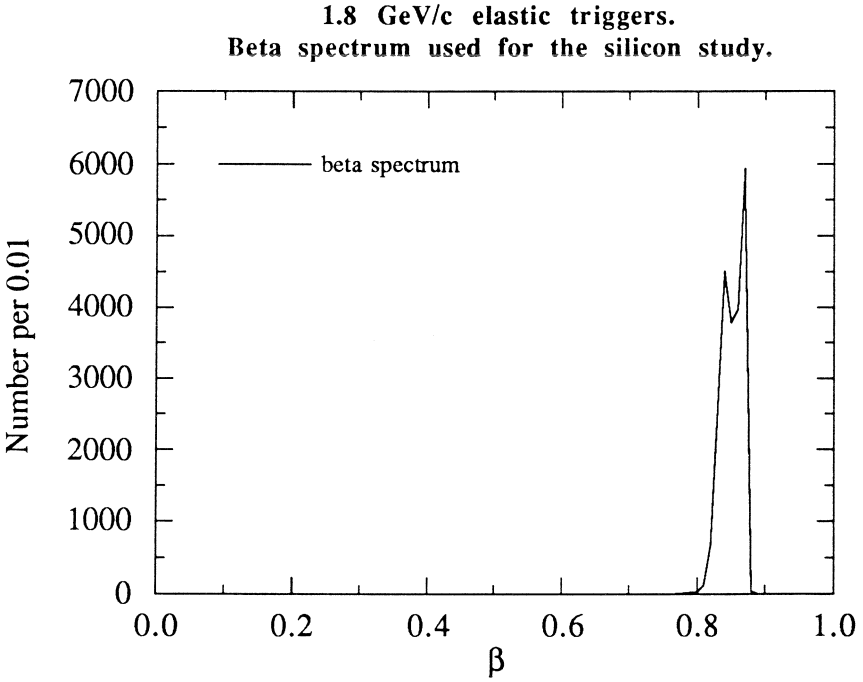

Fig. 4.19 Incident momentum 1.8 GeV/c.

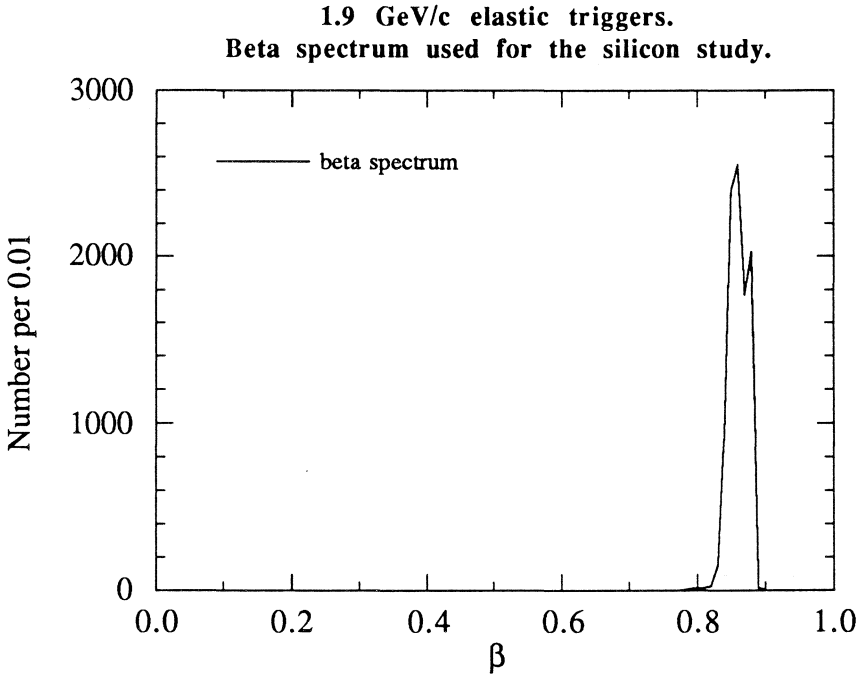

Fig. 4.20 Incident momentum 1.9 GeV/c.

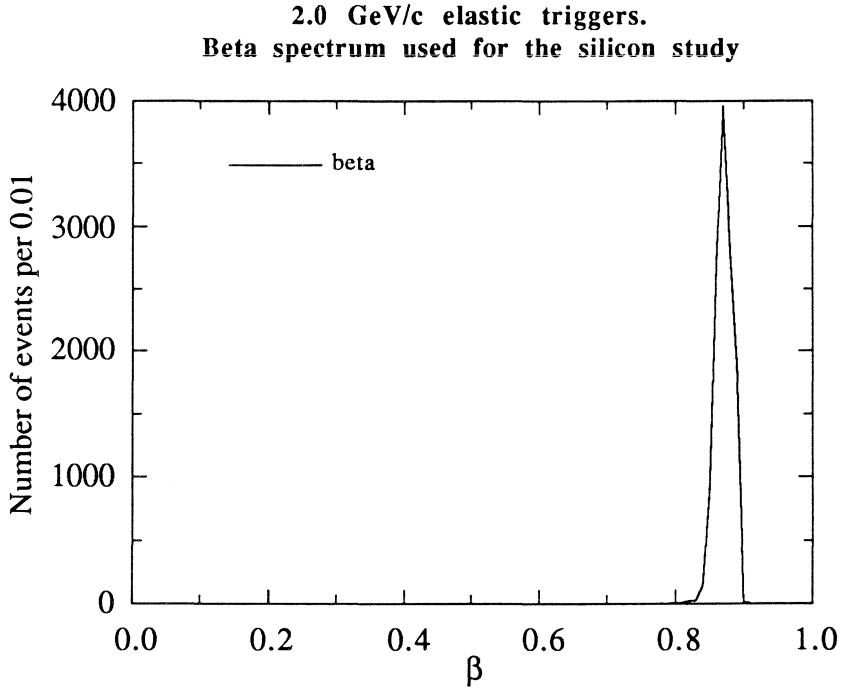

Fig. 4.21 Incident momentum 2.0 GeV/c.

The spectra of the raw signals at each momentum setting appear on figs. 4.22 to 4.31. Two sets of signals are given in each plot. The empty circles represent the distribution of all signals independently of the fact that one or two detector planes have fired. The full circles instead refer to the case where two hits have been detected above background along the track. In this case we have plotted only the smallest signal (*truncated mean*). There is an important reduction in numbers between the single- and the double-plane events. Is this due to silicon inefficiency or rather to an anomalously high frequency of single hits ? These and similar questions should be answered by people more familiar with the detctor than ourselves.

Features of the data appear to be remarkably similar over the momentum region with the notable exception of the results at 0.6 GeV/c. These data are too scarce to allow definite conclusions; the only thing one can say for sure is that the signals here are quite large. The consequence of this will be discussed below. Notice also that in these and other plots there is evidence of the *pedestal* creeping through at a small but non negligible level.

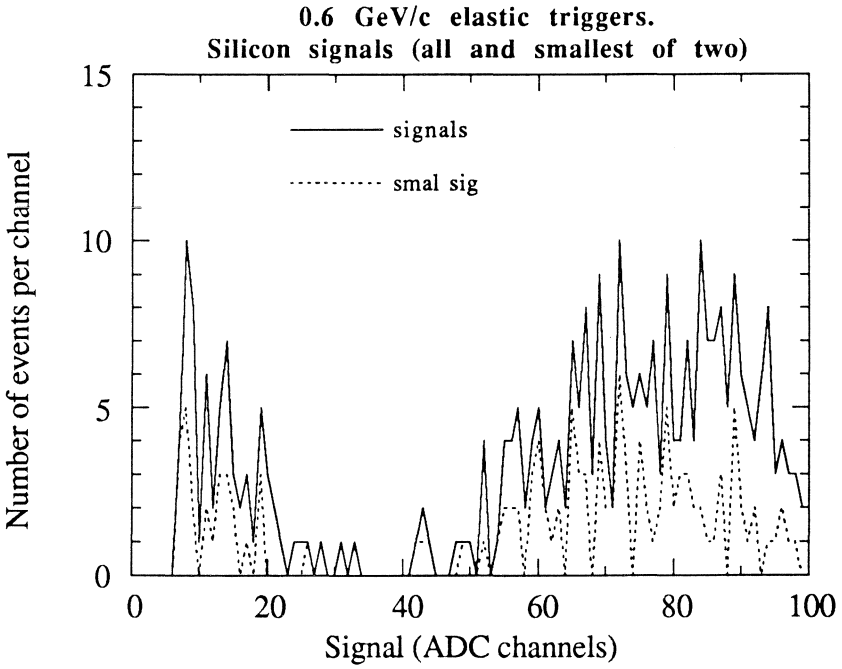

Fig. 4.22 Incident momentum 0.6 GeV/c.

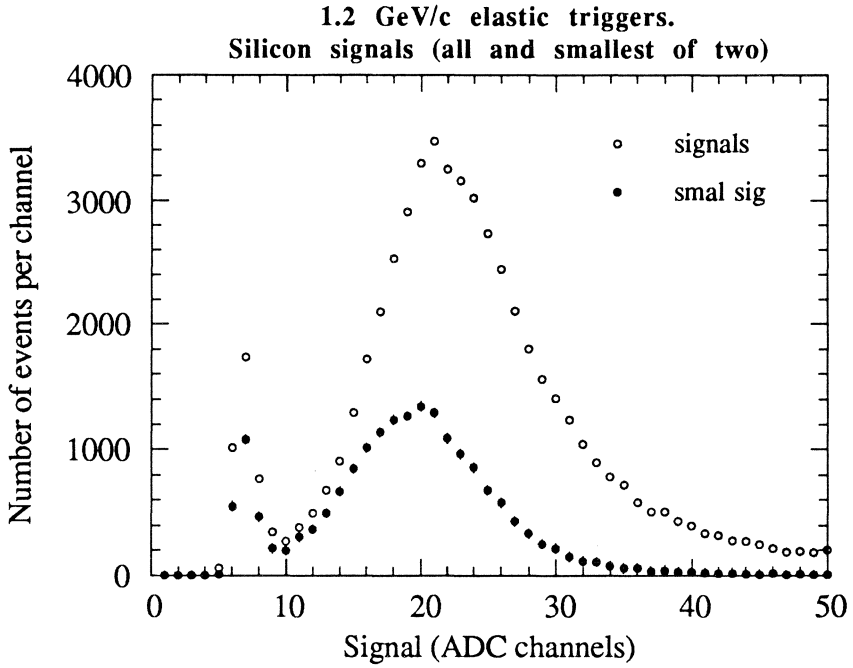

Fig. 4.23 Incident momentum 1.2 GeV/c.

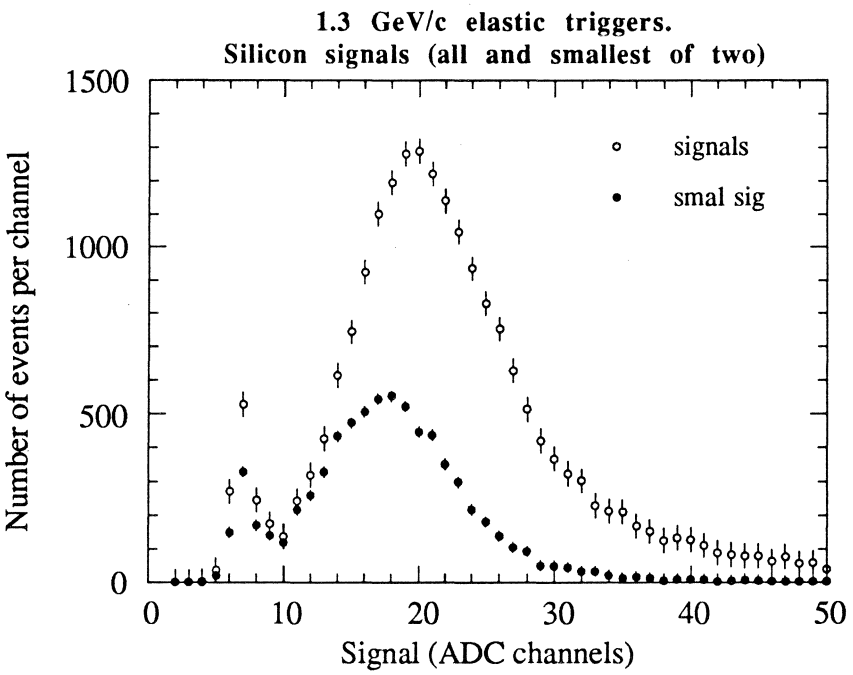

Fig. 4.24 Incident momentum 1.3 GeV/c.

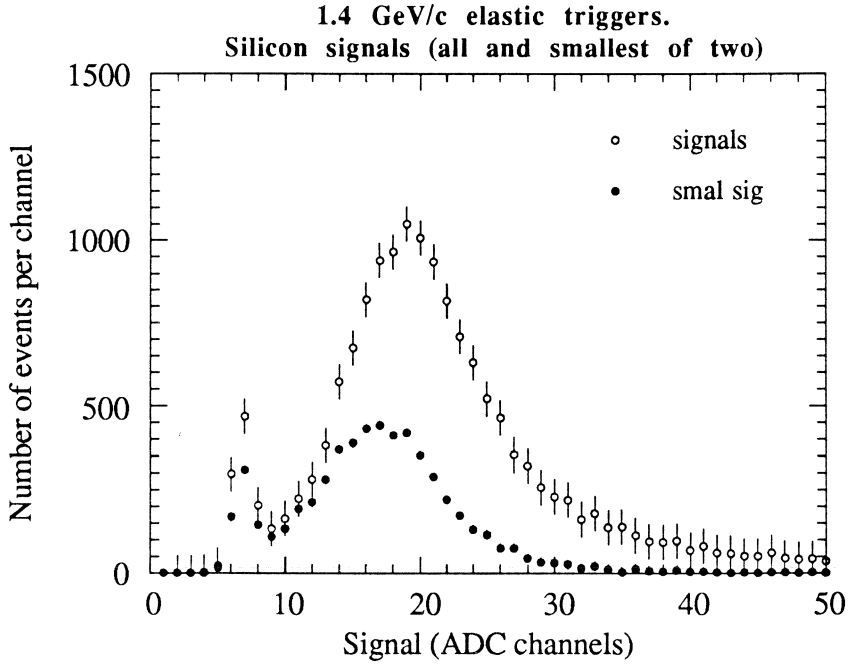

Fig. 4.25 Incident momentum 1.4 GeV/c.

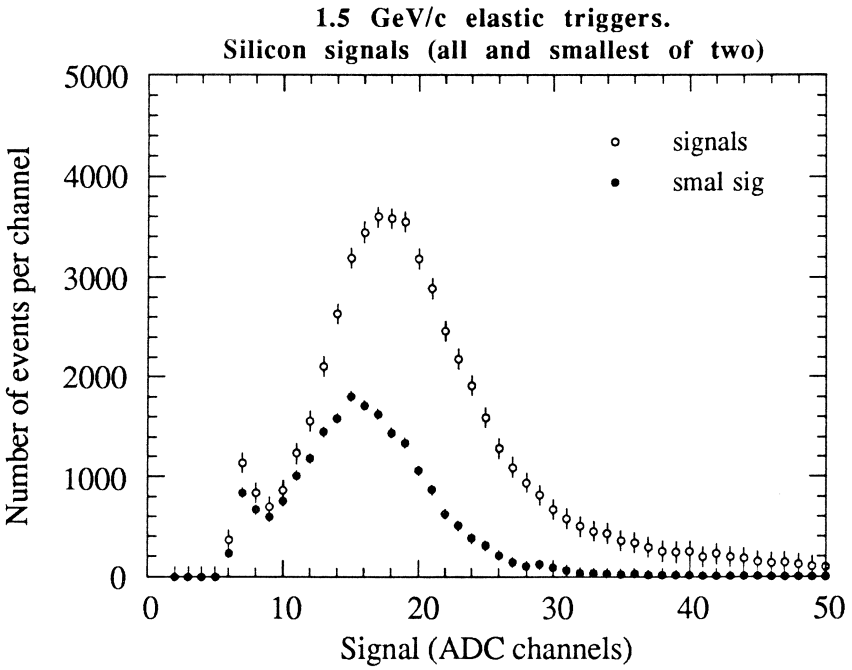

Fig. 4.26 Incident momentum 1.5 GeV/c.

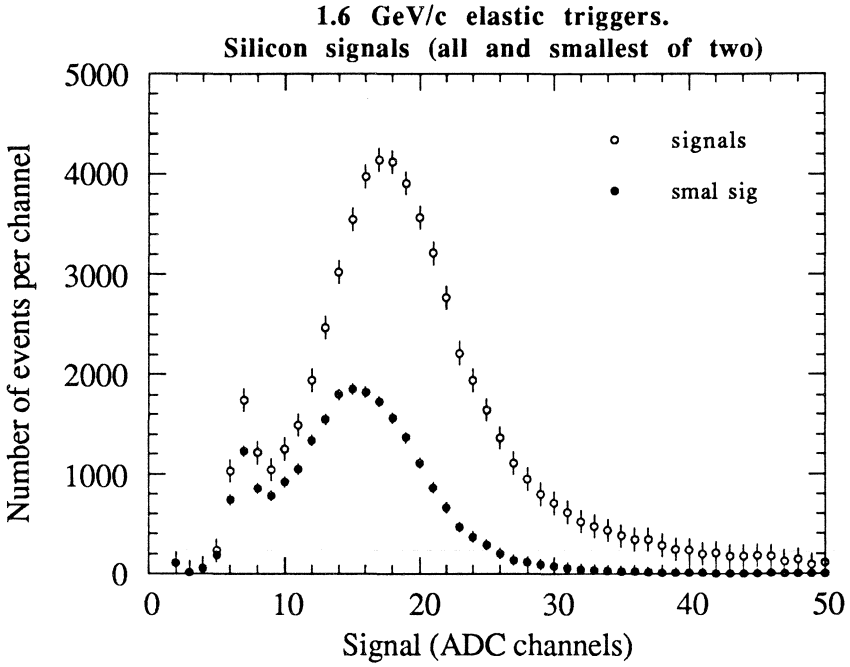

Fig. 4.27 Incident momentum 1.6 GeV/c.

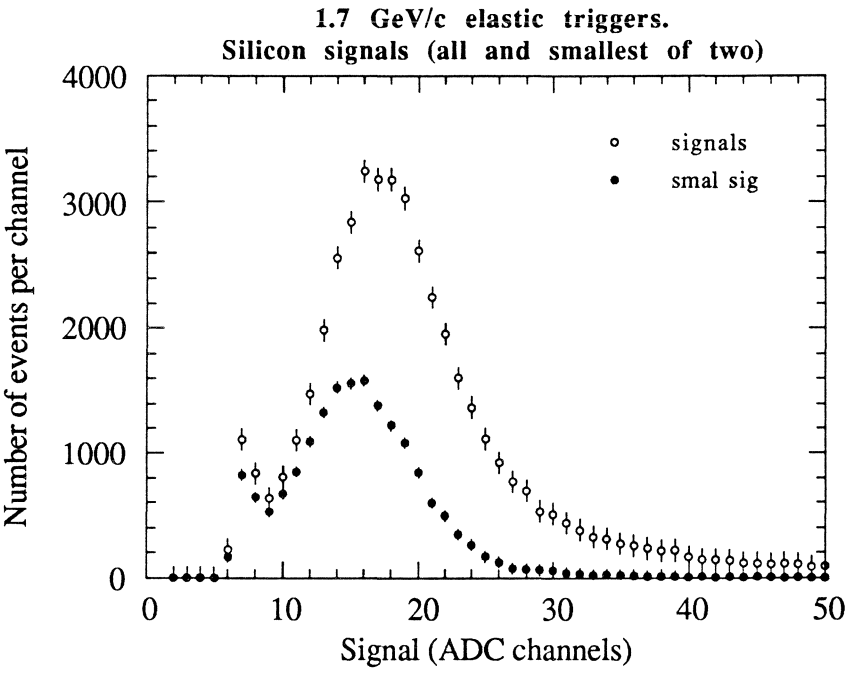

Fig. 4.28 Incident momentum 1.7 GeV/c.

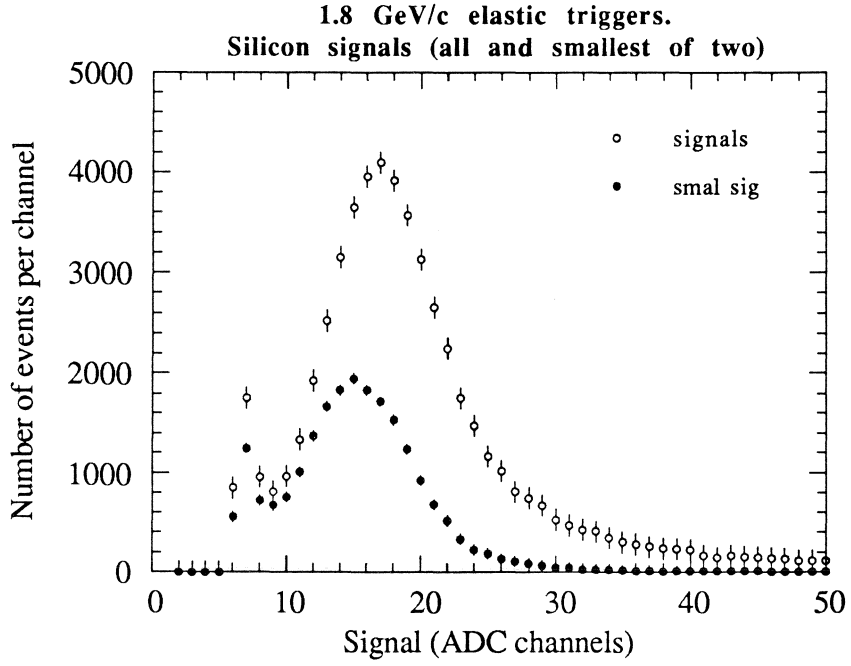

Fig. 4.29 Incident momentum 1.8 GeV/c.

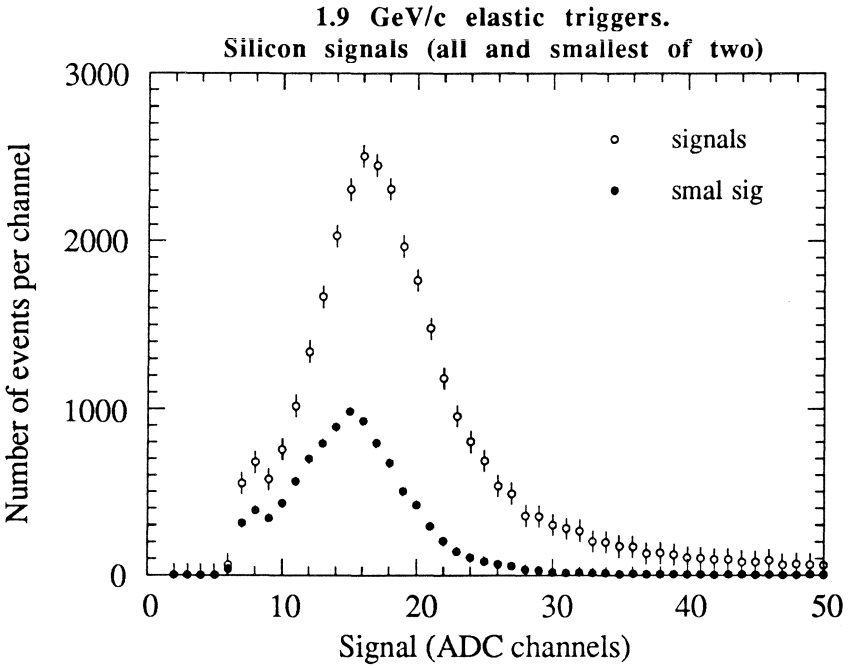

Fig. 4.30 Incident momentum 1.9 GeV/c.

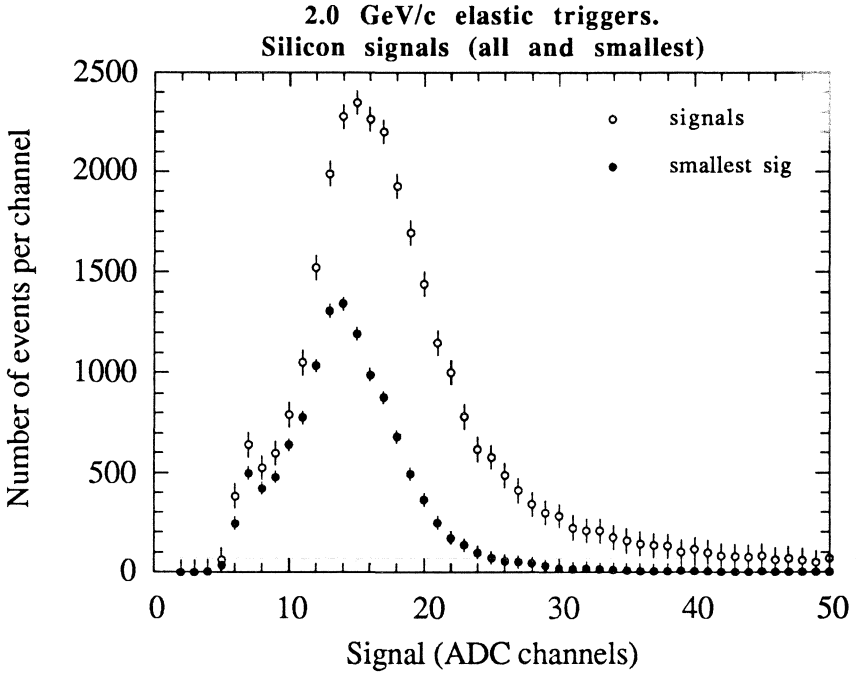

Fig. 4.31 Incident momentum 2.0 GeV/c.

Here again we have proceeded as with the Cherenkov signals, calculating the expected energy loss ΔE on the basis of the standard (simplified) formula:

$$\Delta E = \frac{dE}{dx}\,\delta \quad with \quad \delta = 0.03\ cm\ and$$

$$\frac{dE}{dx} = \frac{0.431\,(11.04 + ln\,(\eta^2) - 2.375 - \beta^2)}{\beta^2}$$

(here η is the usual abbreviation for P/M). By dividing the individual measurements by these values we obtain the normalisation factors.

The results appear in figs. 4.32 to 4.41. These plots give the normalisation factor needed to transform the energy loss from MeV to ADC channels. Why are the data frequently scattered around (or oscillating) is something that needs more careful examination. It may be a "binning" effect similar to the one have noticed in the confidence level plots to be discussed below.

On the other hand there is a remarkable consistency about the average values. We find all these values clustered around ≈ 105 channels per MeV, as shown on fig. 4.42. On this figure we have pointedly not drawn the value at 0.6 GeV/c ($\beta \approx 0.45$) because we did not feel confident at all about its significance. Nevertheless, if one is willing to take the data at face value, then we would have to plot it somewhere in the vicinity of 160 - 170 channels per MeV, in stark contrast with the other values. To put it another way, the average value of the

velocity necessary to generate the observed signal (at ≈ 75 channels ?) with our normalising factor would need to be in the $\beta \approx 0.30$ region, a long way from the $\beta \approx 0.45$ of the 0.6 GeV/c setting.

Notice that we have not forgotten the existence of material in the detector. The energy lost by each particle on its way from the origin to the Silicon planes has been accounted for. The value of β used for the expected signal had been accordingly corrected. The energy-loss treatment that has been applied[9] may not be the most accurate in the world but should give a reasonable account of the major material effects along the particle's path. In particular we have verified that drastic increases in the amount of material existing before the detector did not alter things appreciably. Thus for example when we introduced a factor of two in the vacuum-pipe thickness (from 300μm to 600μm) we found no significant effect as far as the Silicon expectation was concerned.

As already mentioned in sect. 1 we feel that — barring mistakes always possible on our side or trivial read-out errors — the effect must be due to the presence of spurious reactions which are more liable to occur at these low momenta than at higher ones. Antiprotons are notorious for interacting and annihilating; the lower the energy the more enthusiastically they do it. We may be recording the end-products of secondary (very low energy) particles with velocities bearing little relation to the putative β's assumed in the calculation.

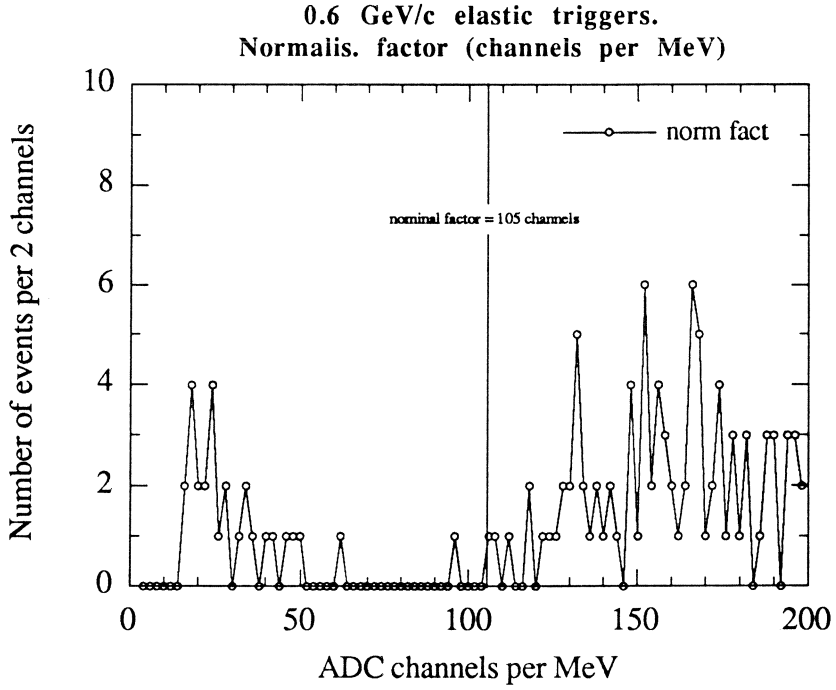

Fig. 4.32 Incident momentum 0.6 GeV/c.

[9] Program listing in JETSET note 91-03 (M.F.-L.) 7 June 1991.

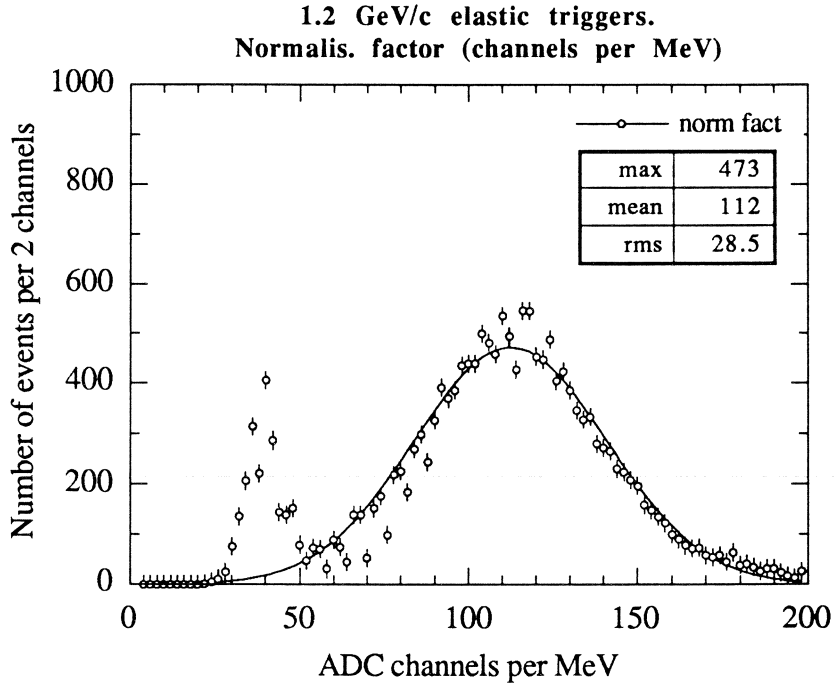

Fig. 4.33 Incident momentum 1.2 GeV/c.

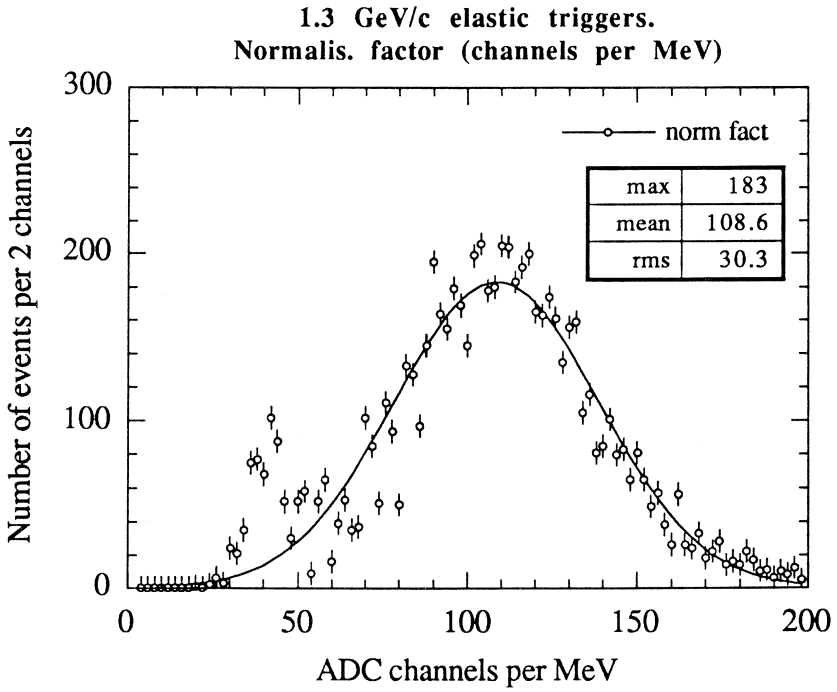

Fig. 4.34 Incident momentum 1.3 GeV/c.

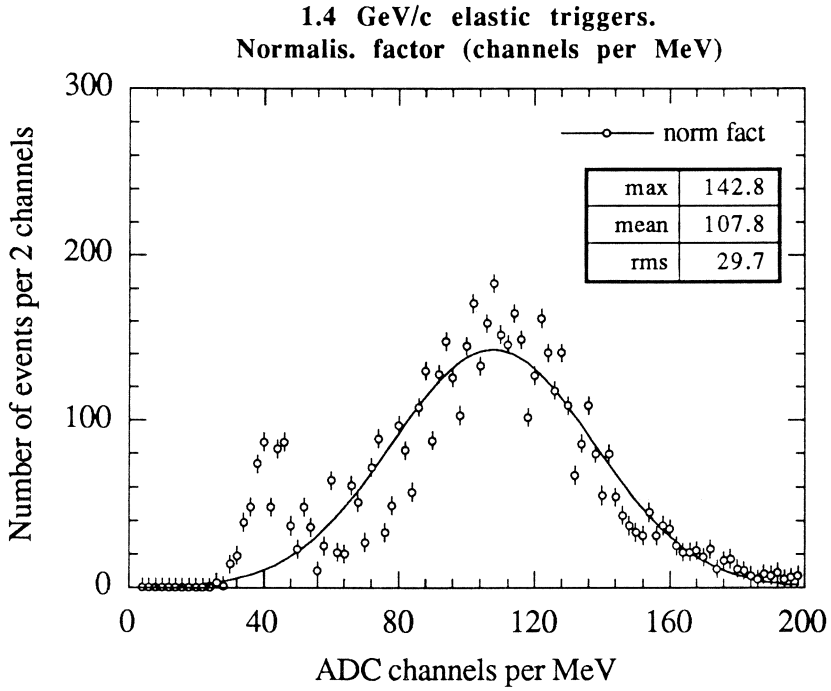

Fig. 4.35 Incident momentum 1.4 GeV/c.

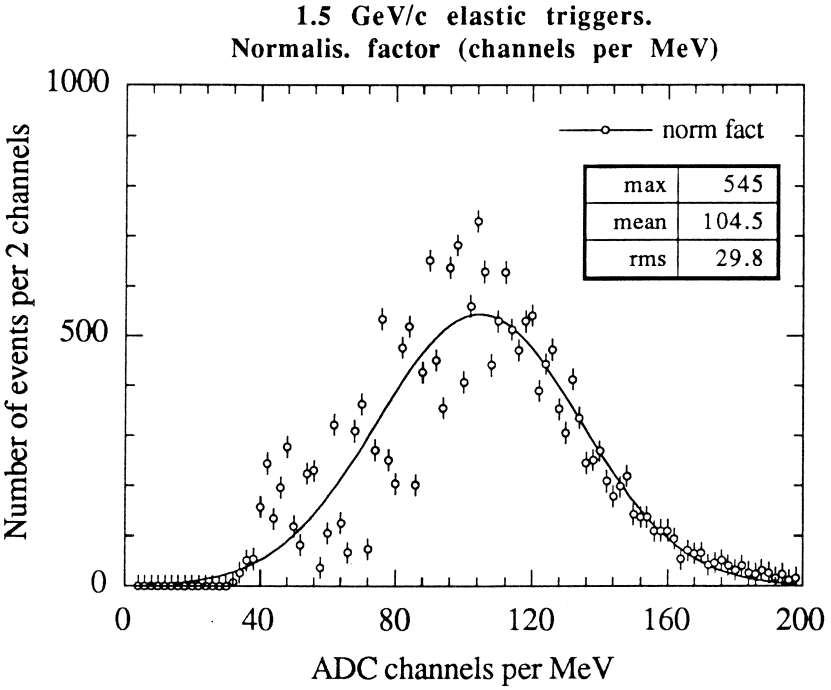

Fig. 4.36 Incident momentum 1.5 GeV/c.

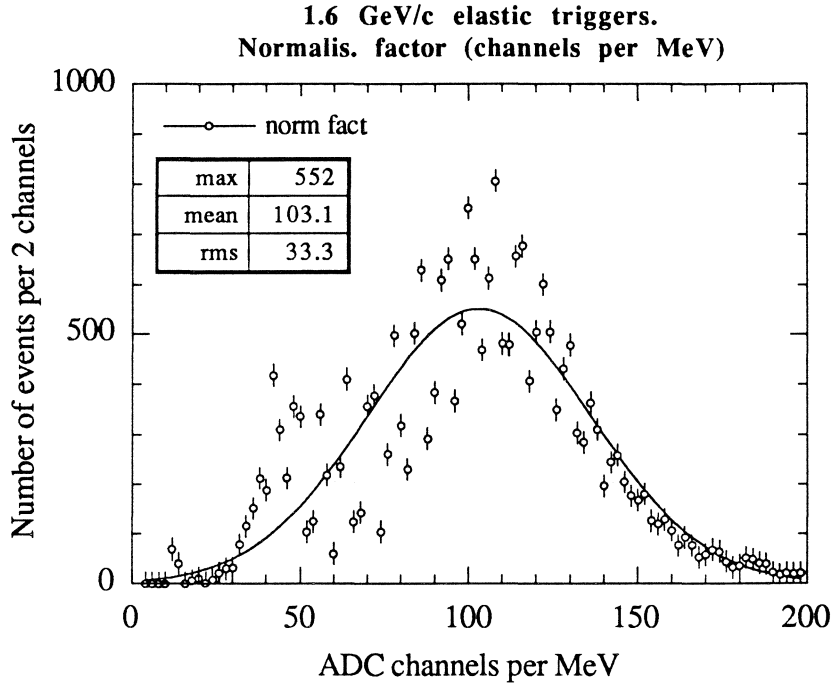

Fig. 4.37 Incident momentum 1.6 GeV/c.

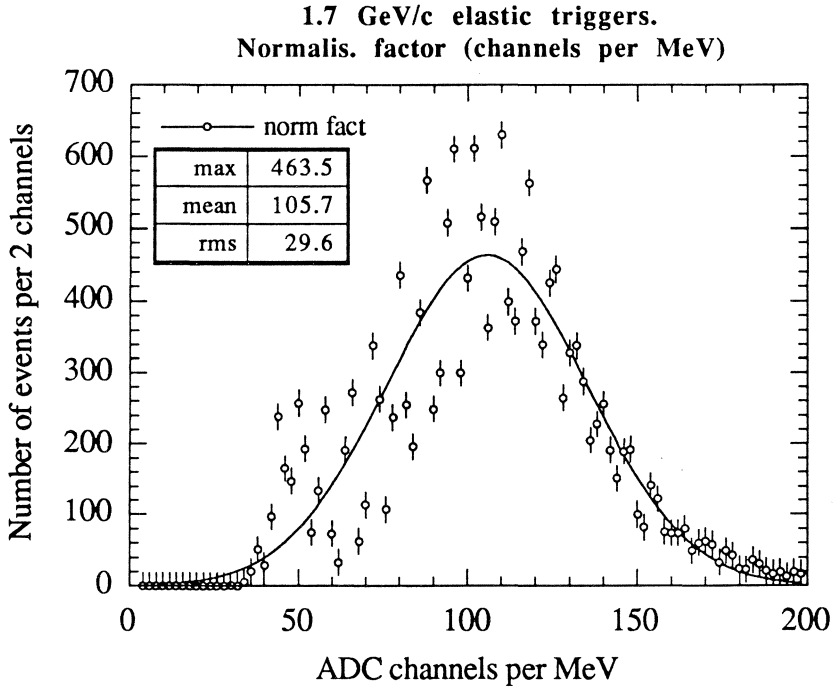

Fig. 4.38 Incident momentum 1.7 GeV/c.

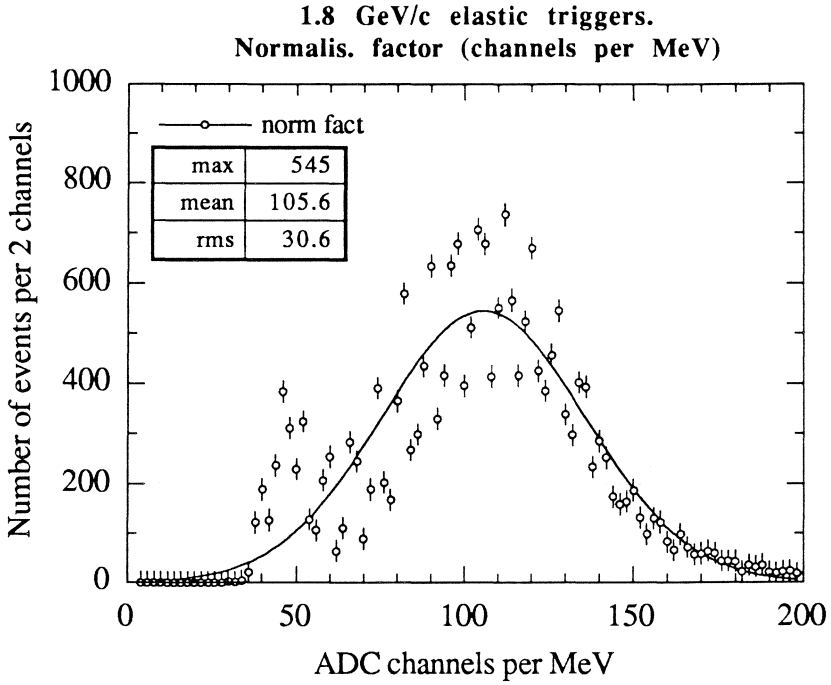

Fig. 4.39 Incident momentum 1.8 GeV/c.

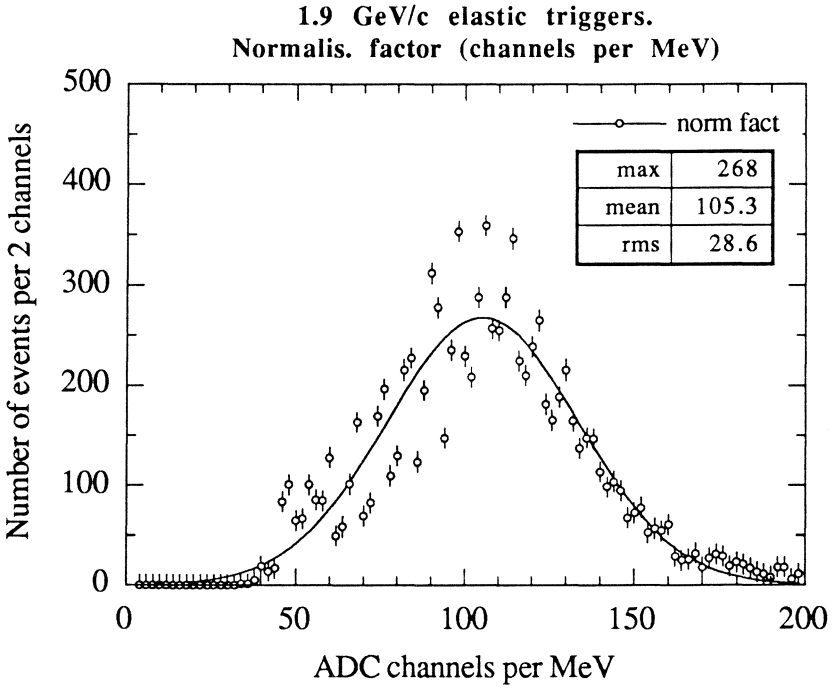

Fig. 4.40 Incident momentum 1.9 GeV/c.

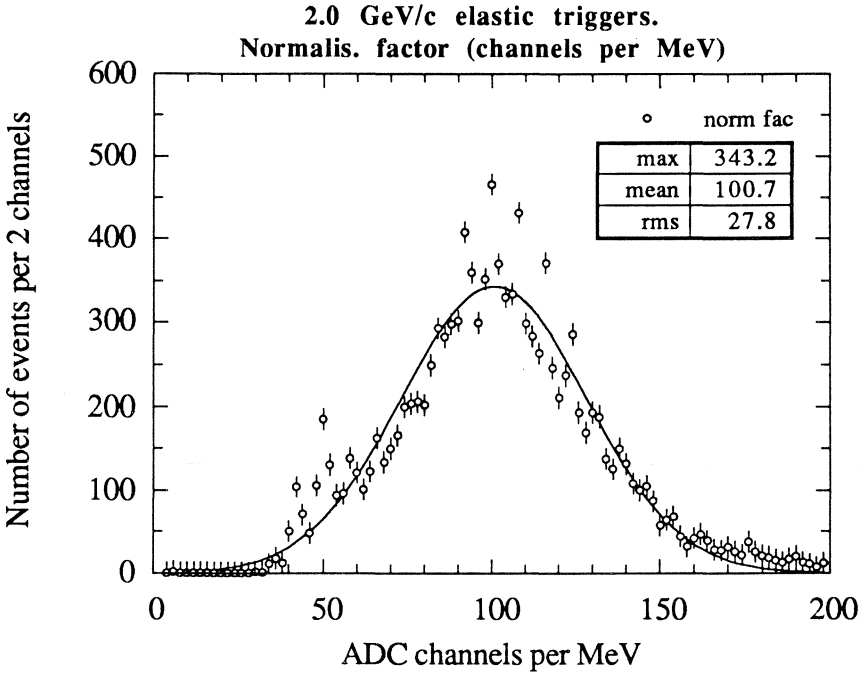

Fig. 4.41 Incident momentum 2.0 GeV/c.

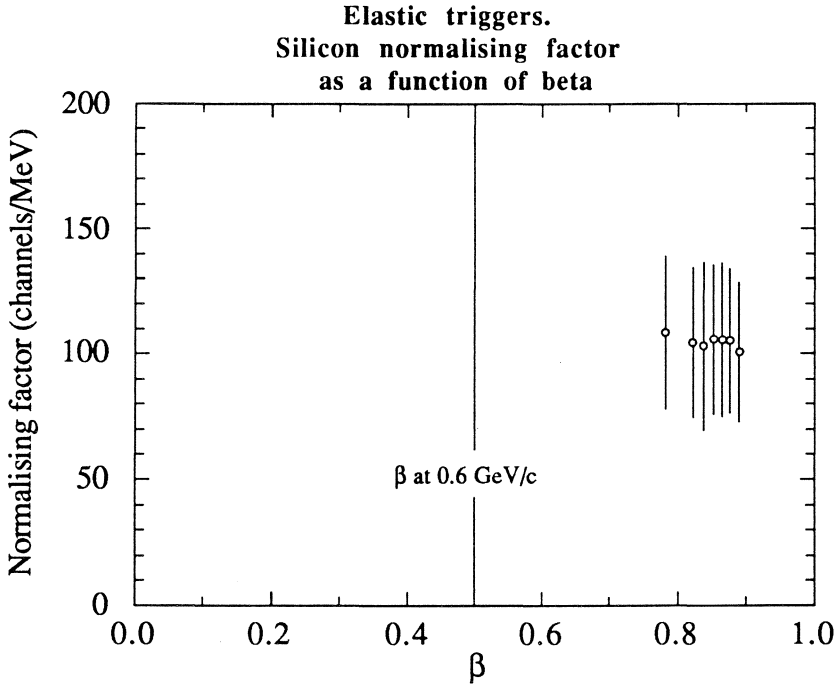

Fig. 4.42 Normalisation factor as a function of the average β.

Leaving the question of the 0.6 GeV/c data aside for the moment, we have verified that the normalisation factors derived at higher energies make sense.

The plots in figs.4.43 to 4.52 have been obtained using the 105 channels/MeV factor to convert expected signals into ADC channels. These plots show the "measured-minus-expected" distributions at all momenta. With the usual 0.6 GeV/c exception they all are reasonably well described by Gaussians.

As already mentioned, the small enhancement at low values appearing in many (but not all) of these distributions is probably due to "pedestal leakage" occurring when the on-line subtraction fails for one reason or another.

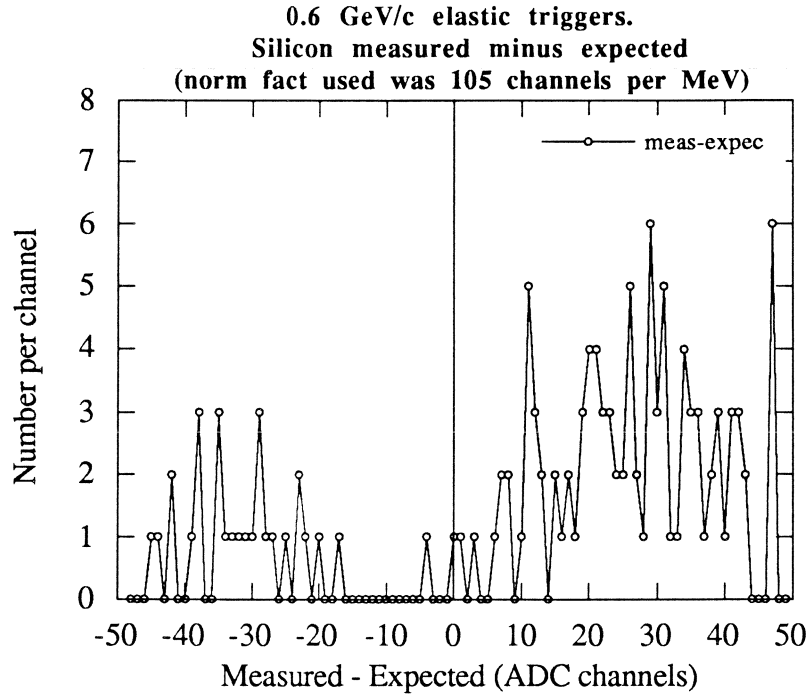

Fig. 4.43 Incident momentum 0.6 GeV/c.

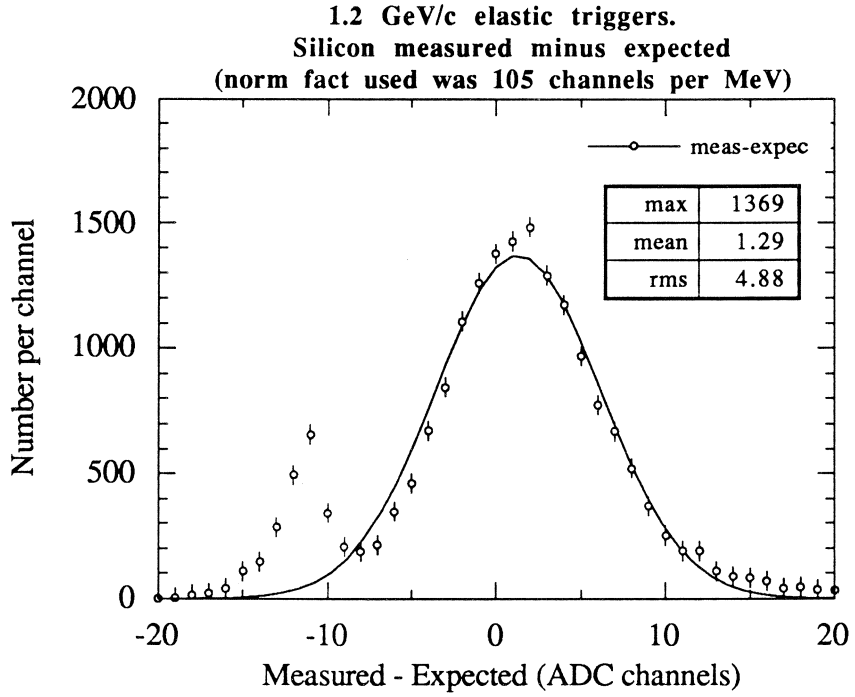

Fig. 4.44 Incident momentum 1.2 GeV/c.

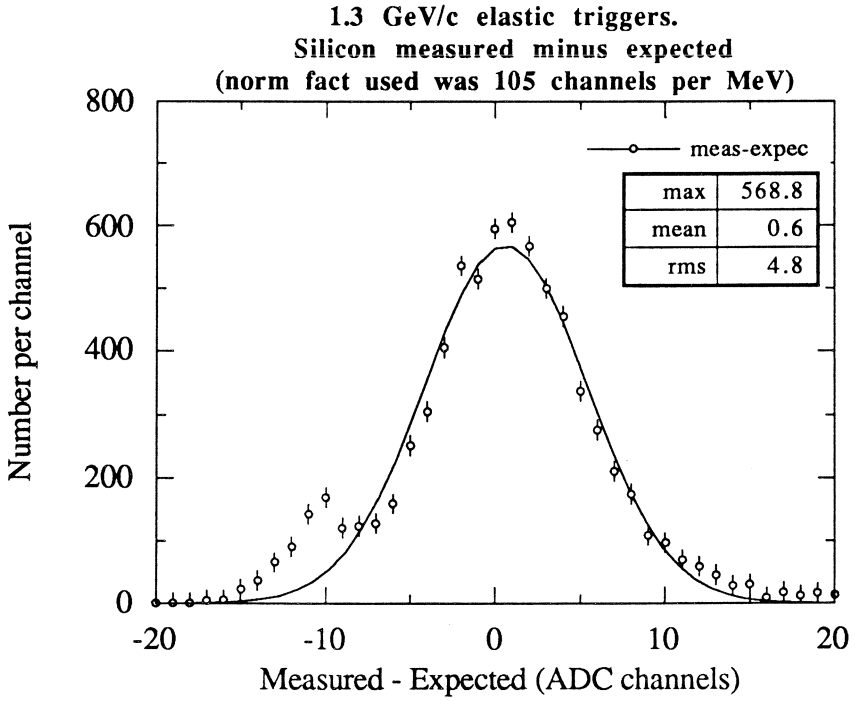

Fig. 4.45 Incident momentum 1.3 GeV/c.

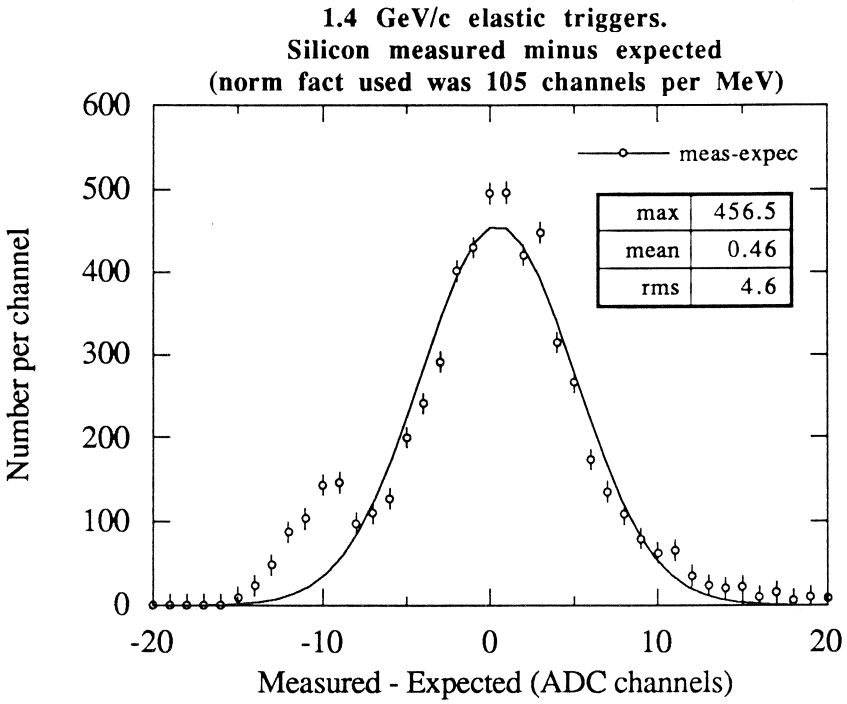

Fig. 4.46 Incident momentum 1.4 GeV/c.

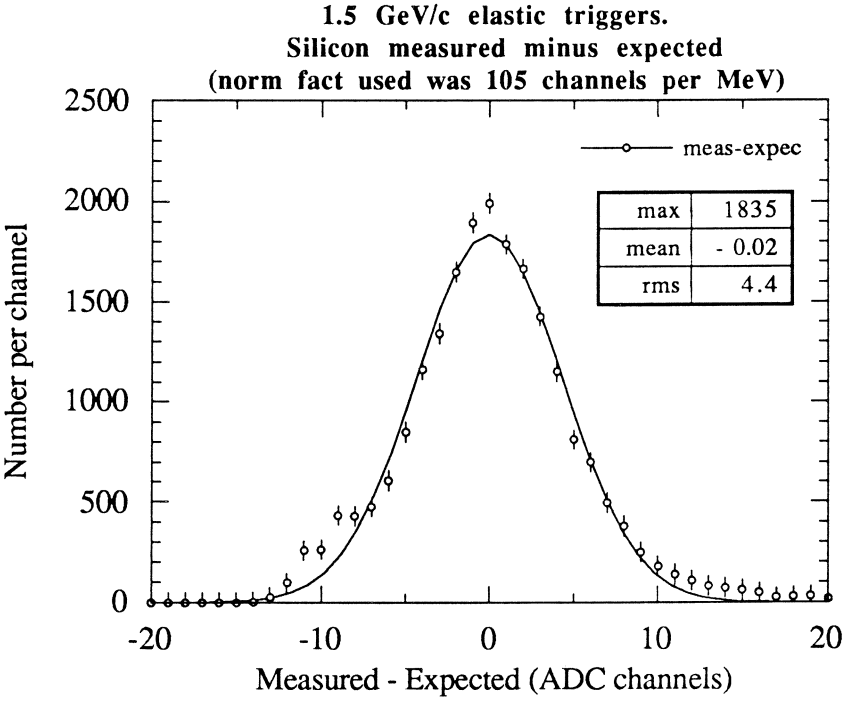

Fig. 4.47 Incident momentum 1.5 GeV/c.

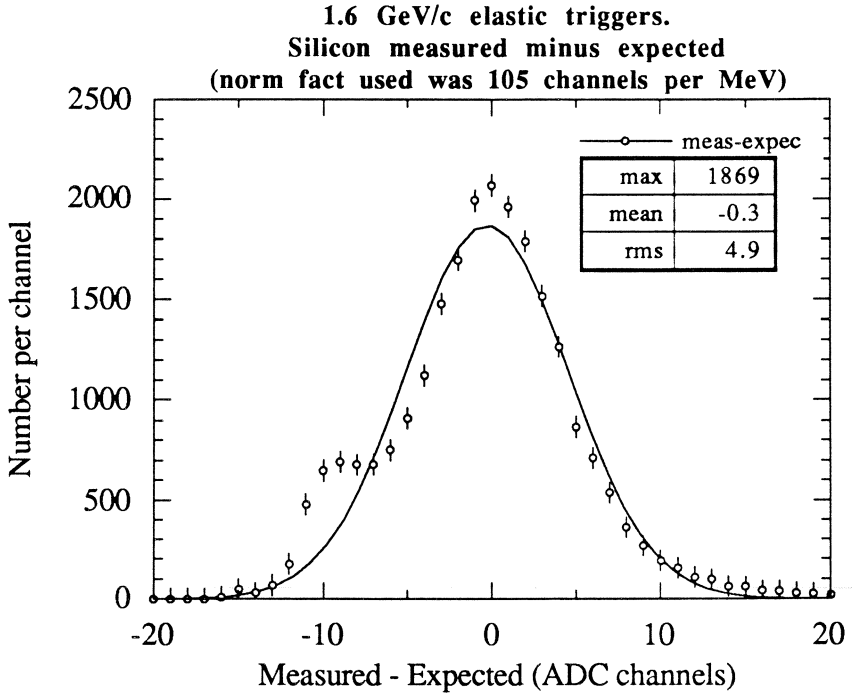

Fig. 4.48 Incident momentum 1.6 GeV/c.

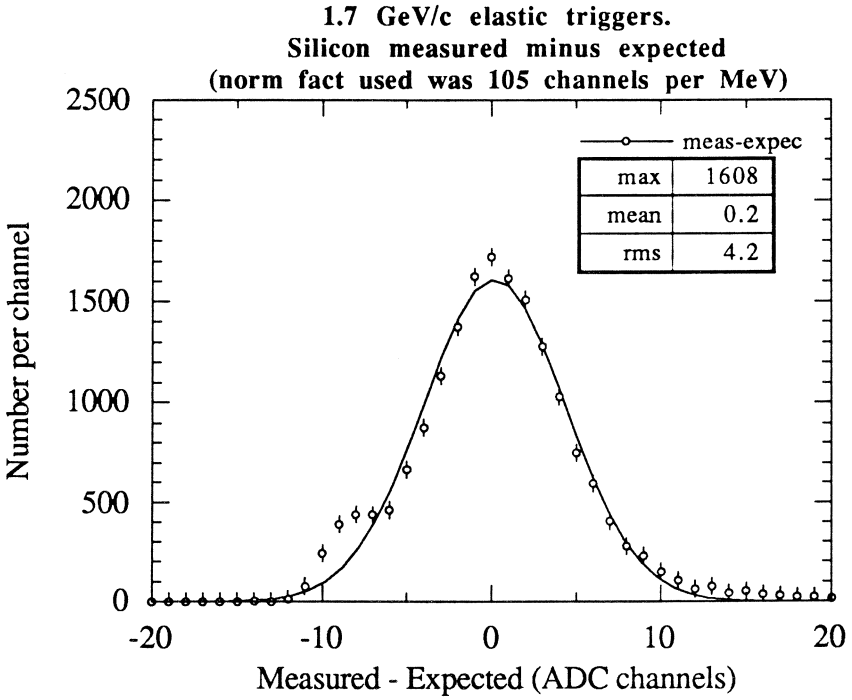

Fig. 4.49 Incident momentum 1.7 GeV/c.

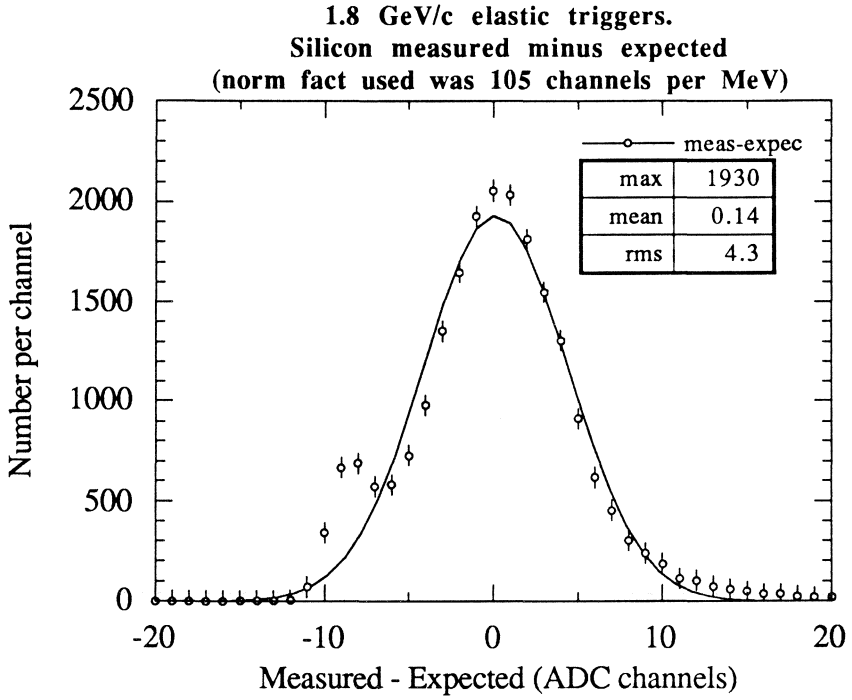

Fig. 4.50 Incident momentum 1.8 GeV/c.

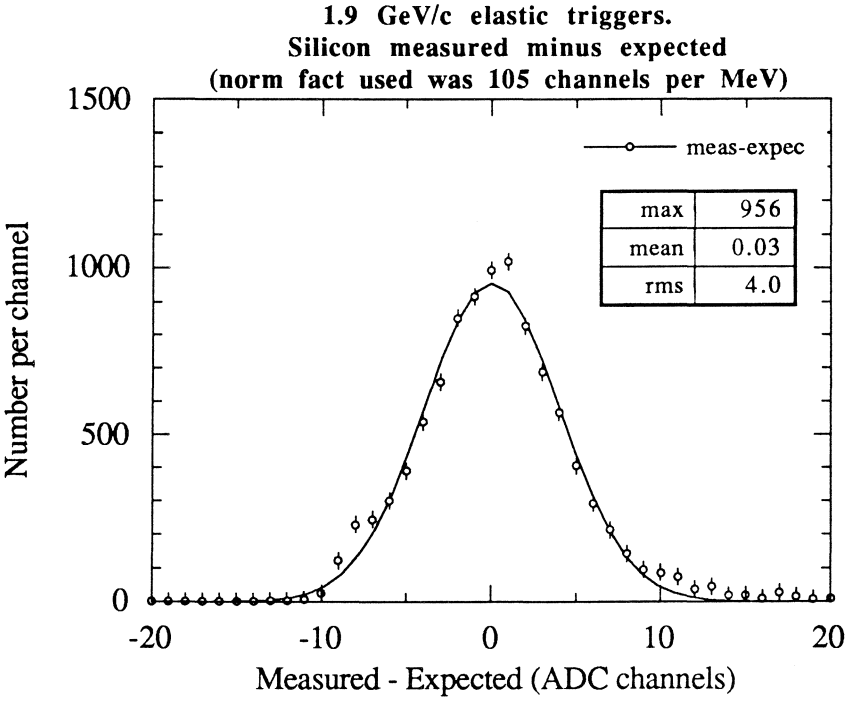

Fig. 4.51 Incident momentum 1.9 GeV/c.

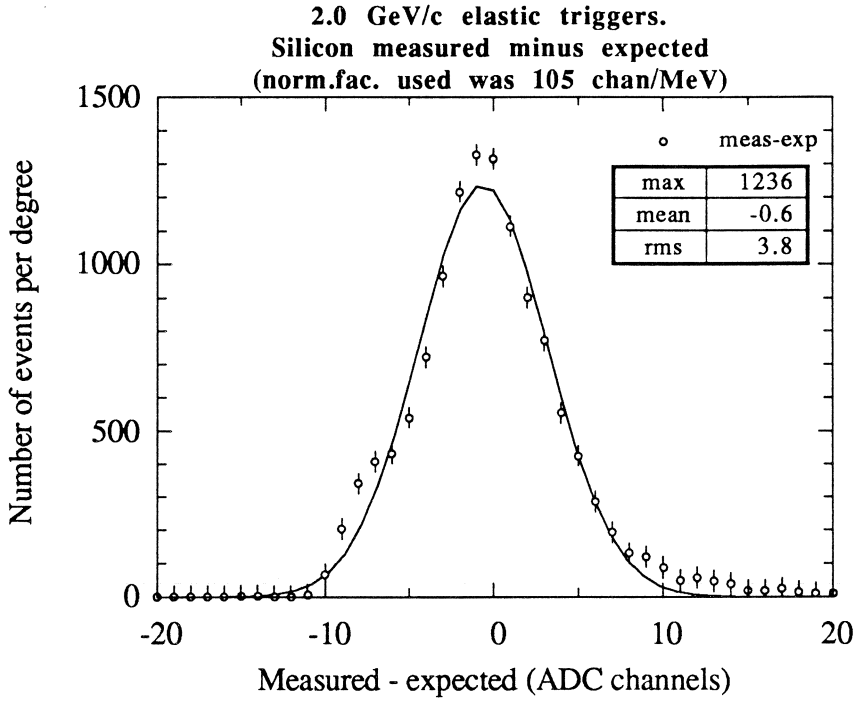

Fig. 4.52 Incident momentum 2.0 GeV/c.

Finally we present the **confidence level** distributions (labelled "probability" on the plots) of the silicon measurements in figs. 4.53 to 4.62. They have been obtained as for the Cherenkovs, by calculating a chisquare with the measured and expected values and using 4.7 channels for the rms (the average value observed in the above plots 4.43 to 4.52). We recall that by *expected values* we mean — as in the Cherenkov case — those obtained from the values of β derived by the elastic kinematics on the basis of the forward angle.

These distributions look reasonably uniform, as they should, if one forgets about the funny oscillations which are simply due to the limited precision of the ADC measurement of the signals and should not be taken seriously[10]. A hint of a wrong rms attribution (too large....) is instead apparent in the distributions of figs. 4.61 and 4.62 at the two highest momenta.

This is the end of our cursory examination of the *Silicon* detector. We hope that other important but still unsettled questions will be answered in later and more thorough studies: what is the β-resolution achievable with this detector ? what is its efficiency ? can we use the hits as pattern recognition elements ? All these are very important points which greatly affect the future of the experiment and we hope that everybody will try their best to answer them.

---

[10] In these measurements the ADC readings span a small set of integers numbers. The corresponding line spectra are then converted into broadened but still quantised spectra when calculating the confidence level.

One last consideration is that if we have learned anything out of this study of the *Silicons* it is that in the future it will be very important for the understanding of this detector to take abundant data in the neighbourhood of 1 GeV/c and below.

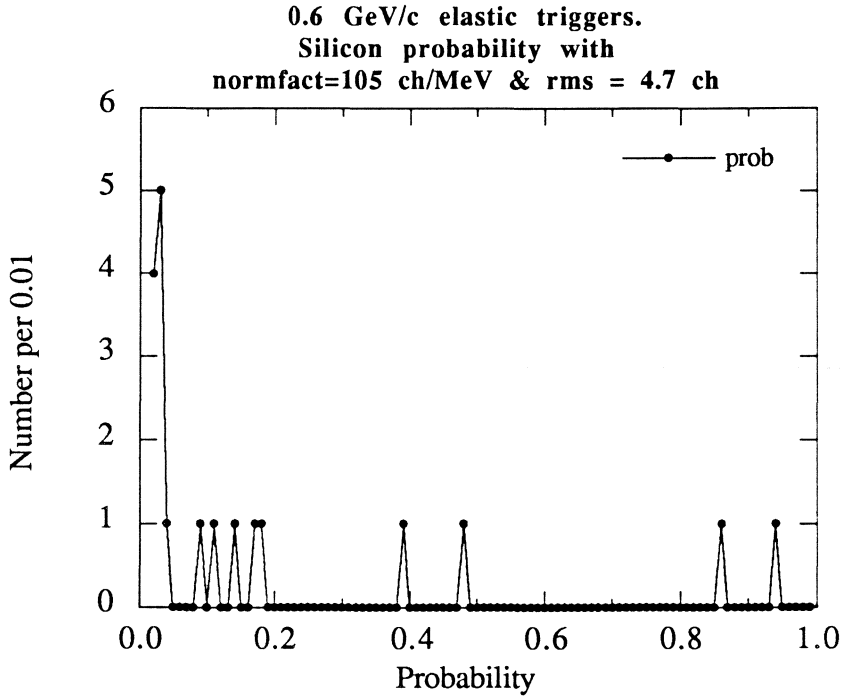

Fig. 4.53 Incident momentum 0.6 GeV/c.

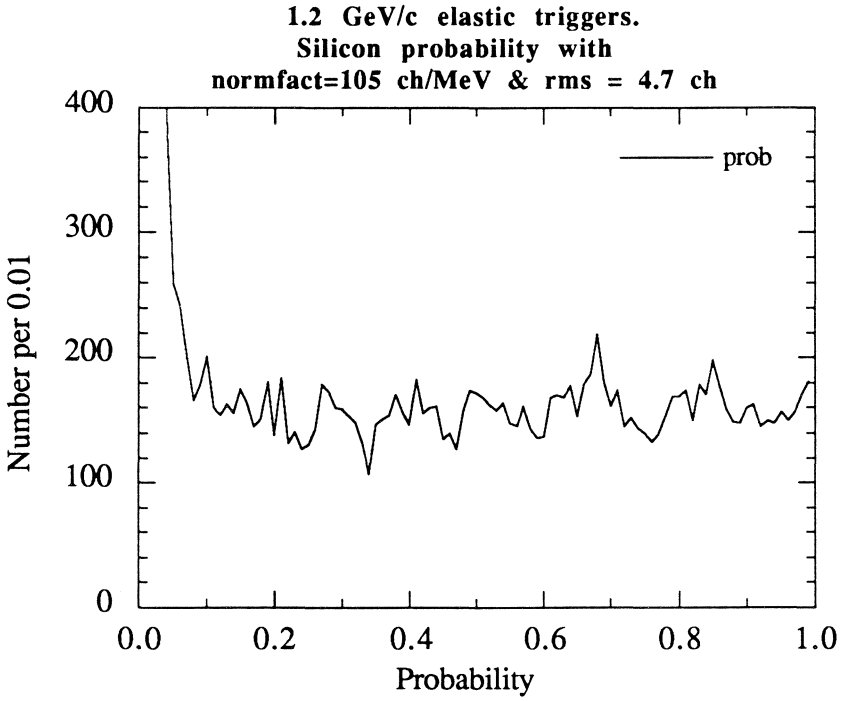

Fig. 4.54 Incident momentum 1.2 GeV/c.

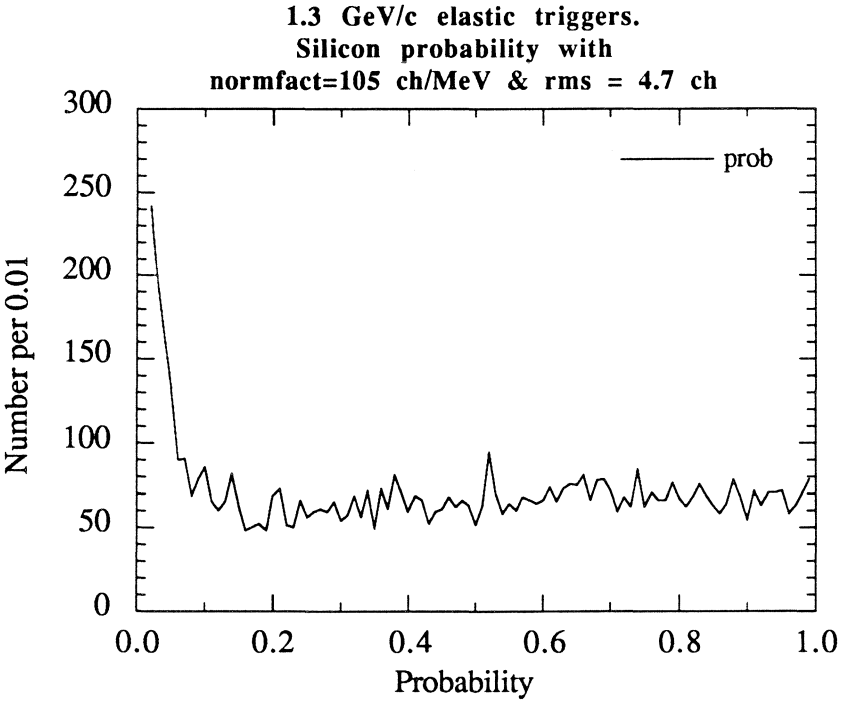

Fig. 4.55 Incident momentum 1.3 GeV/c.

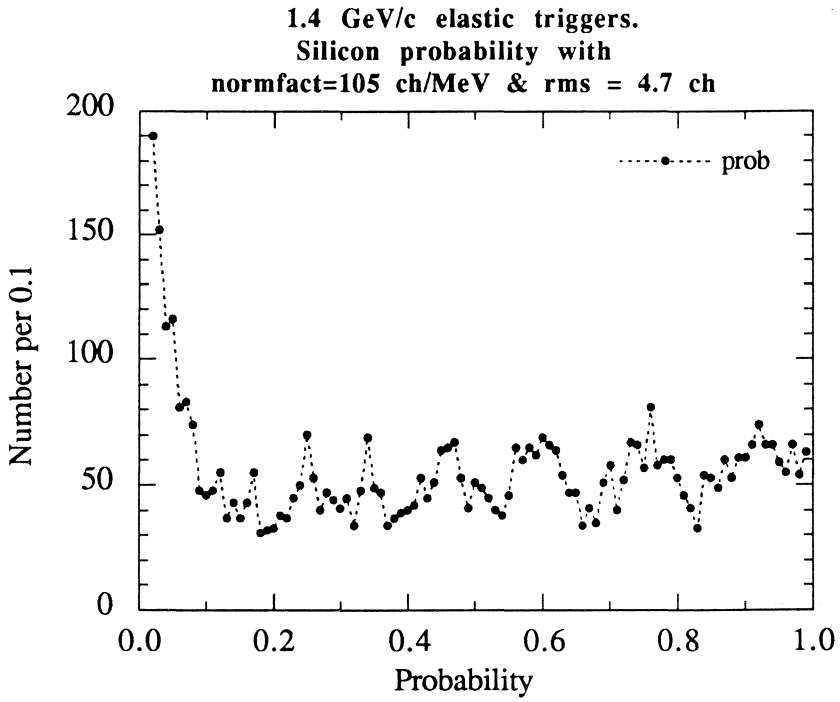

Fig. 4.56 Incident momentum 1.4 GeV/c.

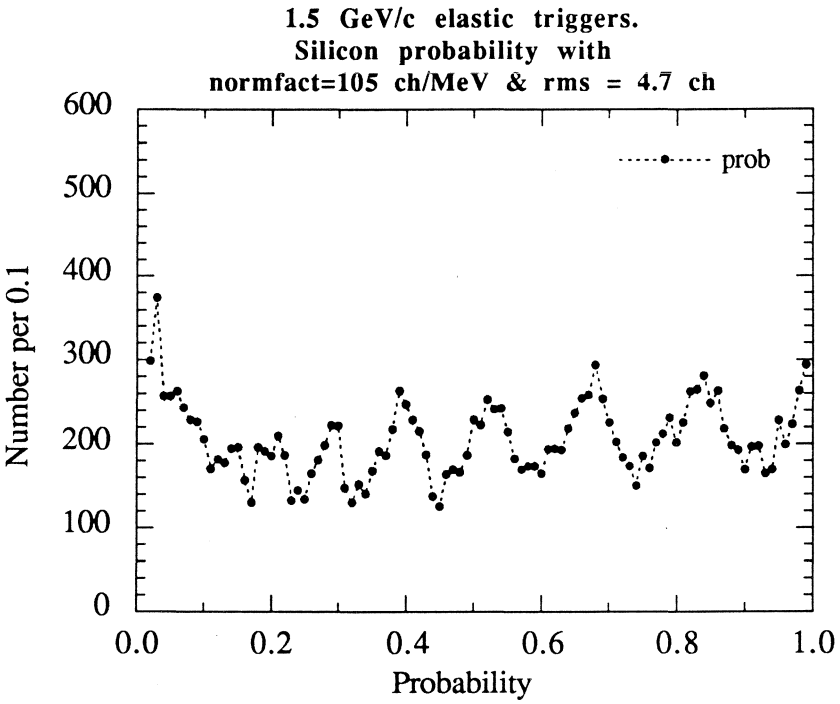

Fig. 4.57 Incident momentum 1.5 GeV/c.

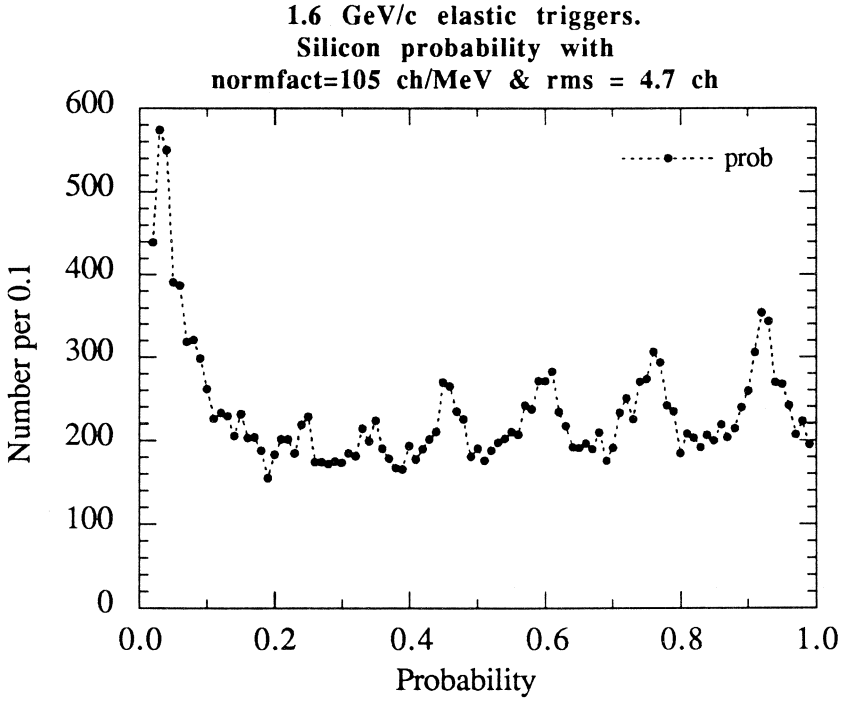

Fig. 4.58 Incident momentum 1.6 GeV/c.

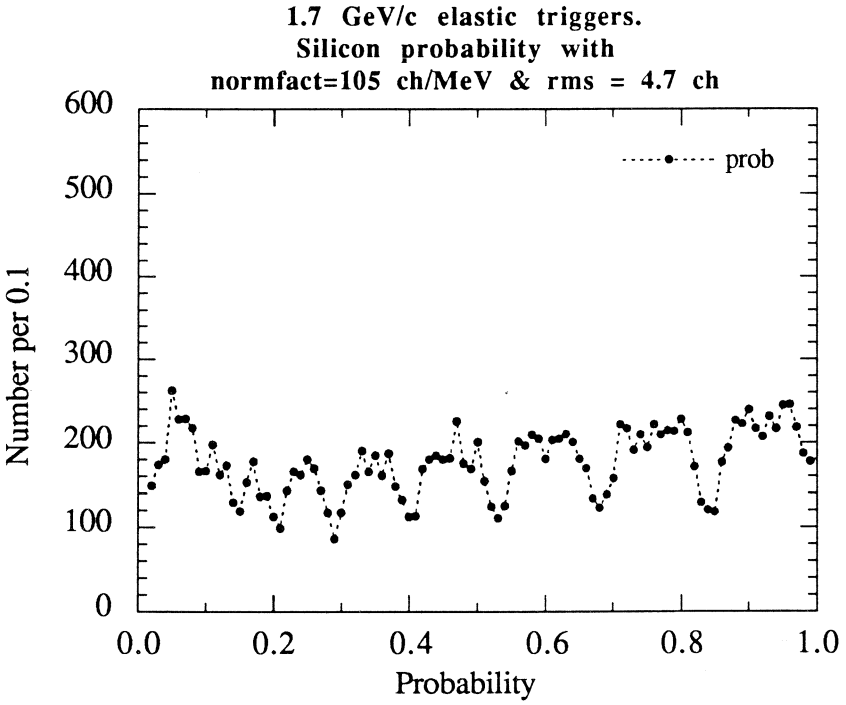

Fig. 4.59 Incident momentum 1.7 GeV/c.

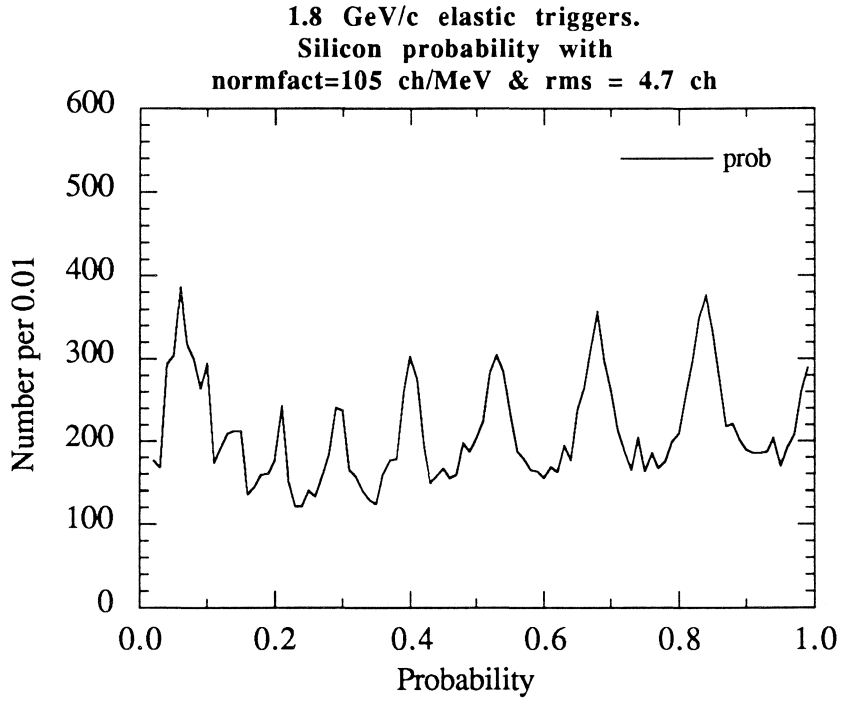

Fig. 4.60 Incident momentum 1.8 GeV/c.

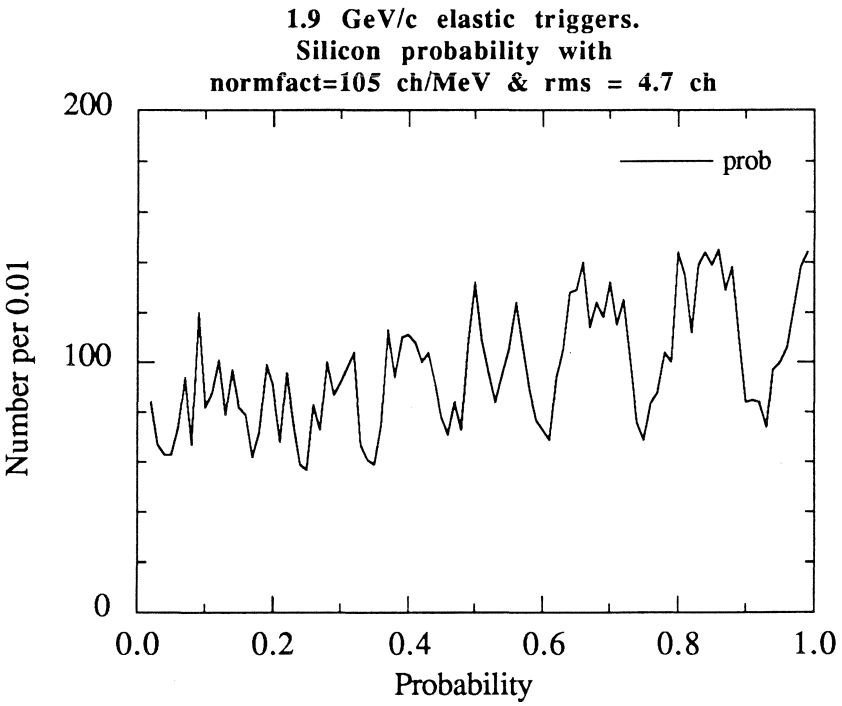

Fig. 4.61 Incident momentum 1.9 GeV/c.

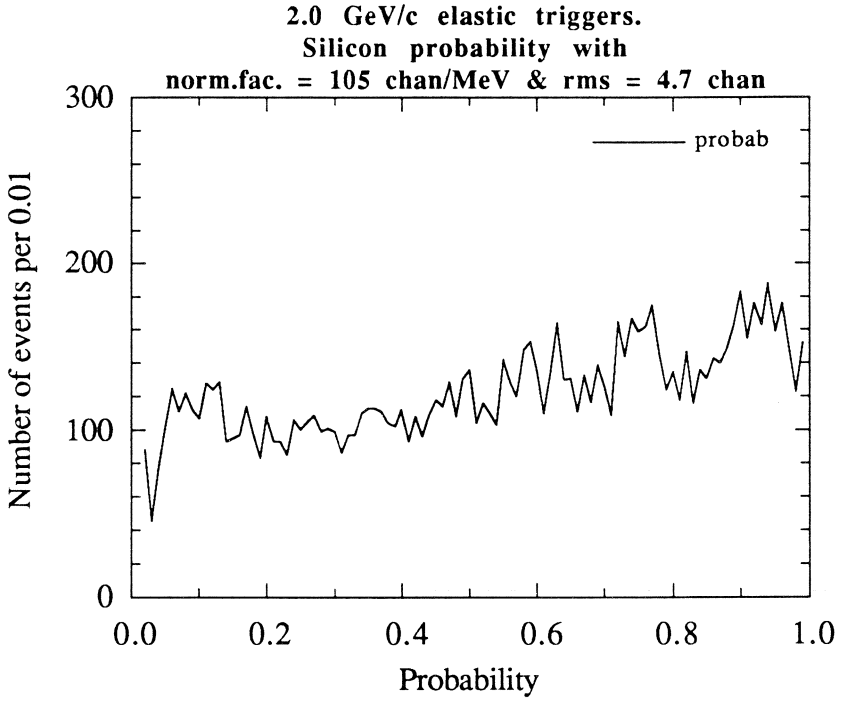

Fig. 4.62 Incident momentum 2.0 GeV/c.

Imprimé au CERN. Prix: 3.95 Fr.